Copyright Warning & Restrictions

The copyright law of the United States (Title 17, United States Code) governs the making of photocopies or other reproductions of copyrighted material.

Under certain conditions specified in the law, libraries and archives are authorized to furnish a photocopy or other reproduction. One of these specified conditions is that the photocopy or reproduction is not to be "used for any purpose other than private study, scholarship, or research." If a, user makes a request for, or later uses, a photocopy or reproduction for purposes in excess of "fair use" that user may be liable for copyright infringement,

This institution reserves the right to refuse to accept a copying order if, in its judgment, fulfillment of the order would involve violation of copyright law.

Please Note: The author retains the copyright while the New Jersey Institute of Technology reserves the right to distribute this thesis or dissertation

Printing note: If you do not wish to print this page, then select "Pages from: first page # to: last page #" on the print dialog screen

ABSTRACT

POLYMERIC NITROGEN BY PLASMA ENHANCED CHEMICAL VAPOR DEPOSITION

by
El Mostafa Benchafia

With the urgent need for new environmentally-friendly energetic materials, the field of polymeric nitrogen, predicted to be a high energy density energetic, is now at a critical stage in its development. In spite of extensive first principles calculations regarding the existence and stability of different polymeric nitrogen structures, their successful syntheses have been rare. This dissertation describes the first detailed study of a plasma-enhanced chemical vapor deposition (PECVD) approach to the synthesis of polymeric nitrogen. PECVD provides non-equilibrium conditions known to produce high pressure-temperature phases. Molecular nitrogen mixed with hydrogen and argon is used as the gas phase precursor to provide nitrogen and passivating hydrogen species. In addition, either solid sodium and lithium azide or azide solution infiltrated sheets of carbon nanotube substrates have been used to initiate plasma polymerization to a polymeric nitrogen phase. Characterization of the samples produced were conducted using micro-Raman spectroscopy, attenuated total reflectance-Fourier transform infrared spectroscopy, powder X-ray diffraction, and temperature programmed desorption. Sample morphologies and compositions have also been performed using scanning electron microscopy combined with energy-dispersive X-ray analysis. The results show that a mixture of polymeric nitrogen phases is formed that is stable under ambient conditions and decompose near 400°C. The long-sought-after cubic-gauche polymeric nitrogen (cg-PN) phase, produced only in a diamond anvil cell at high pressure high temperature conditions and not recoverable under ambient conditions, is shown by the powder diffraction data to be one of the polymeric nitrogen phases synthesized by the plasma process. Density

Functional Theory (DFT) calculations were also used to investigate the metastability of cg-PN and that of related nitrogen clusters at ambient conditions in order to understand some of the results. Although these phases were obtained with and without carbon nanotube substrates, the spectroscopic results suggest that carbon nanotubes play a significant role in faster and more efficient plasma synthesis possibly due to stabilization of a PN phase inside the walls of carbon nanotubes. The effect of carbon nanotubes on polymeric nitrogen growth will be investigated by transmission electron microscopy in future studies.

POLYMERIC NITROGEN BY PLASMA ENHANCED CHEMICAL VAPOR DEPOSITION

by
El Mostafa Benchafia

A Dissertation
Submitted to the Faculty of
New Jersey Institute of Technology and
in Partial Fulfillment of the Requirements for the Degree of
Doctor of Philosophy in Materials Science and Engineering

Interdisciplinary Program in Materials Science and Engineering

January 2015

APPROVAL PAGE

POLYMERIC NITROGEN BY PLASMA ENHANCED CHEMICAL VAPOR DEPOSITION

El Mostafa Benchafia

Dr. Nuggehalli M. Ravindra, Dissertation Co-advisor — Date
Professor, Department of Physics, NJIT

Dr. Zafar Iqbal, Dissertation Co-advisor — Date
Research Professor, Department of Chemistry and Environmental Science, NJIT

Dr. Xianqin Wang, Committee Member — Date
Associate Professor, Department of Chemical, Biological and Pharmaceutical Engineering, NJIT

Dr. Frank Owens, Committee Member — Date
Research Professor, Department of Physics, City University of New York

---

Dr. Cristiano L. Dias, Committee Member — Date
Assistant Professor, Department of Physics, NJIT

BIOGRAPHICAL SKETCH

Author: El Mostafa Benchafia

Degree: Doctor of Philosophy

Date: January 2015

Undergraduate and Graduate Education:

- Doctor of Philosophy in Materials Science and Engineering,
  New Jersey Institute of Technology, Newark, NJ, 2015
- Master of Science in Condensed Matter Physics,
  Mohammed V University, Rabat, Morocco, 2008
- Bachelor of Science in Physics,
  Mohammed V University, Rabat, Morocco, 2000

Major: Materials Science and Engineering

Presentations and Publications:

El Mostafa Benchafia, Chi Yu, Marek Sosnowski, N.M. Ravindra, and Zafar Iqbal, "Plasma Synthesis of Nitrogen Clusters on Carbon Nanotube Sheets," *The Journal of The Minerals, Metals and Materials Society (TMS)*, vol. 66, pp 608-615, 2014.

Zhiyi Wu, El Mostafa Benchafia, Zafar Iqbal and Wang Xianqin, "N_8^- Polynitrogen Stabilized on Multi-Wall Carbon Nanotubes for Oxygen-Reduction Reactions at Ambient Conditions," *Angewandte Chemie International Edition*, vol. 53, pp 12555-12559, 2014.

El Mostafa Benchafia, "Encapsulating Polymeric Nitrogen in Carbon Nanotubes," *2014 TMS RF Mehl Medal Symposium on Frontiers in Nanostructured Materials and Their Applications*, San Diego, February 16, 2014.

El Mostafa Benchafia, "Plasma Synthesis of a Polymeric Phase of Nitrogen," *2013 MS&T Conference and Exhibition*, Montreal, Canada, October 27, 2013.

Experience without theory is blind, but theory without experience is mere intellectual play.

Immanuel Kant

ACKNOWLEDGMENT

This research project would not have been possible without the support of many people. I would like to express my sincerest gratitude to my Co-advisor Zafar Iqbal for providing me with the opportunity to work in this project. I was lucky enough to benefit from his guidance and motivation. I would also like to gratefully acknowledge the support of my Co-advisor Nugehalli Ravindra who encouraged me throughout this endeavor from beginning to end and enabled me in many occasions to present my work at international conferences where I could meet other members from the materials science community and also discover beautiful places in the country and abroad. I would like to take this opportunity to thank Professor Xianqin Wang who has been instrumental in the completion of this project and has been generous in assisting me and making me a part of her research team. I greatly appreciate Professor Marek Sosnowski for his help with the Plasma enhanced chemical vapor deposition. I would also like to thank Professor Cristiano L. Dias for allowing me access to the high performance research computing cluster at NJIT and for serving on my dissertation committee. A special thanks also goes to Frank Owens who graciously accepted to serve as a committee member for my thesis defense. Many of the results presented in the course of this thesis are obtained with the help of many collegues. I thank Jade Ying for sharing her knowledge on Raman spectroscopy, Amir Hussein Rajabi for his guidance in the SEM and FTIR, Zhiyi Wu for his help in the lab and the dicussions about polynitrogen clusters, Sarang Mulley and Chiranjivi Lamsal for computer time in Professor Ravindra's laboratory, Gu Yuan for X-Ray analysis and Maocong Hu for his help with temperature programmed desorption. I wish to thank my grandmother, my parents, brothers and sisters for their unconditional support throughout the years. Finally, a very special thanks goes to my fiancée Hana, who brought a meaning to my life and endured a hard lifestyle during my Ph-D years at NJIT.

TABLE OF CONTENTS

TABLE OF CONTENTS
(Continued)

Chapter **Page**

TABLE OF CONTENTS
(Continued)

Chapter **Page**

LIST OF TABLES

LIST OF FIGURES

LIST OF FIGURES
(Continued)

Figure **Page**

LIST OF FIGURES
(Continued)

Figure **Page**

CHAPTER 1

INTRODUCTION

1.1 Historical Background

Some 40 years ago a new terminology for nitrogen started to see light: *POLYMERIC NITROGEN*. Predictions pointed towards the existence of a new phase and structure beyond the only two all-nitrogen-compounds known at that time : molecular nitrogen N_2 and the azide anion N_3^- [1]. More to the prediction of a polymeric crystalline form a greater surprise came; the crystalline form itself is an unusual one that has never been seen before in any other material: This was the *cubic gauche* structure depicted in Figure. 1.1 and was suggested for the first time in 1992 by Mailhiot et al. [2]. However, even though the transformation from molecular nitrogen to cubic gauche structure (abbreviated cg-PN in the rest of this dissertation) was predicted to take place at pressures around 50 GPa which was within the reach of the diamond anvil cells that were in use at that time, no successful synthesis was reported for 16 years. In the meanwhile, a major breakthrough had come in 1999 with the successful synthesis of pentazenium N_5^+ cation by Criste et al. [3], The chemistry involved took advantage, in the presence of hydrozoic acid HN_3, of the weak N-F bond in the N_2F^+ cation and the strong H-F bond to eliminate HF and produce N_5^+ according to the following reaction:

$$[F - N \equiv N]^+ + H - N = N = N \longrightarrow [N \equiv N - N = N = N]^+ + HF \qquad (1.1)$$

The bent linear structure of the N_5^+ in Figure. 1.2 is of C_{2v} symmetry and was characterized by NMR, IR and Raman spectroscopy in complete agreement with density functional theory calculations.

[1]Historical accounts attribute the azide anion N_3^- discovery to Curtius in 1890. However, Phenyl azide [$C_6H_5^+$,N_3^-]was first synthesized by Peter Graß in 1864 [1] .

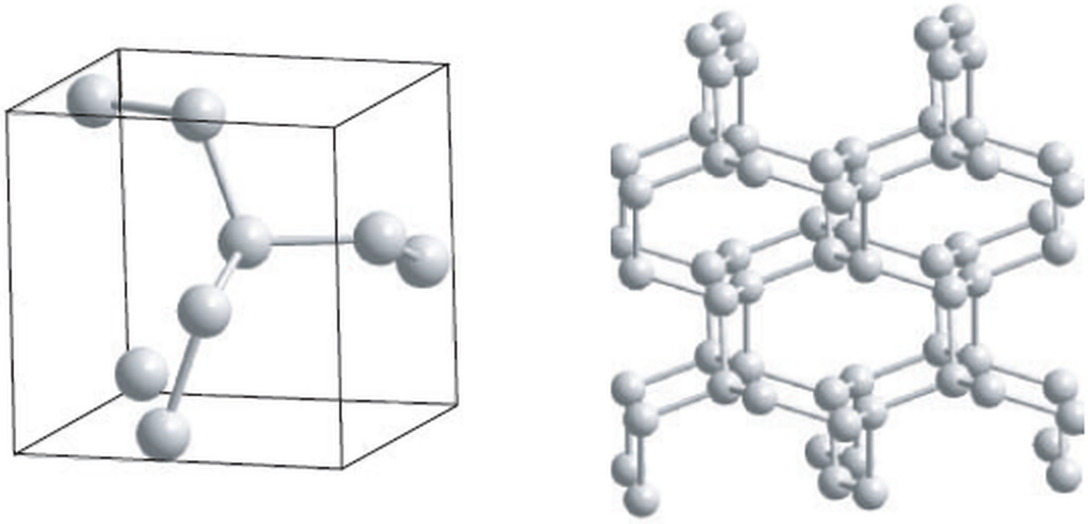

Figure 1.1 Polymeric nitrogen cubic gauche (cg-PN) structure, primitive cell (left) and an extended structure (right).
Source: *Mikhail I. Eremets, Alexander G. Gavriliuk, Ivan A. Trojan, Dymitro A. Dzivenko1 & Reinhard Boehler. Single-bonded cubic form of nitrogen. Nat Mater, 3, 558-563, 2004.*

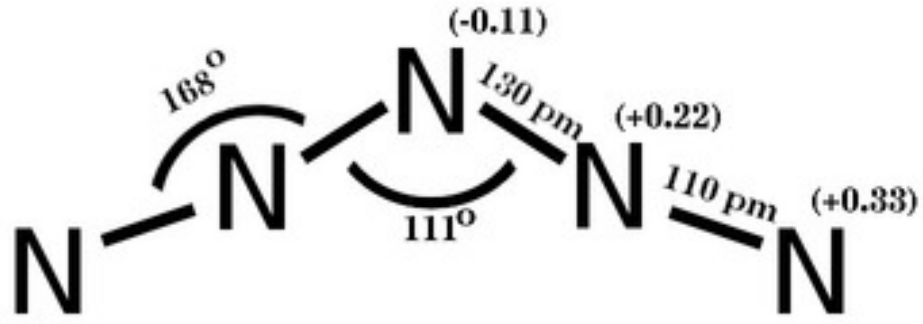

Figure 1.2 C_{2v} N_5^+ structure.
Source: *http://en.wikipedia.org/wiki/Pentazenium#mediaviewer/File:Pentazenium.png*
(accessed June 14, 2014)

The long sought after cg-PN was synthesized by Eremets et al. [4] in 2004. Extreme conditions allowed such an extensive synthesis at temperatures and pressures beyond 2000 K and 110 GPa. The diamond anvil cell high pressure-high temperature apparatus, was equipped for in-situ characterization with X-Ray diffraction measurements and Raman spectroscopy. The cg-PN structure was as predicted and Raman spectroscopy provided a conclusive proof as it fitted nicely with the theoretical predictions of Barbee [5].

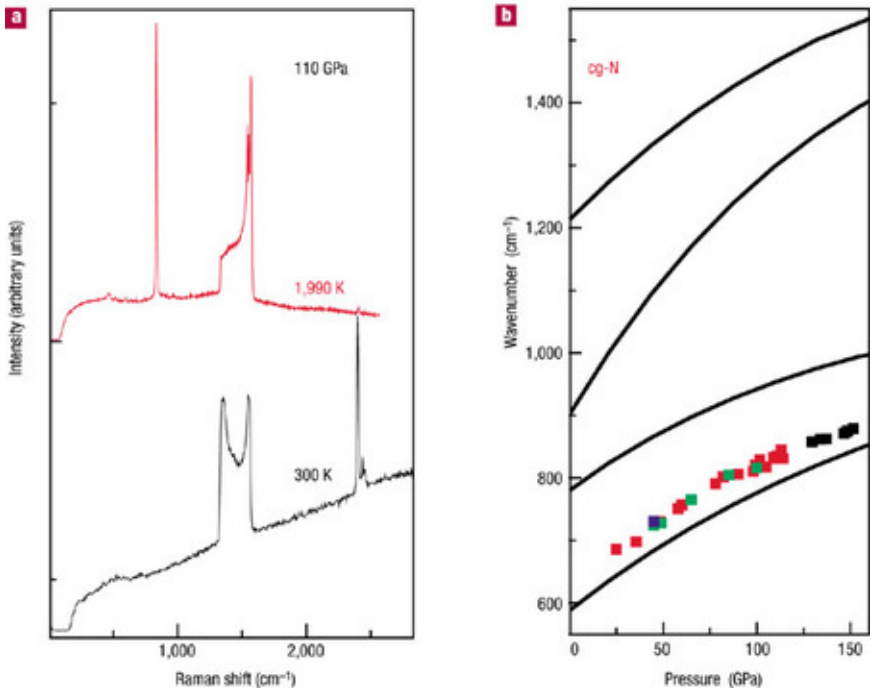

Figure 1.3 Left: Raman spectra of the cg-PN at 1990K, 110GPa compared to molecular nitrogen at 300K,110GPa. The N_2 vibron at 2400 cm^{-1} vanishes at 1990K and is replaced by the peak at 840 cm^{-1}. Right: Colored data points depict the pressure dependence of the cg-PN frequency, solid lines are from Barbee calculations for cg-PN.
Source: *Mikhail I. Eremets, Alexander G. Gavriliuk, Ivan A. Trojan, Dymitro A. Dzivenko1 & Reinhard Boehler. Single-bonded cubic form of nitrogen. Nat Mater, 3, 558-563, 2004.*

Some other forms of polynitrogen have been detected ephemerally, notably N_3, N_4 and N_5^- [6, 7, 8]. The expected high energy form of cyclic N_3 was directly formed

by UV photodissociation of chlorine azide ClN_3 [2], time-of-flight (m/z=42) detections were attained 100 μs after the cyclic polynitrogen was formed. Tetranitrogen N_4 on the other hand had a lifetime of about 1 μs at 298K, the open-chain geometry was interestingly seen as the best candidate made of two closely linked N_2 fragments joined by a weaker relatively longer bond that is not necessarily of the Van Der Waals type. This is unlike the N_4^+ obtained along with N_3^+ by mass spectrometry [9]. Cyclic N_5^- in Figure. 1.4 was formed and detected by electrospray ionization mass spectrometry (ESI-MS) [10]. Its lifetime is debatable and is probably of the order of few seconds. Its decomposition to N_3^- and N_2 was inevitable in the ESI-MS procedure, but it was the detection of N_3^-, not present as a starting material, that confirmed the formation of the cyclic N_5^- anion.

1.2 Polynitrogen Compunds: Motivations

1.2.1 Polynitrogens: High-Density-Energetic-Materials

The strength of the molecular nitrogen triple bond N≡N is much larger than any other homopolar bond [11] with an energy content of about 4.94 ev.atom^{-1} compared to -0.83 ev.atom^{-1} for the N-N single bond [12]. Therefore a high amount of energy of about 2.3 ev.atom^{-1} [13] is expected to be released from the single to triple bond transformation. Consequently, an all-single-nitrogen bond or at least a single-double-nitrogen bond compound should, in principle, be a High-Density-Energy-Material (HDEM), a storage medium that can be used as explosives, propellants [3] and energetic binders. Estimations for such Polynitrogen compounds envisage up to tenfold more detonation pressure than that of one of the most powerful explosives in use today: HMX($C_4H_4N_8O_8$).

[2]Warning:ClN_3 is highly unstable and can explode without any provocation.

[3]Solid nitrogen rocket fuel could make for smaller, lighter spacecraft. An excerpt from "New rocket fuel?" `http://www.nature.com/news/2002/020514/full/news020513-2.html` (accessed online Dec 15, 2014)

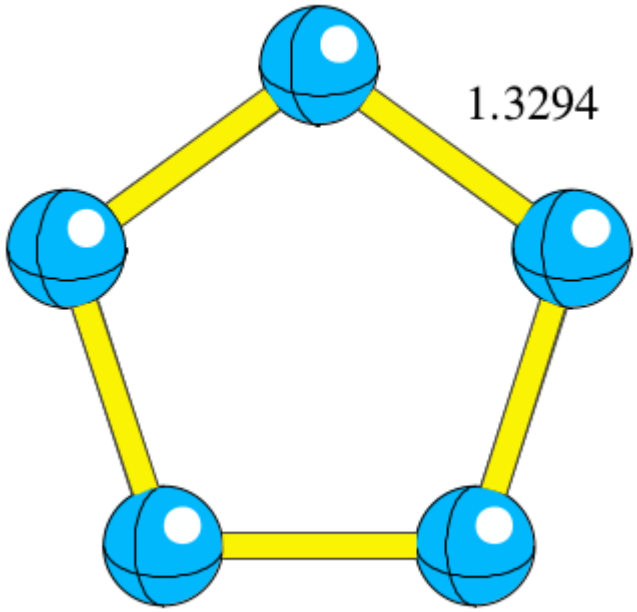

Figure 1.4 Optimized geometry of the planar pentazolate anion N_5^- of D_{5h} symmetry at the B3LYP level of theory.
Source: *Rodney J. Bartlett.* ***http://www.clas.ufl.edu/users/rodbartl/pdf_files/polynitrogen\%20Tobita.pdf***
(accessed May 20, 2014)

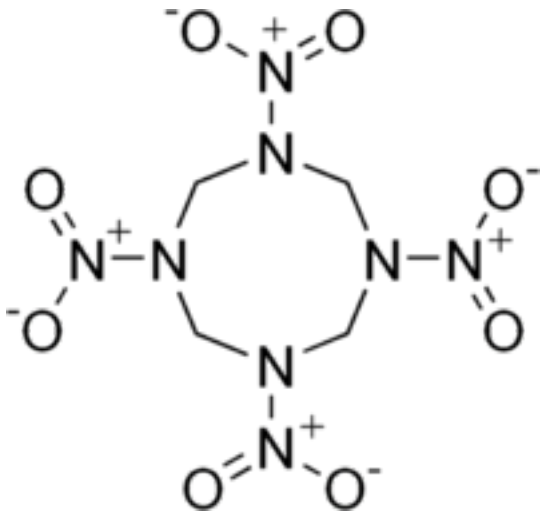

Figure 1.5 HMX: One of the most powerful explosives in use.
Source: *http://commons.wikimedia.org/wiki/File:HMX.png*
(accessed December 5, 2014)

1.2.2 cg-PN is a Nitrogen-based Diamond!

The cg-PN structure is not only interesting because of its eventual energy storage capabilities; it can also compete with diamond in terms of hardness as it has similar lattice parameters and low compressibility [13]. Moreover, the three-fold coordination of cg-PN makes it analogous to the sp^2 covalency found in graphite, but the nonbonding orbital of the lone-pair on each nitrogen site gives the structure a near tetrahedral sp^3 hybridization analogous to diamond [14]. In the absence of experimental data regarding the mechanical properties of this unique structure, claiming its full resemblance to diamond cannot be made. In fact only the bulk modulus of about 300GPa was reported from the high pressure/high temperature synthesis which is still less than diamond's bulk modulus of about 443GPa [15]. Theoretical predictions suggest only the C_{12} elastic constant to be higher in cg-PN than diamond (160GPa versus 130GPa at the GGA level of theory) [14, 16].

1.2.3 Polynitrogen for Catalysis

As discussed above, the lone-pair carried in each nitrogen provides extra stability in cg-PN by directing the bonding towards a tetrahedral sp^3 coordination. A more useful source of electron-transfer can be achieved from this material for Oxygen-Reduction-Reactions (ORR), particularly in hydrogen fuel cells as demonstrated by Wu et al. [17]. The need for a catalyst that can replace the expensive and scarce platinum metal is urgently required for the commercialization of these automotive fuel cells. In addition to the very recent work of Wu et al., various papers in the literature have described nitrogen-containing materials for catalytic activity in oxygen reduction reaction. For example, vertically aligned nitrogen-containing carbon nanotubes discussed by Gong et al. [18] showed good ORR performance where it appears that the pyridinic nitrogen incorporated releases the adjacent carbon atoms from their relatively higher positive charge, thus facilitating the weakening of the oxygen O-O bond to initiate ORR . Similar strategies have been implemented for graphene [19, 20] where nitrogen can occupy three different sites: Pyridinic, quartenary or pyrrolic (see Figure. 1.6). In this context, polymeric nitrogen can serve as a good catalyst without the need for stabilization on graphene or carbon nanotubes, although nitrogen clusters like the N_8^- anion would require stabilization on a carbon based or metal support.

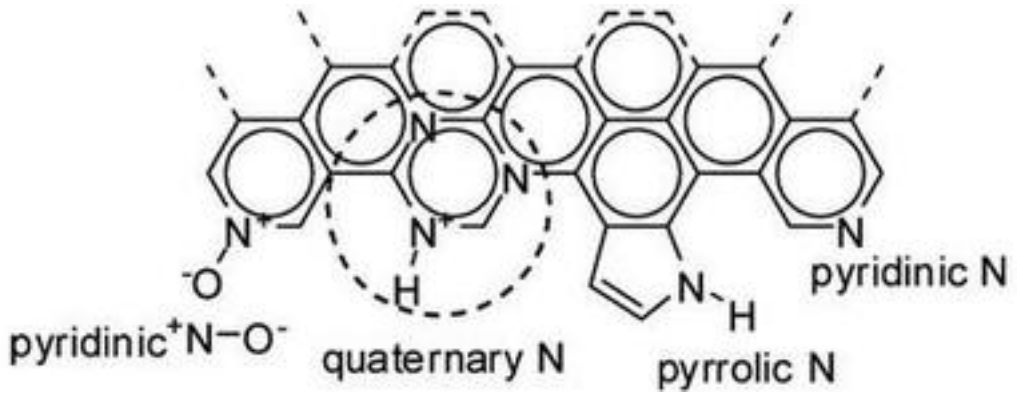

Figure 1.6 Nitrogen-containing graphene.
Source: *Elizabeth J. Biddinger, Dieter von Deak, Umit S. Ozkan. Nitrogen-Containing Carbon Nanostructures as Oxygen-Reduction Catalysts. Top Catal, 52, 1566-1574, 2009.*

CHAPTER 2

NITROGEN REVOLUTION FROM MOLECULAR TO POLYMERIC

2.1 Extended, Polymeric and HDEM

Gasoline is a daily source of energy for people all over the word. Energy from gasoline is obtained from a combustion process that transforms the hydrocarbon into carbon dioxide and water. The energy storage medium is primarily derived from the strong covalent bond within each gasoline molecule (C_8H_{18}). The molecules interact with each other via weak forces of Van Der Waals type; these weak forces are weak bonds between all molecules that have an insignificant contribution to the overall energy that can be stored. Moreover, weaker bonding also means larger volumes to be occupied making the energy density even lower. An unprecedented energy gain will take place if only covalent bonds were extended throughout the whole medium. Extended solids or polymeric forms are thus terms used to define such materials with high energy content per unit volume consisting of a network of molecules or atoms connected in a polymeric fashion, examples include nitrogen (a polymeric nitrogen discussed in this dissertation), carbon (diamond), carbon monoxide and boron. A comparison is made in Table. 2.1 to show the energetic aspect of these materials. Diamond can be thought of as the "ultimate" carbon-based polymer [21]. It is the ideal extended solid or super molecule that is cross-linked at every atom and site of the entire diamond network.

Table 2.1 Energy density expressed in KJ/cm^3

Compound	Energy density (KJ/cm^3)	Reference
Polymeric Nitrogen	34	[2]
Metalic bct Boron	26	[22]
bc8 Carbon	21	[23, 24]
HMX	12	[25]

2.2 The First Steps for Polymeric Nirogen Synthesis

2.2.1 The Early Signs

One of the earliest attempts to make the world of extended solids a reality came from the same people that theorized about their possible existence and feasibility of a synthesis, especially that the pressures involved for a transformation to a polymeric form were within reach of the diamond anvil cells of the day. In the 90's, T. Barbee, A.K McMahan, C. Mailhiot and co-workers [25] examined the behavior of nitrogen and carbon monoxide at megabar pressures and through laser heating. The brown color manifested in nitrogen samples under pressure gave signs of the weakening of the bonds in molecular nitrogen as it transitions to a polymeric phase. On the other hand, the molecular vibron of nitrogen at a Raman frequency around 2325 cm^{-1} exhibits a shift to higher frequencies with pressure increase (Figure. 2.1) due to initial strengthening of the bond followed by a turnover to decrease in frequency due to bond weakening as a result of triple to double and finally to single bond formation in the polymeric phase.

2.2.2 Transition to Non-molecular Phases in the 150-200 GPa Range

Goncharov and co-workers [26] provided optical spectroscopic evidence using visible, near IR/Raman and synchrotron techniques for the transformation of molecular nitrogen to a non-molecular phase in the 140-160 GPa range. Among their findings is one of the important features in the Raman/IR spectra that will be key to the interpretations of the experiments proposed in this dissertation. It is the appearance of a broad Raman line at 640 cm^{-1} along with the related infrared line about 1450 cm^{-1} and 900 cm^{-1} (Figure. 2.2). The intensities of these new lines appear to increase while molecular nitrogen line intensities decrease upon pressure increase implying that the molecular and non-molecular phases coexist at these high pressure ranges. While still transparent up to 140 GPa, beyond this pressure the phase starts to look yellow till becoming totally opaque at 160 GPa.

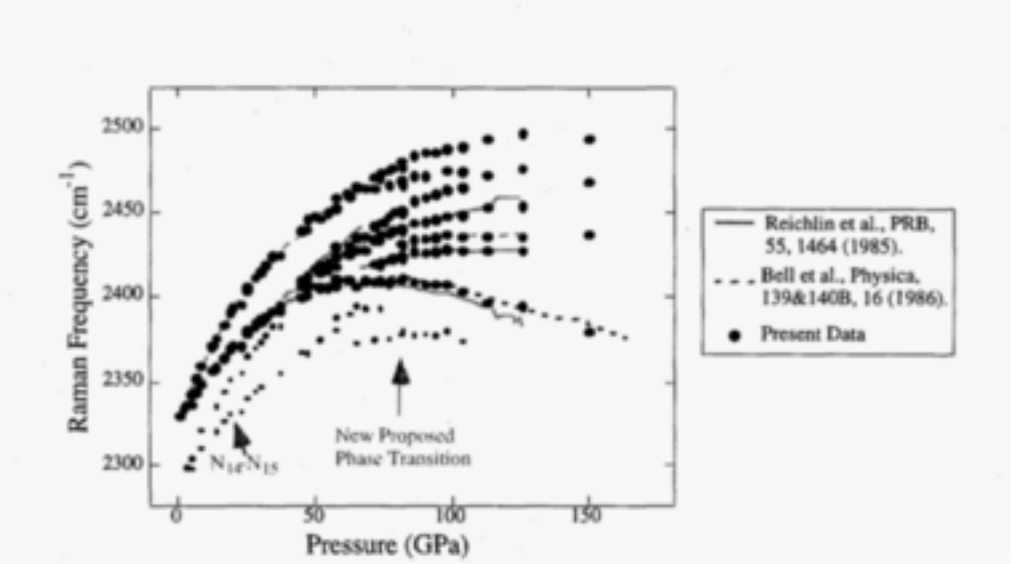

Figure 2.1 Raman stretch modes in N_2 vs. pressure. The analysis of the data demonstrates that the N_2 triple bond is severely weakening.
Source: *H.E. Lorenzana, C.S. Yoo, M. Lipp, T. III Barbee, A.K. McMahan, and C. Mailhiot. Novel high energy density materials: Synthesis by megabar hot pressing. Laboratory Directed Research and Development, 1996, Final Report.*
`http://www.osti.gov/scitech/servlets/purl/231384`
(accessed December 1, 2014)

This change in color to complete opacity is a manifestation of band gap-closing, a small band gap would be related to a semiconducting phase rather than a metallic phase, such as in the predicted simple cubic structure [27]. The IR/Raman modes obtained were also speculated to undergo a splitting (typically a consequence of intermolecular interactions in the molecular phase and site symmetry in the extended phases) because of either the non-hydrostatic conditions or symmetry reduction and can provide an explanation for the large linewidths observed. Having a mixture of phases (cubic gauche, black phosphorous, arsenic and chainlike structures, etc ...) that are close in energy also raises this possibility; in such scenario the overall phase would misleadingly look amorphous by spectroscopy techniques [26] unless X-ray or electron diffraction measurements are made.

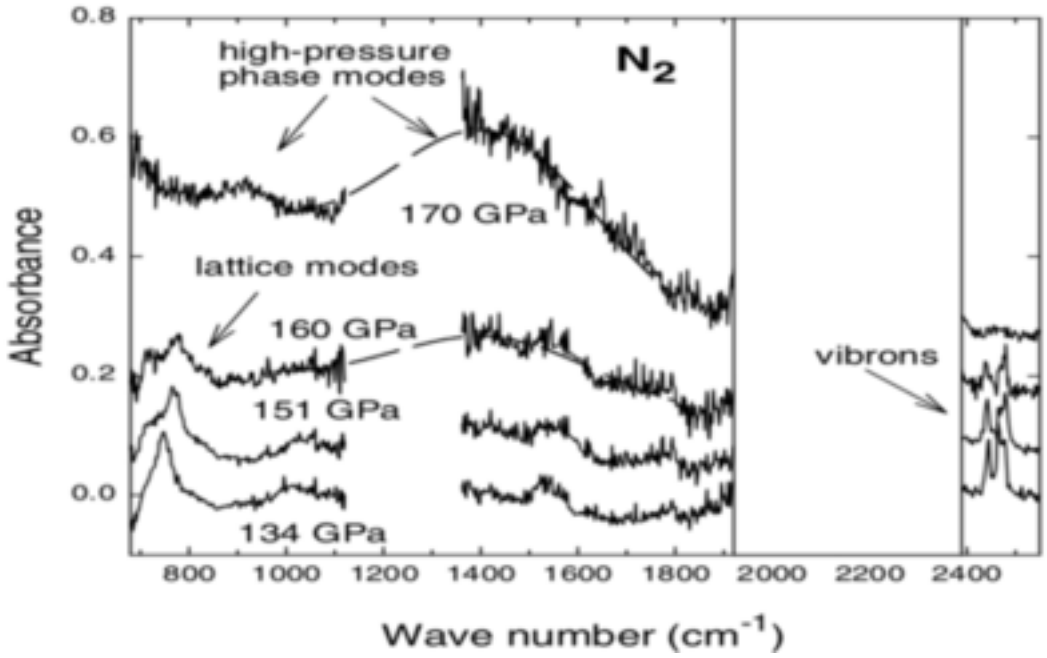

Figure 2.2 IR absorption spectra in the vibrational spectral range through the transition from molecular to non-molecular nitrogen.
Source: *Alexander F. Goncharov, Eugene Gregoryanz, Ho-Kwang Mao, Zhenxian Liu, and Russell J. Hemley. Optical Evidence for a Nonmolecular Phase of Nitrogen above 150 GPa. Physical Review Letters, 85:1262-1265, 2000.*

The semiconducting nature of the nitrogen phase was determined by Eremets and co-workers [28] by electrical resistance measurements but at higher pressures up to 240 GPa and room temperature. The energy gap was estimated to be about 0.4 eV. Interestingly, this phase was successfully retrieved at ambient pressures but at temperatures below 100K. A theoretical investigation of the real nature of these high pressure phases was done by Nordlund and co-workers [29] using molecular dynamic simulations based on density functional theory parametrization that allowed the determination of all the stages of evolution of nitrogen under increase of pressure. The resulting structure obtained was a disordered network of single and double bond nitrogen atoms (Figure. 2.3).

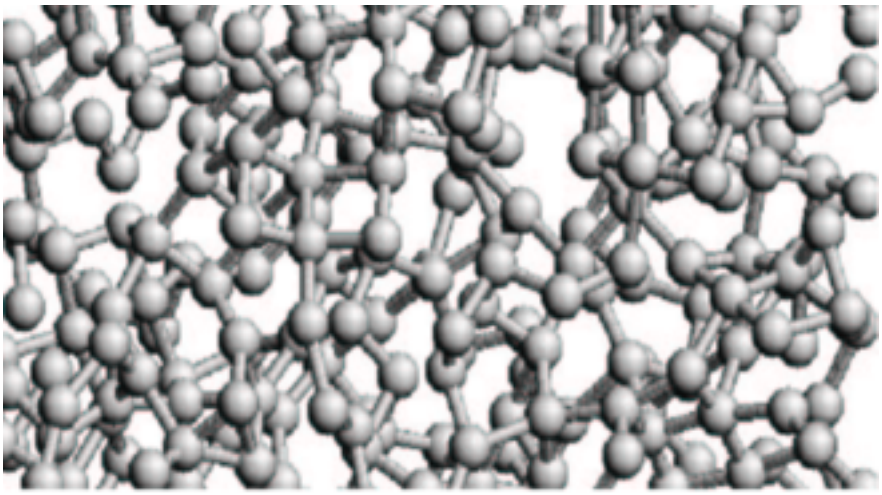

Figure 2.3 Structure of low-coordinated nitrogen at ambient pressure at 100 K produced by molecular dynamic simulation.
Source: *K. Nordlund, A. Krasheninnikov, N Juslin, J. Nord, and K. Albe. Structure and stability of non-molecular nitrogen at ambient pressure. Europ. Lett, 65:400-406, 2004.*

2.3 The Synthesis of the Cubic Gauche Form of Polymeric Nitrogen

The major breakthrough towards a substantial synthesis of polymeric nitrogen occured in 2004 with the work of Eremets et al. [4]. Unlike the predicted amorphous phase, which is opaque as discussed in the previous section, the new phase was found

to be completely transparent. The molecular vibron disappeared completely from the Raman spectra while a new Raman line emerged at 840 cm^{-1} (Figure. 1.3). The synthesis was done at temperatures higher than 1990 K and pressures above 110 GPa in a sophisticated arrangement involving a diamond anvil cell (Figure. 2.4) which could be combined with in-situ Raman and X-ray diffraction measurements. The X-ray patterns were analyzed to see which possible polymeric phase corresponds exactly to the synthesized phase. The cubic gauche structure provided the best fit to the diffraction pattern obtained. At 115 GPa of pressure, the N-N bond was estimated to be 1.346 $\AA$ and the diehedral angle was about 108.87° indicating that the cg-PN structure was strongly bonded covalent structure consistent with the derived bulk modulus in the 300-400 GPa range [14]. Further investigations led to the synthesis of single crystals of cg-PN by Eremets and co-workers [30]. Higher reflection angles were obtained, thus providing stronger proof for the cg-PN structure Figure. 2.5.

2.4 Controversy about the Infrared and Raman Active Lines in cg-PN

Barbee's [5] theoretical investigation on the metastability of cg-PN also shed light on the pressure dependence of the four Raman and infrared active lines associated with the 12 optical branches of this previously unknown structure. Of te four lines, two (the A and E symmetry) modes are Raman-active only while the other two are both Raman and infrared active (see Figure. 2.6). However, only the band at 840 appeared at 110 GPa in the diamond anvil cell experiment reported by Eremets et al. in 2004 [4]. This ambiguity was resolved in 2007 in the theoretical work of Caracas [31] who showed that the polarizability-induced intensity of the the Raman spectrum of the structure will be dominated by the high pressure 840 cm^{-1} line (extrapolated to the vicinity of 600 cm^{-1} line at zero pressure) of A-symmetry while all the other modes will have less than 10% intensity which will make them difficult to detect in the diamond anvil cell. Only by using a special diamond anvil cell that allows larger

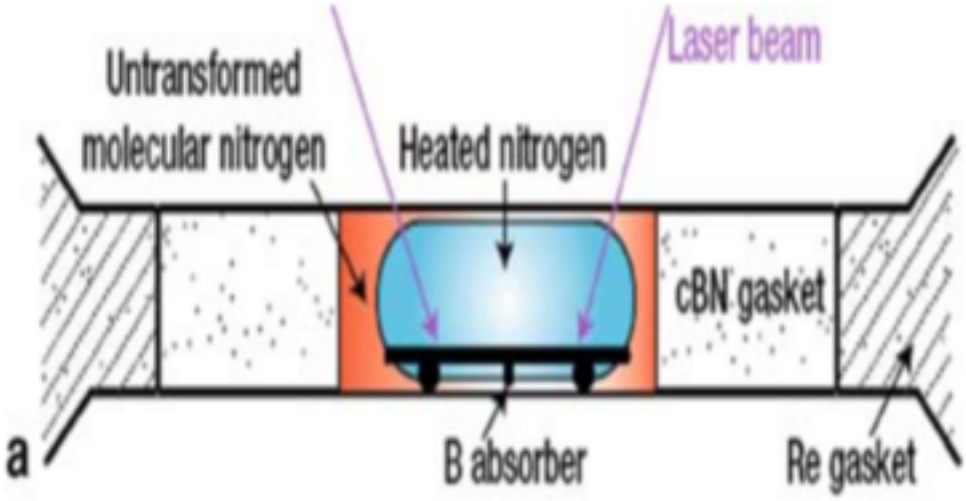

Figure 2.4 Diamond anvil arrangement used for cg-PN synthesis. A laser radiation was used to heat up a 1 μm-thick boron plate, nitrogen was squeezed in the anvil cell through a carbon-boron epoxy gasket.
Source: *M. Eremets, I. A. Trojan, A. G. Gavriliuk, and S. A. Medvedev. Synthesis of High Nitrogen Energetic Material. Shock Wave and High Pressure Phenomena. Springer Berlin Heidelberg, 2008.*

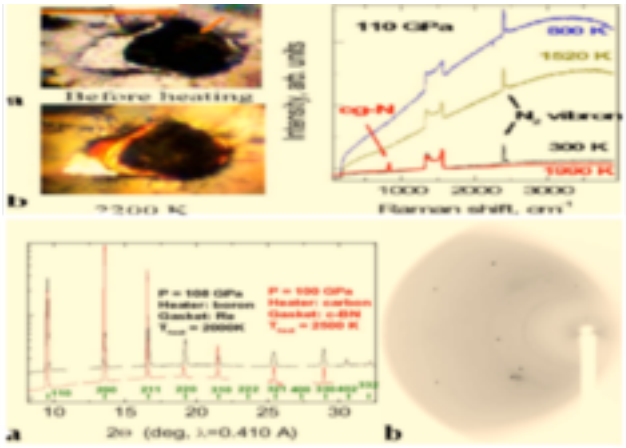

Figure 2.5 Top: Colors that develop for cg-PN (left) and Raman spectra at 110 GPa but different temperatures (right). Bottom : Diffraction spots (right)and X-ray diffraction pattern of the cg-PN single crystals at 2000K and 110 GPa.
Source: *M. I. Eremets, A. G. Gavriliuk, and I. A. Trojan. Single-crystalline polymeric nitrogen. App. Phys. Lett, 90, 2007.*

amounts of the synthesized cg-PN it was possible to grow cg-PN crystals and detect the second Raman-IR-active peak at 963 cm^{-1}, but with very low intensity as evident from (Figure. 2.7) [13].

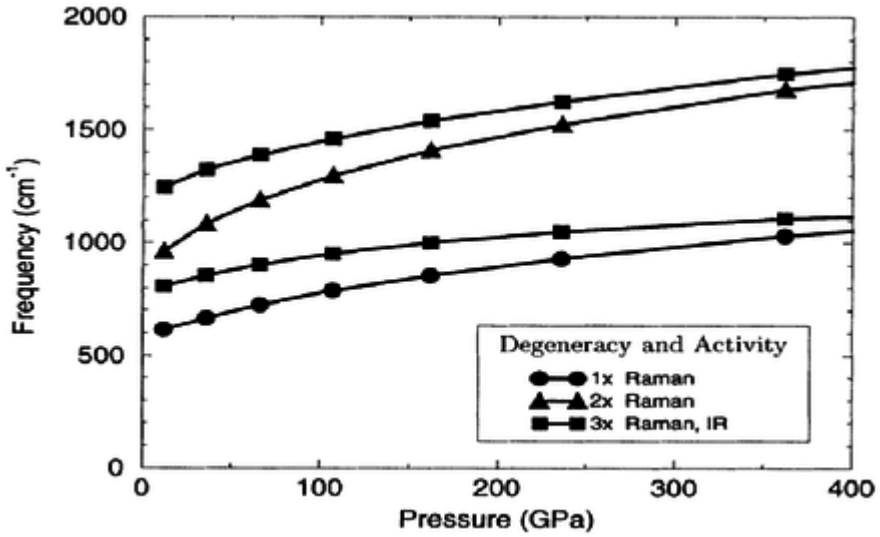

Figure 2.6 Frequencies of zone-center phonon modes in cubic gauche nitrogen as a function of pressure.
Source: *T. W. Barbee. Metastability of atomic phases of nitrogen. Phys. Rev. B, 48:9327, 1993.*

2.5 NaN_3 as a Precursor for Polymeric Nitrogen

As diatomic molecular nitrogen required very high pressures to undergo a phase transition toward polymeic phases, attempts were made to decrease the polymerization pressure by starting from an azide anion N_3^-. Most azides are very sensitive to shock and heating, but sodium azide NaN_3 is one of the least sensitive and was therefore the natural choice for use in the high pressure- high temperature diamond anvil cell experiments. Eremets and co-workers [32] recorded the extensive changes occurring in the Raman spectrum of sodium azide under pressure, where many different phases were obtained upon compression (for example, the so called Phase I and Phase II shown in Figure. 2.8) and upon decompression (for example, phases

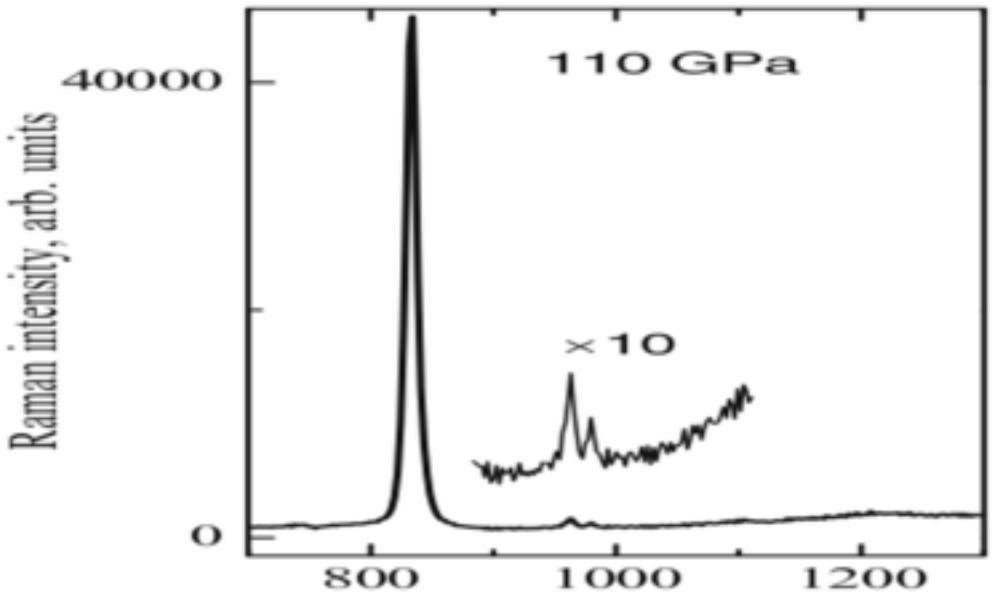

Figure 2.7 Raman spectrum from a large sample of cg-PN at 120 GPa where the second Raman line at 963 cm^{-1} is observed with very low intensity.
Source: *M. Eremets, I. A. Trojan, A. G. Gavriliuk, and S. A. Medvedev. Synthesis of High- Nitrogen Energetic Material. Shock Wave and High Pressure Phenomena. Springer Berlin Heidelberg, 2008.*

III, IV, V and VI). However, the structures of these phases were not determined by diffraction methods. Popov conducted similar experiments by using a different arrangement of the diamond anvil cell [33], where Phase II was attributed to the cg-PN based on Raman and infrared data showing the presence of the four peaks of the cg-PN discussed above. A comparison will be made in Chapter 4 of this thesis between the phases obtained using the non-equilibrium plasma deposition approach for polymeric nitrogen synthesis and some of the high pressure phases obtained from sodium azide.

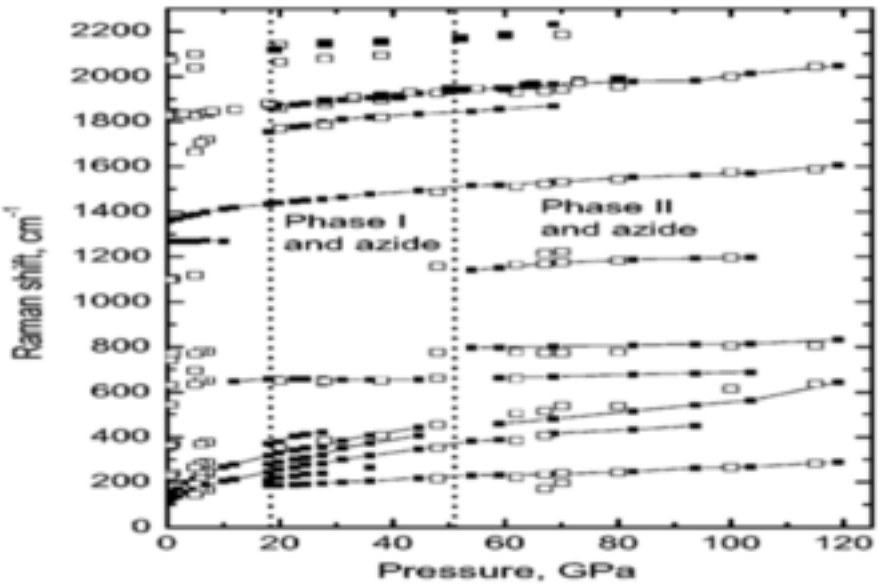

Figure 2.8 Raman line frequencies as a function of pressure for NaN_3 at room temperature. Solid squares are peak positions on increasing pressure, open squares on releasing pressure. The vertical dashed lines show the boundaries of the transitions. Source: *M. I. Eremets, M. Yu. Popov, I. A. Trojan, V. N. Denisov, R. Boehler, and R. J. Hemley. Polymerization of nitrogen in sodium azide. Chem. Phys, 120(22), 2004.*

2.6 Polynitrogen Clusters

2.6.1 N_5^+: The third Homoatomic Polynitrogen Prepared

As discussed in the introductory chapter, the synthesis of N_5^+ cation in the white salt $N_5^+AsF_6^-$ was of big historical importance since this was only the third homoatomic

nitrogen compound prepared after N_2 and N_3^- and the only third polynitrogen that can be produced in a large scale. The N_5^+ in the bent C_2v structure (Figure. 1.2) was first reported by Pyyk and Runeberg [34] in a theoretical investigation of the ABCBA compounds and its vibrational stability was known. Criste and co-workers [3] exploited the availability of the azide moiety in hydrozoic acid HN_3 and what was needed for the synthesis strategy was a compound that could provide two nitrogen atoms. The N_2F^+ found in $N_2F^+AsF_6^-$ was a natural choice. Due to the strength of the H-F bond and the weakness of the N-F bond, HF elimination was possible, thus giving rise to N_5^+ cation (Equation 1.1). The $N_5^+AsF_6^-$ salt was reported to react violently with water, but has reasonable stability at room temperature. It can be stored without decomposition at -78° for extended periods. Calculations of its formation enthalpy $\Delta H_f^{298} = 1469 \text{KJ.mol}^{-1}$ confirms its HDEM characteristics, and its low temperature Raman spectrum (Figure. 2.9) was in excellent agreement with theoretical predictions.

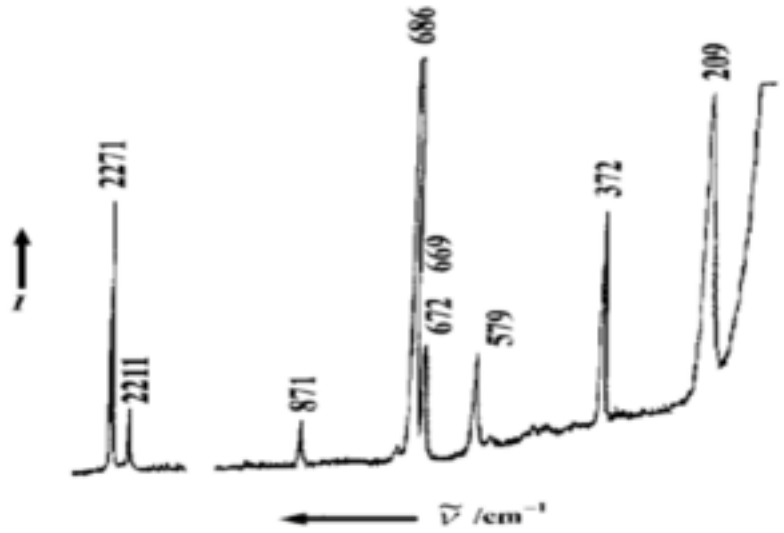

Figure 2.9 $N_5^+AsF_6^-$ Low-temperature Raman spectrum.M. I. Eremets, M. Yu. Popov, I. A. Trojan, V. N. Denisov, R. Boehler, and R. J. Hemley. Polymerization of nitrogen in sodium azide. Chem. Phys, 120(22), 2004.
Source: *K. O. Christe, W. W. Wilson, J. A. Sheehy, and J. A. Boatz. N_5^+ : A novel homoleptic polynitrogen ion as a high energy density material. Angew. Chem. Int. Ed, 38:2004, 1999.*

CHAPTER 3

PLASMA ENHANCED CHEMICAL VAPOR DEPOSITION

"The word "plasma" will be used to designate that portion of an arc-type discharge in which the densities of ions and electrons are high but substantially equal. It embraces the whole space not occupied by "sheaths. ""

Lewis Tonks and Irving Langmuir [35]

3.1 The Plasma State of Matter

3.1.1 Natural Plasmas

The sun, with temperatures reaching millions of Kelvins (10^6 at its corona), it is just too hot for matter to be in the solid, liquid or gaseous state. It is in the plasma[1], commonly referred to as the fourth state, that matter finds itself as assembly of ionized particles and neutrals manifesting collective effects. While plasmas are not often encountered in our daily lives, billions of stars like the sun in our galaxy and other galaxies are immense balls of plasma making this fourth state of matter the most abundant in the universe. We often get glimpses of naturally occurring plasmas in the form of lightning where temperatures in degree Kelvin can reach thousands of degrees (hotter than at the sun's surface). Auroras like northern lights, mostly seen in the high latitude regions of the Arctic, are a spectacular natural show that exhibits colors ranging from green , red and blue, typical colors from ionized oxygen and nitrogen atoms while yellow and pink are usually a combination of the principal colors. The reason we rarely see these natural plasmas comes from the necessary conditions where plasmas can occur which involves mainly a hard vacuum and high temperatures.

[1]From the Greek word $\Pi\lambda\alpha\sigma\mu\alpha$ which means anything that diffuses like a gel. It was used for the first time by Nobel laureate Irvin Langmuir in 1929 as an inspiration from the already known plasma blood.

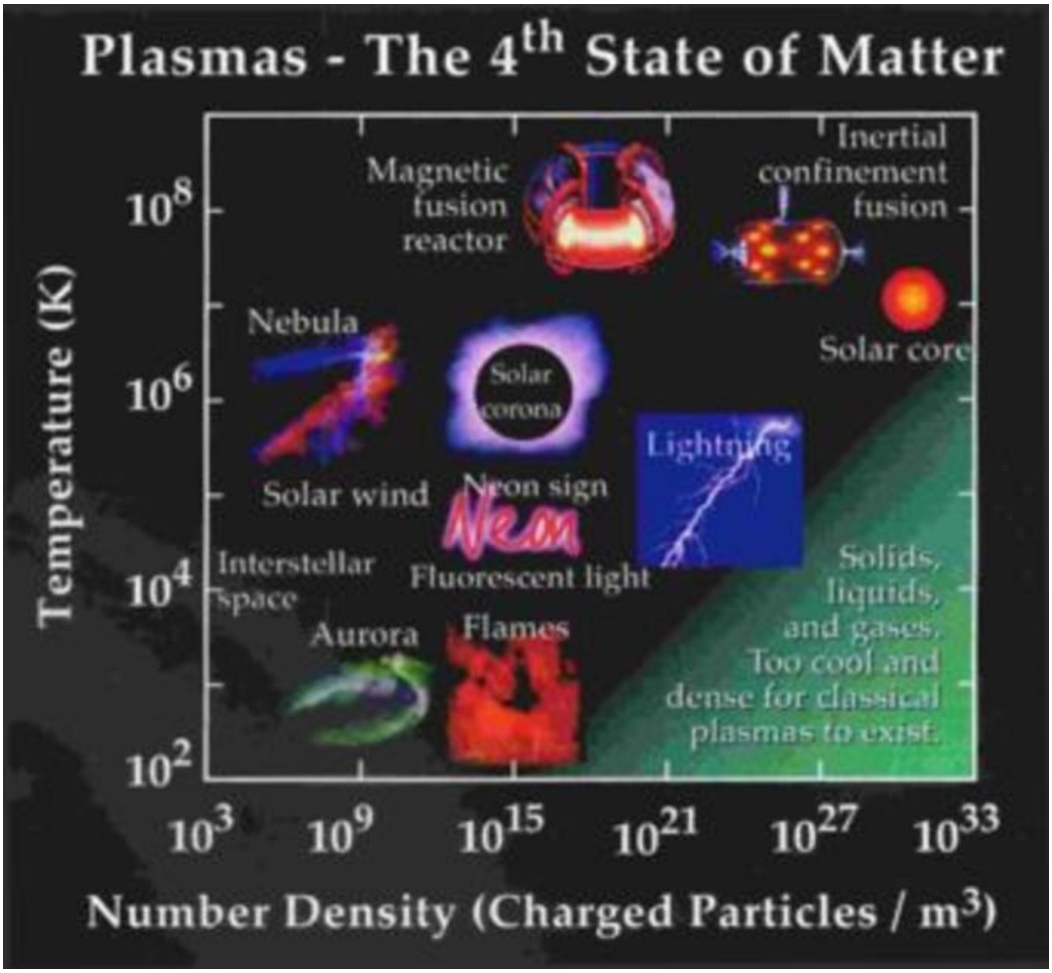

Figure 3.1 Different plasmas at different ranges of temperature and electronic density.
Source: *http://www.plasmas.org/basics.htm*
(accessed December 5, 2014)

A plasma, like the gas phase, has no specific shape but the shape of the reservoir where it is contained. But unlike the gas phase, the plasma state is quasi-neutral and its particles are influenced by and induce electromagnetic forces. Solar flares near the active sunspots and corona mass injections (CMEs) occur when the plasma medium including electrons, protons and heavy ions are accelerated to high speeds and are ejected to outer space. Mass ejections able to reach earth in two days and capable of interrupting electrical grids[2] are all a consequence of the strong interactions between particles and the magnetic forces manifested on the sun.

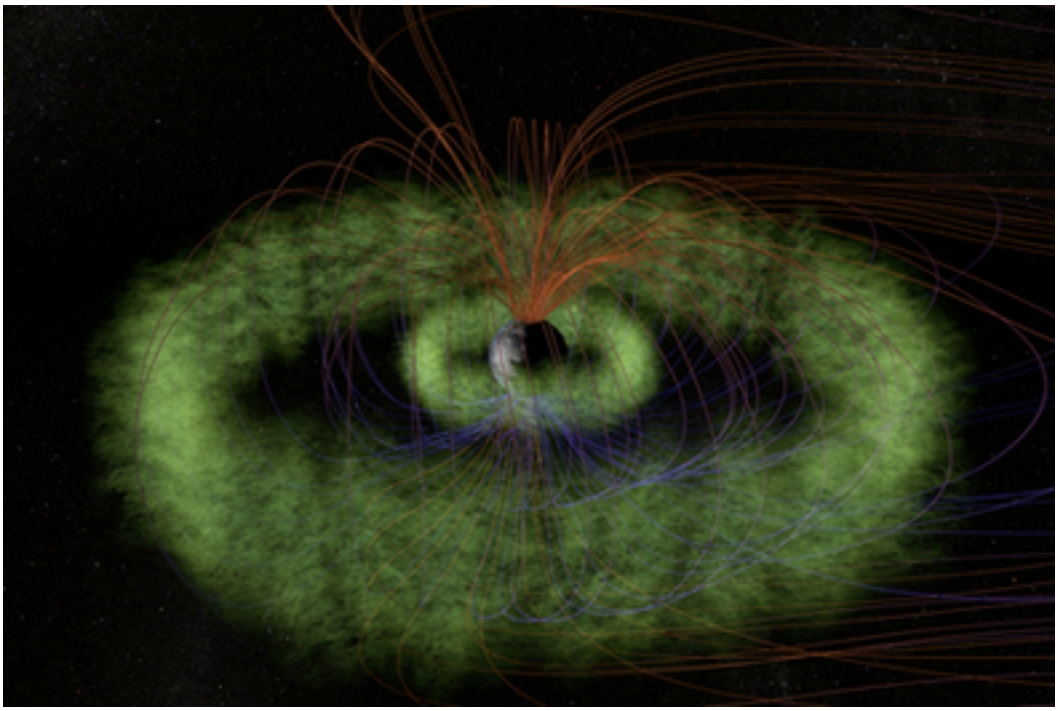

Figure 3.2 Two giant donuts of charged particles called the Van Allen Belts surrounding earth.
Source: *NASA/T. Benesch, J. Carns.* ***http://www.nasa.gov/mission_pages/rbsp/news/electric-atmosphere.html***
(accessed December 5, 2014)

[2]In 1989 a geomagnetic storm hit earth and caused a severe damage to the hydroelectric transmission system in Quebec Canada. Unless earth is lucky, similar storms are predicted to hit earth every eleven years.

3.1.2 Man-made Plasmas

Light up a candle and you have your first man-made plasma, the flame is sufficiently hot to generate a density of ionized atoms and the little flame is able deflect in the presence of an electric field because of the generated charged particles. A plasma is used in a variety of industrial sectors but the largest production line is found in microelectronics. Sputtering, cutting, etching and deposition are highly controlled plasma techniques. Plasma Enhanced Chemical Vapor Deposition (PECVD) has also been successful in the synthesis of carbon nanotubes and it is generally believed that PECVD is a promising technique for large scale synthesis at relatively low temperatures [36]. Plasmas at temperatures of the sun's core is an ongoing effort to come up with a plasma fusion reactor where, unlike nuclear fission of heavy elements like uranium, a hydrogen fusion process takes place to release higher energies.

3.1.3 DC and RF Plasmas

The class of plasmas of interest in this work is a clod plasma, sometimes also referred to as a low temperature plasma and it is by far the most widely used for industrial applications. Electrical discharge of a feeding gas to cause its ionization is generally produced by power sources in the form of a direct current (DC) or alternating current with frequencies in the radio range (RF). Figure. 3.3 depicts a typical apparatus for generating a plasma. A DC plasma is produced between the DC cathode and the grounded electrode while the RF plasma is generated between the RF and the grounded electrodes. In some processes, DC or RF is not a matter of choice and each technique is used according the process involved. In plasma sputtering for instance, the use of DC is more favored if the target is a conductor in order to accelerate the bombardment kinetics. If the the target is a semiconductor a charge build-up occurs with DC that inhibits further sputtering, and RF is used since heavy ions cannot keep up with switching currents. This charge build-up usually seen in a DC plasma in the

form of sparks can also be avoided in an RF plasma by covering the electrodes with a dielectric material that acts like an arc extinguisher. The discharge process is also done by means of the small pulses carried in filaments allowing very weak currents [37]. Still, the overall density and temperature is capable of ionizing the feeding gas.

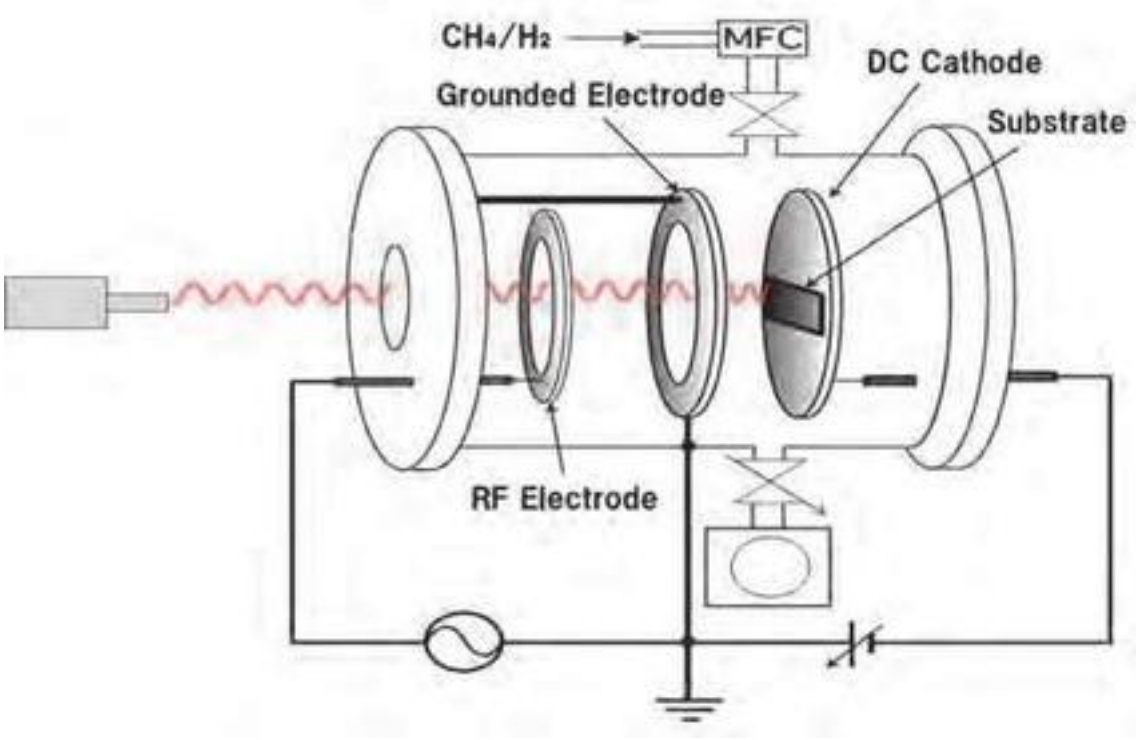

Figure 3.3 Typical experimental setups for a DC/RF discharge plasma chamber. The Plasma is generated between RF and the grounded electrode for RF plasma and between the DC cathode and a grounded electrode for a DC plasma.
Source: *S. Yasuaki, H. Hideto and T. Hideyuki. Growth of Vertically Aligned Carbon Nanotubes by RF-DC Plasma Chemical Vapor Deposition, Carbon Nanotubes-Polymer Nanocomposites. InTech, 2011.*

3.1.4 Nonequilibrium and Equilibrium Plasmas

In plasma processes, a distinction can be made between an equilibrium and a nonequilibrium plasma. In an equilibrium plasma, the kinetic energy gained and temperature are the same among all species present in the plasma (electrons, ions and neutral species). This situation arises at high pressures or when low fields are

applied, particles involved don't have enough space to move far before undergoing a collision, the energy exchange between electrons and ions is dominant that equilibrium is eventually reached rendering this kind of plasma an equilibrium one. In a nonequilibrium plasma, when fields are high or pressures are very low, electrons and some ions will have enough kinetic energy to go farther than the slower neutrals that are not affected by the field. Although electrons and ions are stripped from the neutrals, the overall plasma remains quasi-neutral because the densities of positive and negative carriers are still equal. What is dominant is the high speed gained by electrons due to their light mass compared to that of the ions, and therefore not enough time is available to reach equilibrium making the plasma a nonequilibrium one.

3.2 Plasma Enhanced Chemical Vapor Deposition: PECVD

3.2.1 Plasma Chemistry

Fast electrons in a plasma environment can trigger all chemical processes that can take place. When an electron collides with a gas molecule, the energy loss is gained by the molecule to escalate it from its ground state to an excited state, thus creating radicals with higher reactivity than the precursor molecule. Further reactions can occur with the other molecules and radicals present. Plasma processes thus can be tailored to form new species that are otherwise impossible to produce or only form under harsh conditions. Most of the fundamental reactions that can occur in a plasma are summarized in Table. 3.1 and has been discussed in more details in reference [38] along a variety of other nonequilibrium plasma techniques including glow discharge, corona discharge, silent discharge , RF and microwave discharge.

3.2.2 Advantages of PECVD

One of the main advantages of using PECVD over classical thermal CVD is the low temperatures involved. For example, whereas ordinary CVD to produce high-quality

Table 3.1 Major Chemical Processes in Plasma Reactions

	Electron/Molecular Reactions
Excitation	$e+A_2 \rightarrow A_2^*+e$
Dissociation	$e+A_2 \rightarrow 2A+e$
Attachment	$e+A_2 \rightarrow A_2^-$
Dissociative attachment	$e+A_2 \rightarrow A^-+A$
Ionization	$e+A_2 \rightarrow A_2^++2e$
Dissociative ionization	$e+A_2 \rightarrow A^++A+e$
Recombination	$e+A_2^+ \rightarrow A_2$
Detachment	$e+A_2^- \rightarrow A_2+2e$
	Atomic/Molecular reactions
Penning Dissociation	$M^*+A_2 \rightarrow 2A+M$
Penning Ionization	$M^*+A_2 \rightarrow A_2^++M+e$
Charge transfer	$A^{+/-}+B \rightarrow B^{+/-}+A$
Ion Recombination	$A^-+B^+ \rightarrow AB$
Neutral Recombination	$A+B+M \rightarrow AB+M$
	Decomposition
Electronic	$e+AB \rightarrow A+B+e$
Atomic	$A^*+B_2 \rightarrow AB+B$
	Synthesis
Electronic	$e+A \rightarrow A^*+e$
	$A^*+B \rightarrow AB$
Atomic	$A+B \rightarrow AB$

Source: *P. Chabert and N. Braithwaite. Physics of Radio-Frequency Plasmas. Cambridge University Press, 2011.*

silicon dioxide films requires temperatures in the range of 650-850°C, similar quality films can be deposited at 300-350°C using a plasma-enhanced process [37]. The low deposition temperatures can also inhibit defect formation in the underlying silicon substrate, dopant diffusion and degradation of the metal layers [39]. For diamond synthesis, PECVD also offers the opportunity of getting high quality diamond with different shapes that cannot be produced by any other deposition process.

3.2.3 RF Plasma Parameters

Even though the principles underlying the conditions for plasmas to form are the same among all plasma processes, there are some differences manifested depending on the system used for specific purposes. The main focus in this research effort however are the parameters controlling RF plasma systems since this approach was chosen based on earlier experiments in the group to form polymeric nitrogen by PECVD (discussed in the next chapter) using a radio frequency apparatus built for this purpose. As discussed in the preceding sections, ionization of neutral gases is mainly due to collisions between the charged and neutral particles driven by current and voltage sources in the system. In this regard, an understanding of the power delivered to the system is crucial. The frequencies from the DC to the microwave range are also important since it is through oscillation of the fields due to charged particles that ignite the plasma. The frequency commercially used for PECVD in industry is a 13.56 MHz. This frequency is dictated by treaties among state and federal agencies to avoid interference with telecommunications and military assets. However, a lot of evidence can be found in the literature suggesting better depositions by using different frequencies. Evidence of better deposition rates for silicon using a silane plasma at 70 MHz compared to 13.56 MHz was reported by Howling et al. [40] where a powder-free product can be obtained, indicating the advantages of using higher frequencies for plasma deposition. The gas mixture and the flow rates

are also important. Hydrogen for instance is a key element for diamond deposition from a carbon source like methane [41, 42, 43]. The flow rates of the gases is also taken into consideration and it is generally believed that higher flow rates require more power to produce enough radicals [44]. On the other hand, high flow rates can lead to higher deposition rates that can hinder relaxation of the structure and even sputtering can occur, thus destroying what is being formed. Among other parameters are the charge density of a plasma, temperature, pressure and the plasma reaction time. In fact, there is no general rule for the optimal parameters for successful plasma synthesis because plasma involves a very complex nonequilibrium process with many parameters. Figure. 3.4 demonstrates the effect of some of the parameters in various PECVD processes [45, 46, 47].

3.2.4 Nitrogen in Plasmas

Processes where a nitrogen plasma is used is found in many technological applications, such as the deposition of oxynitrides (SiON, ZrON), silicon nitride and III-V semiconductors (GaN) [48]. Investigating nitrogen plasmas is thus necessary in order to clarify the nature of the different species involved in a nitrogen plasma jet. The most common techniques for such characterizations include mass spectrometry (MS) and optical emission spectroscopy (EOS) as shown in Figure.s. 3.5 and 3.6. Hence, besides measurements of all the parameters discussed in the preceding sections, identification of the active molecular, atomic and radical species are of great importance for a better optimization of the process involved. As an example, Figure. 3.7 is a depiction of an in-situ characterization of the species involved in a RF plasma under the same conditions that will be used as discussed in the following chapter for the synthesis of polymeric nitrogen. When the plasma is on, the mass spectrometer is giving signals attributed to ionized nitrogen atoms generated in the reaction vessel. The ionization energy of nitrogen atoms is of the order of 14.53 eV,

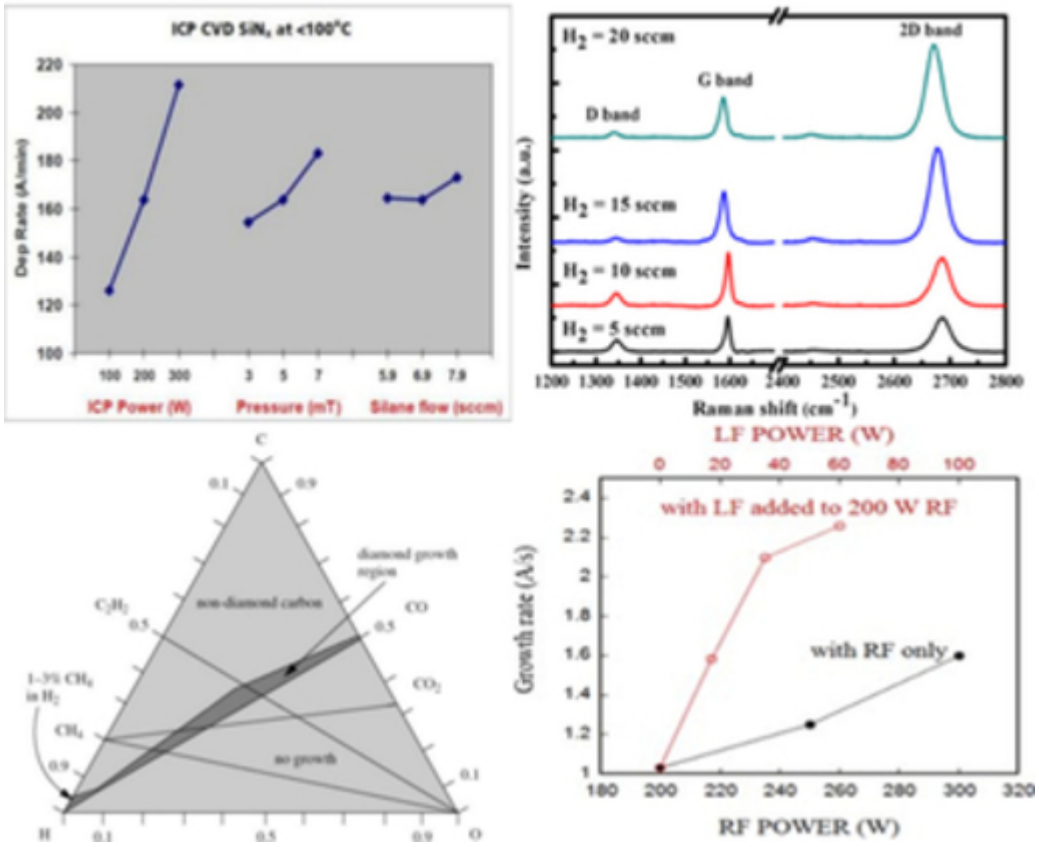

Figure 3.4 Effect of different parameters on plasma synthesis: Top left: Effect of ICP power, pressure and silane flow on the plasma CVD deposition rate of SiN_x. Top right: Raman spectra of PECVD synthesized graphene at 600°C using various H_2 flow rates from 5 to 20 sccm for 5 mins, where the intensity of the deffect D line at 1350 cm^{-1} is a measure of the crystallization quality of graphene. Bottom left: Schematic of the Bachmann atomic C-H-O diagram showing optimal regimes for pollycrystalline diamond from CH_4,CO_2/H_2 gas precursors. Bottom right: TiN deposition rate in an RF plasma and the effect of using a second low frequency plasma simultaneously. Source: *http://www.azom.com/article.aspx?ArticleID=5953*
(accessed December 5, 2014)
& [45],[46],[47].

while dissociation of molecular nitrogen is of the order of 24.3 eV. Hence, for electron energies above 14.53 eV but less than 24.3 eV, N^+ radicals are from an ionization process of atomic nitrogen, while the same radicals form as a result of the dissociation process for energies beyond 24.3 eV (Eq. 3.1. 3.1). While it is beyond the scope of this work to analyze all the nitrogen radicals for a specific plasma process, it needs to be mentioned that there exist a variety of nitrogen species in plasma processes. An extensive spectroscopic investigation was performed by Lofthus and Krupenie [49] on nitrogen species ranging from N_2, N_2^+, N_2^{2+}, N_2^- and N_3. Nitrogen ionization by laser pulses was reported to produce a combination of N_+, N_2^+ and N [50, 51, 52]. Negative nitrogen ions have drawn less attention(THAT in the plasma community. N^- for instance, was reported to have a contribution to the continuum radiation in a nitrogen plasma [53].

$$N + e^- \longrightarrow N^+ + 2e^- \qquad E > 14.53eV \tag{3.1}$$

$$N_2 + e^- \longrightarrow N^+ + N + 2e^- \qquad E > 24.3eV \tag{3.2}$$

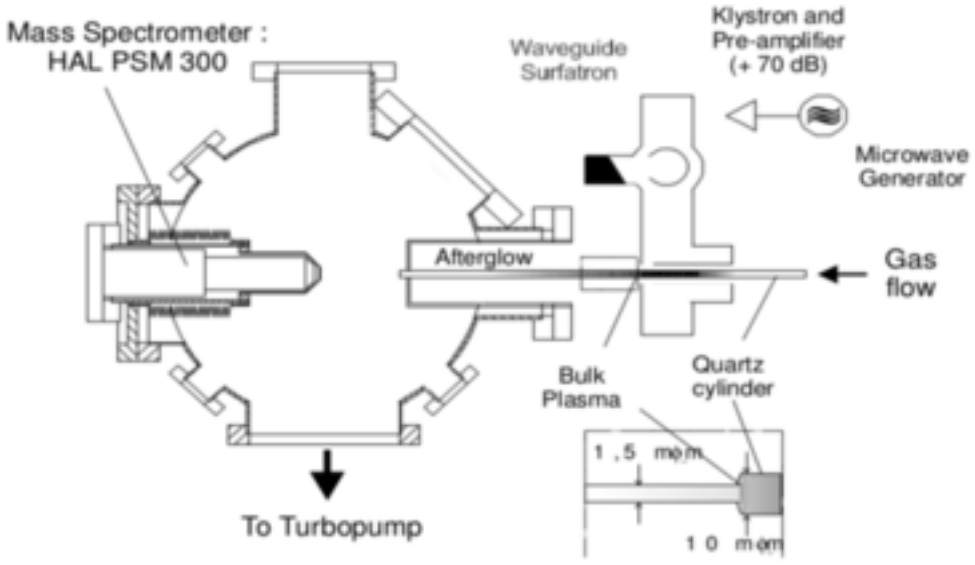

Figure 3.5 Mass Spectrometry set-up for DC and AC discharge experiments. Source: *J. Berndt, J. Winter, and D Douai. Active nitrogen species in the remote plasma of a surface wave sustained discharge. 14. international symposium on plasma chemistry (ISPC-14), with plasma equipment exhibition, Prague (Czech Republic), 1999.*

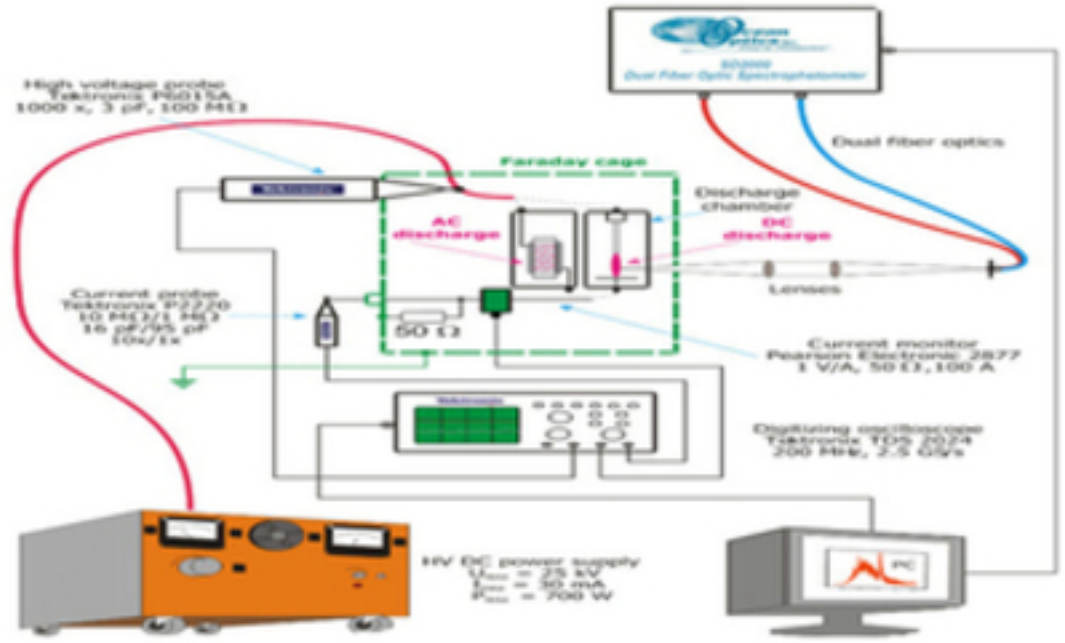

Figure 3.6 Emission spectroscopy set-up for DC and AC discharge experiments. Source: *Z. Machala, M. Janda, K. Hensel, I. Jedlovsk, L. Letinsk, V. Foltin, V. Martiovit, and M. Morvov. Emission spectroscopy of atmospheric pressure plasmas for bio- medical and environmental applications. Journal of Molecular Spectroscopy, 243(2):194-201, 2007. PRAHA2006, The 19th International Conference on High Resolution Molecular Spectroscopy.*

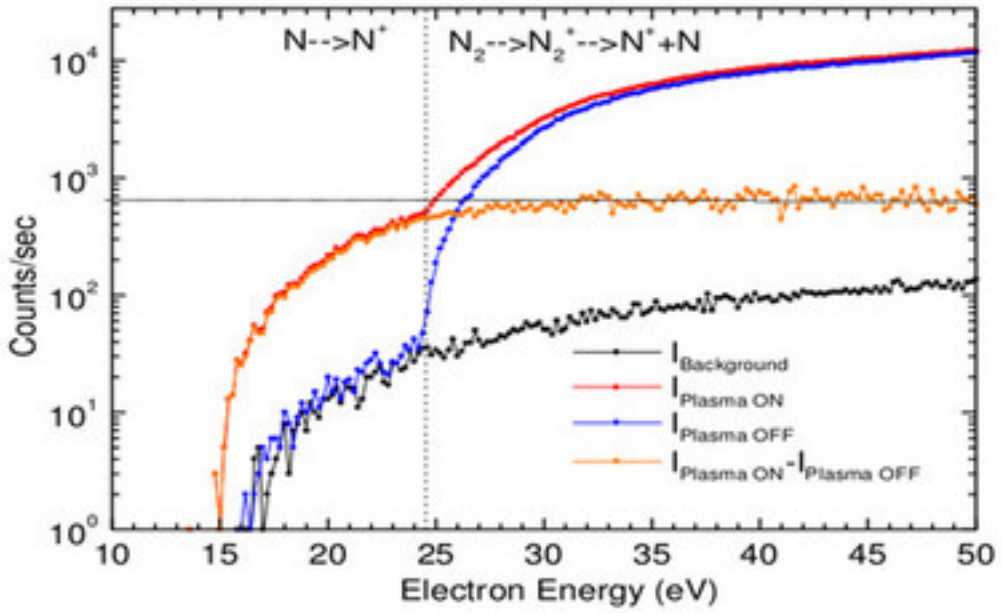

Figure 3.7 m/z=14 Mass spectrometry for a Ar - 50 % N_2 mixture
Source: *J. Berndt, J. Winter, and D Douai. Active nitrogen species in the remote plasma of a surface wave sustained discharge. 14. international symposium on plasma chemistry (ISPC-14), with plasma equipment exhibition, Prague (Czech Republic), 1999.*

CHAPTER 4

POLYMERIC NITROGEN BY PLASMA ENHANCED CHEMICAL VAPOR DEPOSITION

4.1 Diamond Grown near Ambient Pressures: an Inspiration for this Work

Man-made diamond has always been a fascinating material and has a long history that can be traced back to 1880 [54] , but a successful synthesis was not reported until 1950's. The High Temperature- High pressure (HTHP) route was the method of choice since it corresponds to the natural process with which diamond has been formed over billions of years. General Electric is believed to be the first to succeed in making a commercial synthetic diamond. However, HTHP techniques were not the only routes. Plasma enhanced chemical vapor deposition has been successful in synthesizing diamond in the laboratory and in industry . Even more importantly, PECVD methods can provide industry with optical quality diamond disks and thin coating that cannot be obtained from natural diamonds and those from HTHP methods. Another advantage of critical importance for synthesis of an ambient solid form of nitrogen (for example, cg-PN) similar to that of diamond, is the relative ease of PECVD and the ability to stabilize metastable phases on substrates like carbon nanotubes compared to the complications due to scalability and instability on pressure release that arise in HTHP procedures that would be very difficult to mitigate any time soon.

4.2 Rationale for Use of PECVD for PN Synthesis

Since Nitrogen is the element next door to carbon in the periodic table and is the only element that does not exist in a solid form among group- V elements, suggested that it could be synthesized in an extended or polymeric form much as in the carbon structure

of diamond. In view of this and the fact that strong evidence has been obtained from the synthesis of cg-PN by HTHP methods, led to an extensive investigation of PECVD methods for the synthesis of PN phases.

The PECVD method technique involves a dc discharge or radio frequency plasma as discussed in the previous chapter and both have been successful in forming diamond [55, 56, 57, 41]. The metastability related to PN is no different than the metastability of diamond, and the present strategy is to take advantage of the non-equilibrium plasma environment to form PN and then quench it to ambient conditions. Nitrogen precursors suitable for synthesis are nitrogen-rich compounds, such as the azides, ammonia NH_3, and hydrozoic acid HN_3 in a nitrogen-argon carrier gas to a well-chosen substrate. Hydrogen for instance is believed to play an important role for diamond growth by preventing deposition of amorphous carbon which inhibits diamond growth by blocking the nucleation sites. One of the most convincing interpretations of the role of diamond came from Lander and Morrison [42] from Bell Labs in 1966 where it is demonstrated from Low Energy Electron Diffraction (LEED) patterns that hydrogen atoms terminate the dangling bonds normal to the (111) surface planes to give a better stability to the lattice and prevents graphitization. Helium as a carrier on the other hand was crucial for allowing the formation of C_{60} in laser ablation processes. Helium was the cooling carrier that allowed C_{60} deposition from the hot plasma jet in Smalley's revolutionary discovery of this fullerene [58]. The choice of the best gas carrier is a tricky one, what works for the synthesis of one compound does not necessarily work for another compound. To the best of our knowledge, no one has reported a PECVD approach to synthesize PN. In this work, hydrogen or argon has been used as a carrier gas but it could not be determined which works best. As regards the substrate, silicon together with a silicon nitride buffer layer for lattice matching is the substrate of choice for siamond synthesis and deposition. Here, porous silicon was also used as a substrate for the deposition and immobilization

of PN inside its pores, but the results were complicated by surface reactions with the oxide species on the silicon pores during the plasma process. Carbon nanotube sheets or nanopaper, particularly short nanotubes were therefore chosen as substrate for the reasons discussed below.

4.3 Carbon Nanotubes Nanopaper as the Substrate

N_8 chains and N_{24} encapsulation inside carbon nanotubes, shown in Figure.ure 4.1, was proposed by Abou- Rachid et al. [59]. Carbon nanotubes are demonstrated to be ideal hosts to confine the highly metastable PN by providing stability through the hybridization that takes place between the nanotubes and PN conduction bands. Confining PN under ambient conditions is an interesting approach. The relative thermodynamic instability of polymeric nitrogen can be overcome by providing kinetic stability through hybridization by a charge-transfer mechanism and thus the high lattice energy requirement to gain stability and avoid the highly energetic conversion to molecular N_2 . In this work [59], Abou-Rachid et al. also used temperature molecular dynamics to demonstrate the stability of the hybrid Nitrogen-containing compound at ambient conditions. More theoretical evidence of applying nanostructures to confine PN has also been reported [60, 61].

4.4 Sodium and Lithium Azides as Precursors for PN synthesis

Earlier attempts at PN synthesis by PECVD has been made in this research group, from which much has been learnt about the plasma conditions for a PN synthesis. A data-base was created [62, 63] which enabled better control over the PECVD procedure through variations of parameters of gas flow, pressure, power and carrier/precursor combinations. Some of the results of these investigations are summarized in a separate section below where plasma synthesis was conducted without azide precursors. In most of the previous work, molecular nitrogen mixed with argon, hydrogen and ammonia were the precursor gases used. Taking the

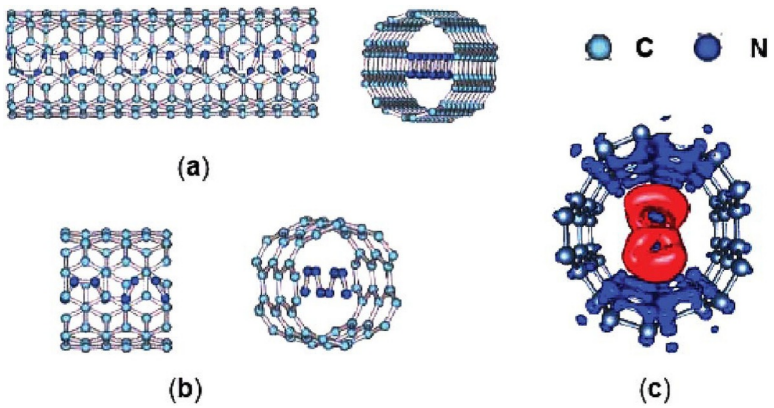

Figure 4.1 Nitrogen clusters stabilized inside single walled carbon nanotubes (SWNTs): (a) N_{24} in (5,5) SWNTs with nine unit cells; (b) N_8 In (5, 5) SWNTs with three unit cells. (c) Electron density of N_8 in (5,5) CNT with three unit cells. Source: *Hakima Abou-Rachid, Anguang Hu, Vladimir Timoshevskii, Yanfeng Song, and Louis-Simon Lussier. Nanoscale high energetic materials: A polymeric nitrogen chain N_8 confined inside a carbon nanotube. Phys. Rev. Lett., 100:196401, May 2008.*

cue from HTHP studies on sodium azides [32, 64] and theoretical work on lithium and heavier metal azides [65, 66], which indicated the formation pressures for PN can be substantially reduced by using these solid nitrogen rich compounds, detailed experiments have been performed using both sodium and lithium azide as precursors together with nitrogen as the precursor gas mixed with the carrier gases such as argon and hydrogen to modify the RF plasmas used

Photolysis of compressed sodium azide as a pathway to nitrogen has also been studied by Suhithi et al. [67]. A controversial N_7^- or Cl_2N_6 (where Cl is coming from the NaCl used as the pressure medium) were suggested as the possible candidate species from infrared and Raman data. Nevertheless, the N_7^- chain-like-structure was shown to be unstable at ambient conditions.

In the present work, the use of sodium azide turned out to be an important turning-point in the PECVD synthesis of PN in spite of the complication from sodium, it has shed a lot of light on the feasibility of the process which enabled further plasma experiments on other azides to validate this approach. Plasma synthesis

was thus also carried out with lithium azide LiN_3 where the same PN phases were obtained. Unfortunately, nitrogen-rich ammonium azide with the interesting N_4H_4 ($NH_4^+N_3^-$) formula, which is more than 90% nitrogen totally disappears from the plasma system under vacuum because of its volatility as it dissociates into ammonia NH_3 and hydrozoic acid HN_3.

4.5 Experimental Details

Short multiwall carbon nanotubes were obtained from Cheap Tubes Inc. (Brattleboro, VT). The as-received nanotubes used were about 400-600 nm in length and were intentionally chosen to be short in length to allow for the nitrogen oligomer to form inside the tubes. The carbon nanotubes were mixed with sodium dodecyl sulfate (SDS) surfactant followed by horn sonication and a vacuum filtration process to produce free-standing nanopaper substrates (Figure. 4.2). Longer multiwall carbon nanotubes and single wall carbon nanotubes were also studied, but as expected short carbon nanotubes proved to be more efficient substrate for the plasma synthesis of PN. Distinction is made throughout the dissertation whenever short carbon nanotubes are not used. The multiwall nanotube nanopaper is an entangled mesh and is very porous, the horn sonication (Fisher scientific Sonicator 3000) process that takes about 45 minutes allow for a a uniform dispersion of carbon nanotubes, the suspension is then filtrated with a membrane filter (10 LC-millipore MITEX) to finally produce the nanopaper that is cut into 2×2 cm^2 pieces used as substrates in PECVD. The nanopaper substrates are then dipped in sodium azide in a pH=4 aqueous buffer solution overnight and then dried in air for a few hours. For plasma runs with lithium azide, lithium azide solution (Sigma Aldrich, 20 wt. % in water) was used. The carbon nanotubes were dipped in lithium azide and the solution was evaporated at 100 °c to obtain carbon nanotube nanopapers coated with lithum azide. Some experiments were also run on pure lithium azide powders. Lithium azide is more sensitive to

plasma conditions than sodium azide. Deflagrations in the plasma reaction tube take place in the first 5 minutes when using plasma powers higher than 50 watts for short periods and even at lower powers for extended periods of time. The schematic of the plasma apparatus used for the synthesis is depicted in Figure. 4.3. Nitrogen or ammonia and argon or hydrogen were fed into the quartz tube through needle valve flow meters allowing control of the flow rate of the gas precursors. An adjustable radio frequency generator delivering up to 500 Watts was attached to an adjustable impedance matching box. The real plasma power was thus the difference between the incident power from the generator and the reflected power. This provided flexibility to choose from a large range of powers. Tuning this power to between 65 Watts and 70 Watts was crucial for getting the best possible synthesis and deposition. Throughout this study, a power range of 65-100 Watts was maintained. Gas mixtures of 50% nitrogen and 50% argon were introduced into the deposition chamber where a quartz boat was used to hold a 2×2 cm^2 nanopaper substrate. A vacuum pump was used to evacuate the deposition chamber to pressures below 1 Torr. When pressures above 1 Torr were used, there was no evidence of PN formation. Flow rates of 10-15 sccm (standard cubic centimeters per minute) were maintained for each gas. Optimal PN synthesis by Raman and ATR-FTIR spectra, on the nanopaper substrates was not obtained at higher flow rates. The deposition time was typically between 2 hours and 3 hours, and at least 2 hours was required for optimal synthesis in the case of sodium azide (few plasma runs were conducted in 30 minutes especially for lithium azide and a few runs up to six hours for sodium azide).The temperature of the substrate throughout each experiment was monitored using a thermocouple even though external heat was not applied to the reactor. Temperatures of the plasma jet were in the range of 200-300 °c and were monitored by using a thermocouple floating inside the quartz tube. As the temperature of the substrate is not necessarily the temperature of the plasma, a thermal infrared imaging camera (FLIR E65 Thermal

Imager) was used to monitor the temperature of the substrates used (Figure. 4.4). In the case of sodium azide, up to 200°c at 65 Watts was obtained by intrinsic plasma heating and had to be maintained below 300 °c for sodium azide to avoid extensive sodium azide decomposition during the plasma deposition process. In the case of lithium azide, lower temperatures of up to 110 °c were maintained.

Figure 4.2 Carbon nanotube nanoper obtained after the sonication- filtration procedure.

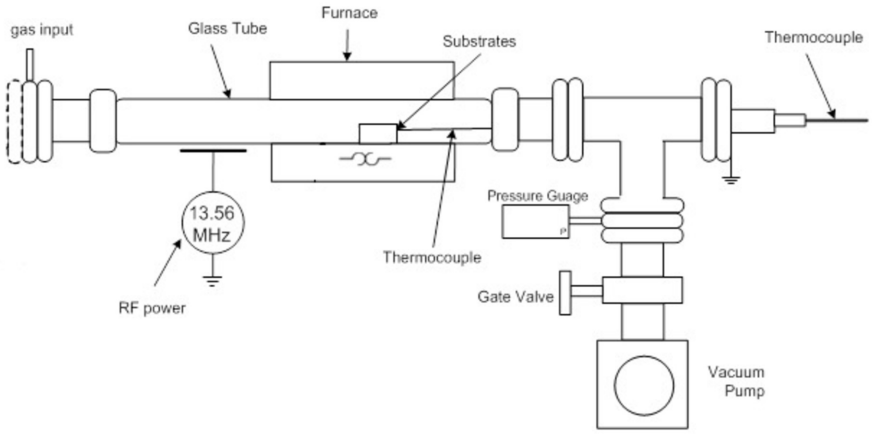

Figure 4.3 Schematic of the plasma system used in this study.

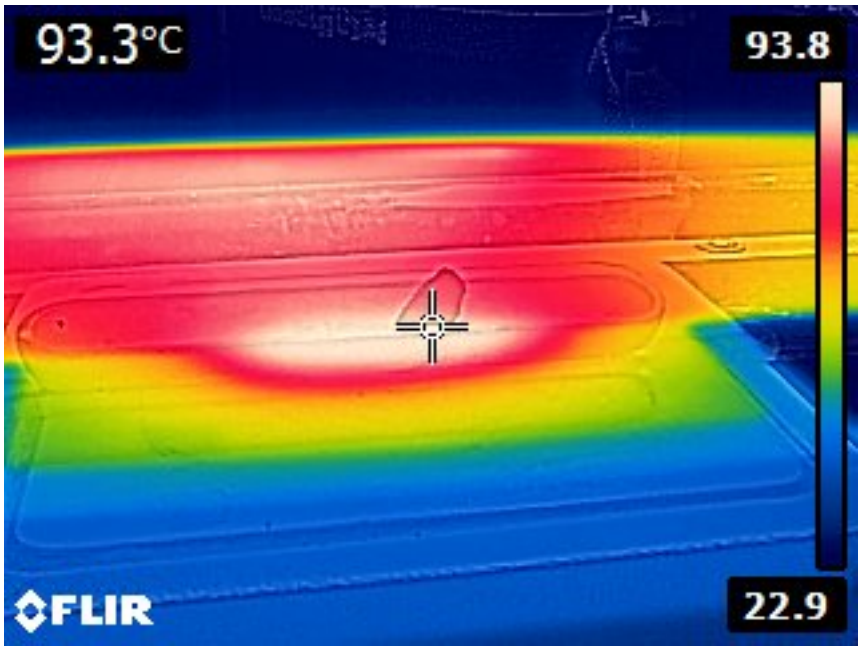

Figure 4.4 Infrared thermal image showing temperatures of the substrate and the surrounding plasma.

Fourier transform infrared (FTIR) spectroscopy was conducted using a Magna Model 560 instrument (Nicolet Instrument Corporation, Madison, WI, USA) attached to an attenuated total reflectance (ATR) accessory with a single reflection ZnSe crystal (Pike Technologies, Madison, WI, USA). The reacted and pristine carbon nanotube nanopaper samples were directly sampled in a range from 600 cm^{1-} to 4000 cm^{1-} at a spectral resolution of 4 cm^{1-} . Raman spectroscopy was carried out with a Thermo Scientific DXR micro-spectrometer (Thermo Scientific, Waltham, MA, USA) with 532-nm laser excitation at a spectral resolution of 2 cm^{1-} and a spatial resolution of $10\mu m$. Scanning electron micro- scope (SEM) images were obtained with a VP-1530 Carl Zeiss LEO (Carl Zeiss, Peabody, MA, USA) field-emission SEM. The samples were mounted on aluminum stubs using double-sided carbon tape. X-ray powder diffraction was carried out on a Philips PW3040-X-Ray diffractometer with Cu Kα radiation.

4.6 Results and Discussion

4.6.1 Plasma Polymerization Strategy

For the related synthesis of diamond by plasma techniques, carbon precursors, such as methane and hydrogen, are usually introduced into the deposition chamber to allow diamond growth on a silicon substrate at temperatures above 800°C. In the current work, carbon nanotubes provided the ideal substrate for the reasons discussed above, whereas azide nuclei from sodium azide, and gases such as nitrogen, ammonia and hydrogen or argon provided the precursor/gas carrier fois made r PN synthesis. The building block toward N_5^+ synthesis [3] was to get N_5^+ by letting hydrozoic acid HN_3 react wih a N_2F^+ salt. A mechanism that starts the polymerization can be as follows:d) and e) are for .

$$\left[|\overline{\underline{N}} - N \equiv N|\right]^- + N^+ \rightarrow [< N = N = N = N >]^0 \tag{4.1}$$

$$[< N = N = N = N >]^0 + N^+ \rightarrow [< N = N = N = N = N >]^+ \tag{4.2}$$

Ionized atoms or molecules from molecular nitrogen or ammonia can involve N_2^+, N^+, N_2^- and N^-. The polymerization, driven by structural and electronic stability, can go beyond N_5^+ as follows:

$$[< N = N = N = N = N >]^+ + N^- \rightarrow [< N = N = N = N = N = N >]^0 \tag{4.3}$$

$$[< N = N = N = N = N = N >]^0 + N^+ \rightarrow [< N = N = N = N = N = N = N >]^+ \tag{4.4}$$

Polymerization to PN can take place by alternating between different nitrogen species as needed to transition to a more favorable structure by feeding ionized nitrogen from the plasma jet. The nonequilibrium environment of the plasma facilitates quenching to occur on the surfaces and the insides of the carbon nanotubes. The mechanism does not have to start with the azide anion but can also initiate with N_2^+ and N_2^- changing

to N_4. This strategy of designing the plasma synthesis to allow polymerization can be thus summarized as follows : the target azide anion has weaker bonding compared to molecular nitrogen and carries a negative charge that can be attracted to a positive ion, this is provided by the nitrogen plasma jet that is mainly composed of N^+ and N_2^+ radicals to allow longer chains to form, any positively formed entity will either attract to another azide anion from the substrate or a negative plasma radical formed by combination. Linear chains of nitrogen clusters or oligomers are thus allowed to grow. This is consistent with the fact that lines above 2000 cm^{-1} in the FTIR and Raman spectra were observed in the plasma synthesized samples as discussed below, which is unlikely for most closed or benzen-like structures.

4.6.2 Plasma-reacted Sodium Azide: Raman and ATR-FTIR Results

Sodium Azide- Raman- and Infrared-active Vibrational Modes Sodium azide NaN_3 is an ionic crystal where the azide N_3^- anions are arranged in layers perpendicular to sodium atom planes. In its high temperature β-phase, NaN_3 has three Raman active modes: the symmetric stretch ν_1 at 1360 cm^{-1}, the azide ion librational mode at 120 cm^{-1} and the Raman- active first overtone of the IR active bending ν_2 mode of the azide ion at 1268 cm^{-1}. The other IR active modes beside ν_2 at 638 cm^{-1} are the antisymmetric stretching mode of the azide ion, ν_3 at 2100 cm^{-1} and three lattice modes at 174, 195 and 243 cm^{-1} [68].

Raman Spectroscopy of the Plasma Synthesized Phase Transformation of sodium azide throughout different runs can be clearly seen from different Raman spectra before and after the plasma synthesis (Figure.s. 4.5 and 4.6). Raman lines due to PN phases produced from sodium azide without a substrate as the starting material and from sodium azide deposited on single and multiwall carbon nanotube sheets can been seen in Figure. 4.5. After plasma reaction, a new low frequency line at 210 cm^{-1} is observed. Other lines in this region on single wall carbon nanotubes (SWNTs)

substrates are due to SWNT radial breating modes, together with an intense line at 637 cm^{-1} when short multiwall carbon nanotubes (MWNTs) are used. Moreover, there is a line at 719 cm^{-1}, a narrow line at 1080 cm^{-1} with varying intensities, a low intensity broad band comprising of peaks at 1985, 2050 and 2095 cm^{-1} and finally a sharp line at 2325 cm^{-1}, probably from trapped N_2. In addition, the line near 1247 cm^{-1} corresponding to the Raman-active $2\nu_2$ overtone of the azide ion, which appears to be broadened due to splitting, is observed in all spectra in Figure.s. 4.5 and 4.6. The key result is that the Raman spectra of the plasma reacted samples show that introducing sodium azide by dipping on short MWNTs brought about a huge enhancement on plasma reaction of the 637 cm^{-1} line. Shortened MWNTs in particular thus appear to function as hosts to confine the highly metastable PN clusters and oligomers, as also shown recently by the stabilization of a catalytically active N_8^- PN cluster, synthesized by electrochemical cyclic voltammetry [17] on MWNTs.

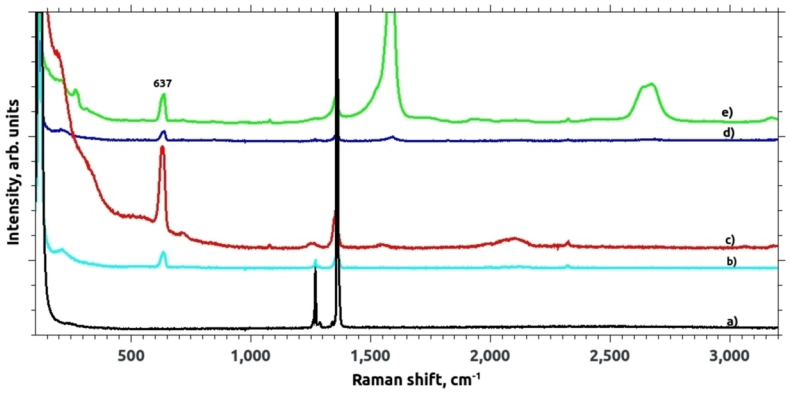

Figure 4.5 Raman spectra showing the effect of the nanotube substrate on PN synthesis. Spectra a) and b) are taken from pure NaN_3 without carbon nanotubes before and after plasma reaction, respectively; Spectrum c) is from plasma reacted NaN_3-deposited on short MWNTs; spectrum d) is from plasma-reacted NaN_3-deposited on long MWNTs; and spectrum e) is from NaN_3-deposited on long SWNTs.

Appearance of colors, as dark gray, black , purple and pink on sodium azide which is originally of a translucent white color, or coloration of the NaN_3-dipped

carbon nanotubes to purple, violet, blue, pink and yellow after plasma reaction indicated a transition of the sodium azide precursor to a new PN phase. Appearance of colors that are sometimes different from run to run have been observed in many plasma processes when nitrogen is involved especially in the presence of alkali metals, the long-lived yellow afterglow on top of the substrate for plasma powers above 80 watts indicates a good interaction between nitrogen radicals from the plasma jet and the sample. However, yellow colors formed on top of the substrate do not give any new features in Raman scattering and it is believed that areas where this coloration occurs consist of disordered phases. It is also likely that the transformation to semiconducting phases of nitrogen is responsible for narrowing the original large band gap in sodium azide and thus the gray to black colors exhibited by the plasma reacted samples. Eremets and co-workers [32], in their high pressure experiments on sodium azide, reported detailed changes that take place in the Raman spectrum at pressures of 15-17 GPa due to the formation of a so-called Phase I that is characterized by an emerging of a line at 638 cm^{-1}, attributed by them to activation of ν_2-IR active lattice modes in NaN_3 into six Raman peaks in the 200-400 cm^{-1} region in Phase I which persist as sharp intense lines up to 86 GPa with intensities much higher than that of the 638 cm^{-1} line. In addition, lines below 2000 cm^{-1} also appear in Phase I which have not been previously observed in any azide.

In the plasma-reacted samples however a medium intensity feature around 2000 cm^{-1} is seen together with a line at 210 cm^{-1} in the librational modes region. More evidence of the 600 cm^{-1} mode can also be seen in the work of Popov [64] on both sodium azide and molecular nitrogen under pressure and high temperature. It is therefore believed that for the plasma synthesized samples, the 638 cm^{-1} line, which is degenerate with the N_3^- ν_2 mode, is the signature of the three-fold coordinated N-N single bonds in cg-PN under ambient conditions.

It has to be emphasized that high pressure vibrational modes observed in high pressure- high temperature studies cannot cannot be compared with lines at ambient conditions in the present plasma synthesis experiments. For example, the high pressure cg-PN structure has a Raman signature around 800 cm^{-1} that extrapolates to about 600 cm^{-1} at ambient pressure. Moreover, the unidentified Phase II structure in reference [32] of the compressed sodium azide at the pressure range between 54 GPa and 160 GPa is mainly characterized by Raman modes at 795 cm^{-1} and 1145 cm^{-1} and a broadening at 580 cm^{-1}, such features disappear on pressure increase which could signal a new transformation to an amorphous phase. The lines in the present synthesis can be compared to features of Phase II seen at 719 cm^{-1} and 1080 cm^{-1} extrapolated to ambient pressures which tends to lower frequencies by about 100-200 cm^{-1}. Such extrapolation needs not to shift all frequencies by the same amount. For instance, In Barbee's calculation [5] of the vibrational modes of cg-PN, the zero-pressure Raman-active modes at 600 cm^{-1} and 900 cm^{-1} should go to about 840 cm^{-1} and 1200 cm^{-1} at 100 GPa . Phase II in reference [64], claimed to be the cg-PN, also reveals lines about 800 and 1200 cm $^{-1}$ along with an unknown line at 270 cm^{-1} which develops by heating. The broad feature at 2000 cm^{-1} consisting of multiple peaks at 1985, 2050 and 2095 cm $^{-1}$ develops in all spectra and it is a clear indication of the delocalization of double bonds in sodium azide and apparently formation of new bonds. In other words, appearance of a band in Raman that is physically only IR active is a total breach in the symmetry of the original sample and a severe weakening of the double bond is undoubtedly taking place as the assymetric stretch cannot be Raman active. Another evidence of the 1080 cm^{-1} can be clearly seen in phase VI in Reference [32] which is a low pressure phase obtained from the decompression procedure. Some nitrogen radicals from the plasma jet and during transition in sodium azide might lead to formation of nitrogen molecules that get

trapped within the new structures and are responsible for the appearance of the nitrogen molecular vibron at 2325 cm^{-1}.

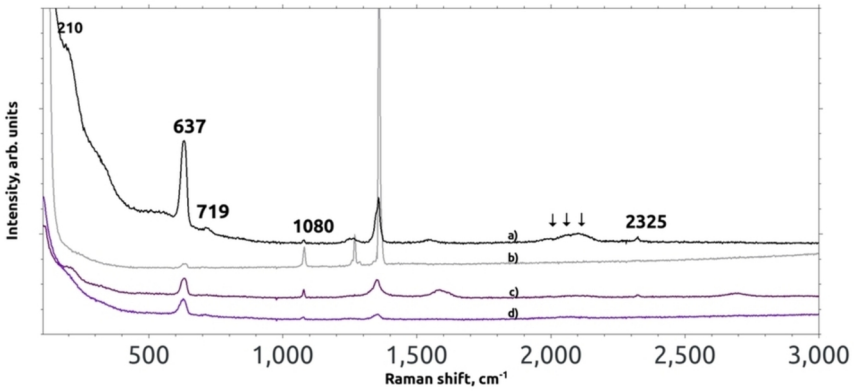

Figure 4.6 Raman spectra of NaN_3-dipped short multiwall carbon nanotube after plasma taken from selected colored regions. a) black, b) white, c) purple, d) violet. Raman lines that only appear after the plasma synthesis are shown and the arrows on top of the broad line at the 2000 cm^{-1} region indicate positions of peaks at 1985, 2050 and 2095 cm^{-1}. The intensity of the 637 cm^{-1} is different in different areas of a particular sample. Note that the the 637 cm^{-1} line intensity is higher when the intensity of the line at 1080 cm^{-1} is lower and vice versa.

Effect of Sodium Azide precursor concentration on PN Formation It was observed taht sodium azide aqueous solutions between 2M and 4M gave the best results based on the same relative intensiy of the 637 cm^{-1} (see Figure. 4.7). The use of saturated solutions however did not bring any improvement.

Changes in the Raman Spectrum of Carbon Nanotubes after Plasma Reaction Figure.ure 4.8 shows the Raman spectra of pristine MWNT nanopaper, the NaN_3-dipped nanopaper, and the plasma-reacted nanopaper. The D (deffect) and G (graphitic) lines of pristine MWNT-nanopaper are located at 1343 cm^{-1} and 1576 cm^{-1}, respectively, with a ratio of $\frac{I_d}{I_g} = 0.90$. The D and G frequencies shifted slightly in the sample dipped in sodium azide to 1348 cm^{-1} and 1586 cm^{-1} , respectively, and their ratio changed by a small amount to 1.06. However, after the plasma synthesis, the nanopapers exhibited a dramatic change. Although the D and

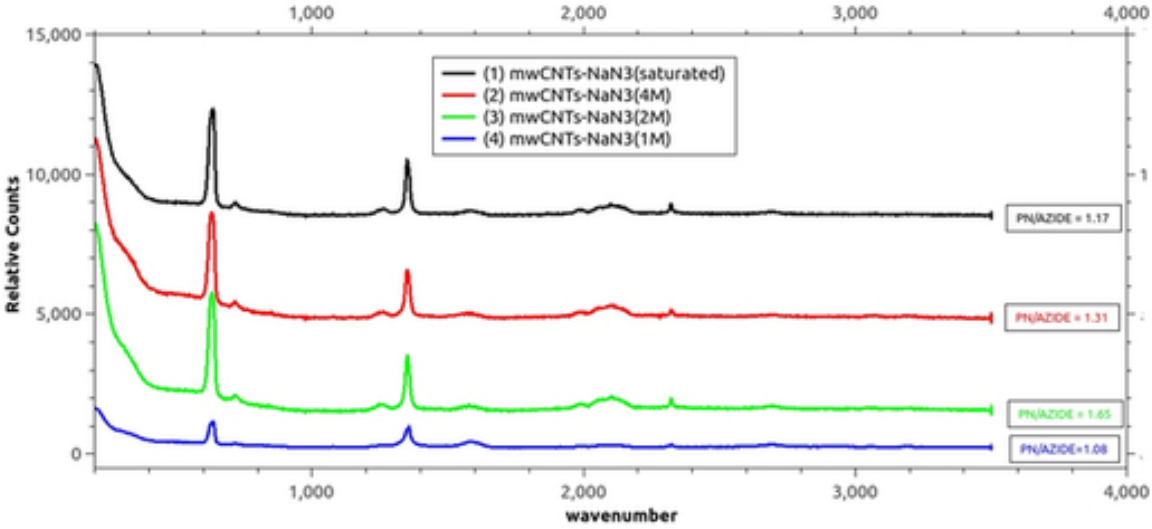

Figure 4.7 Raman spectra of plasma-reacted NaN_3 as a function of azide concentration in dipping solutions used to deposit the azide precursor. The ratio of the intensity of the 637 cm^{-1} line assigned to the new PN phase and the intensity of ν_1 line due to unreacted NaN_3 is a measure of the effectiveness of plasma reaction indicated in the figure (see inserts on the right)

G bands did not exhibit a noticeable shift in frequency relative to the dipped sample (D at 1350 cm^{-1} and G remained at 1586 cm^{-1}), the increase of the D mode intensity was huge, resulting in a rise of the I_d/I_g to 1.40. This can be clearly attributed to functionalization of the nanotube sidewalls due to the plasma induced PN formation and concomitant creation of defects. The sharp lines, at 116 cm^{-1} and 1360 cm^{-1}, can be assigned, respectively, to the librational and symmetric stretching vibrations of the linear azide ion in unreacted sodium azide on the substrate.

ATR-FTIR Spectroscopy of the Plasma Synthesized Phase A typical FTIR-ATR spectrum of the NaN_3-dipped short multiwall carbon nanotube is depicted in Figure. 4.9, the two lines at 1428 cm^{-1} and 880 cm^{-1} are reproducible after each plasma run and are believed to be relevant to the new phase formed after the plasma synthesis. In the IR data taken for polmeric phases of nitrogen synthesized by high pressures routes, bands at 853 and 1428 cm^{-1} were reported in the work of popov [33]. The line at 1428 is accompanied by a doublet about 1300 and this doublet has been

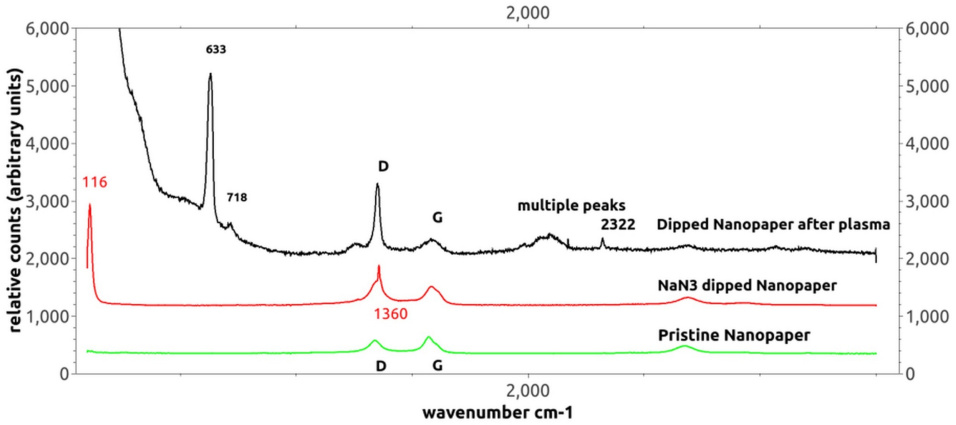

Figure 4.8 Raman spectra of the (a) pristine multiwall CNTs, NaN 3 -dipped CNTs, and plasma synthesized of the NaN 3 -dipped CNTs.

seen in some plasma runs especially when the sample is exposed to heating. A similar doublet is more pronounced in the work with lithium azide. Molecular nitrogen under pressures up to 170 GPa was investigated by Gornachov et. al[69], a broad band about 1450 cm^{-1} and a less intense band around 900 cm^{-1} carried the IR signature for the synthesized high-pressure phase along a weak and broad 640 cm^{-1} Raman line. As was discussed for Raman spectra, a direct comparison between the plasma synthesized samples and the high-pressure data cannot be done without some extrapolation to ambient condition, the similarities are however striking. Goncharov et. al[69] argued that single-bond structures (cg, black phosphorus, chain-like etc which are close in energies can coexist as a mixture in the synthesized phase and misleadingly make it look amorphous in IR and Raman. It is also hihgly likely that combination of Raman and IR spectra don't necessarily stem from the same structure. Only the 840 cm^{-1} Raman line was reported for cg in the work of Eremets et al. [4, 30] among four predicted optical branches. No FTIR data was possible in the extreme conditions of the synthesis to shed some more light. However, it is likely that the spectrum of the cubic-gauche structure will be dominated by the Raman line around 600 cm^{-1} (about

800 at high pressure) and a weaker line at 900 (about 1200 at high pressure) while the two IR-Raman active modes are very weak. A computational investigation is carried out in the chapter 5 to help clarify the controversy of the vibrational frequencies of the cg-PN phase.

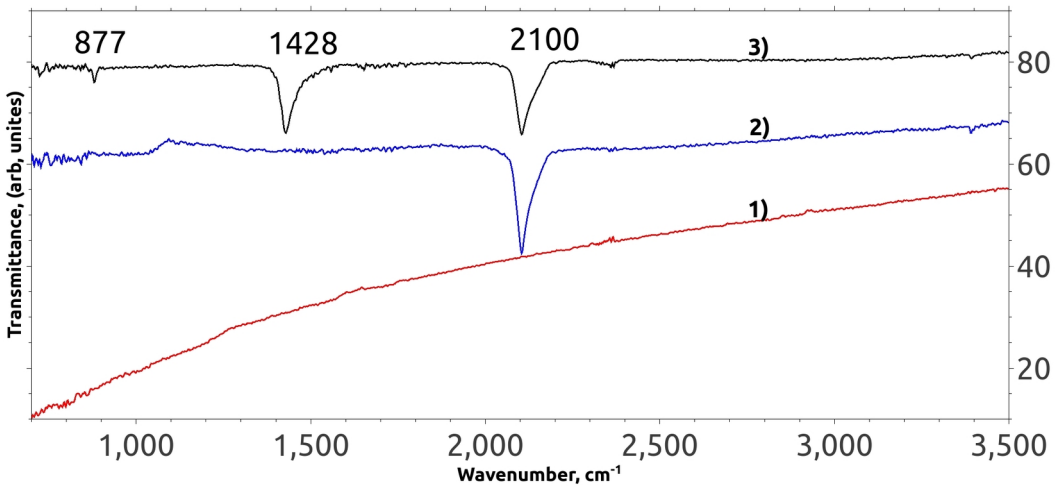

Figure 4.9 ATR-FTIR spectrum of NaN_3 dipped multiwall carbon nanotube before and after plasma

4.6.3 Plasma-reacted Lithium Azide: Raman and ATR-FTIR Results

Lithium Azide- Raman- and Infrared-active Vibrational Modes ν_1, ν_2 and ν_3 for lithium azide are at 1373, 635 and 2090 cm^{-1} respectively. The Raman-active librational mode around 120 cm^{-1} undergoes a shift to a higher frequency depending on temperature and exhibits a splitting into two peaks at 131 and 153 cm^{-1} respectively [70]. The IR-active librational modes are reported to be at 218 and 470 cm^{-1} [68].

Raman spectroscopy of the Plasma Synthesized Phase Depending on a variety of plasma conditions, the plasma synthesized samples from lithium azide bear red regions or are totally black, the change of color from the originally white lithium azide actually appears in the first few minutes of the plasma procedure. Lithium

azide dramatic transformation can be clearly seen in the Raman spectrum shown in Figure. 4.10. The new lines that appear in Raman are the same lines observed for sodium azide which gives a stronger proof that polymerization of nitrogen to the new phase is truly coming from the N_3^- azide anion. However, the plasma process that produced this Raman spectrum comes from lithium azide alone without any carbon nanotubes involvement. Raman features were not as clear while carbon nanotubes were used as can be seen in Figure. 4.11. In addition, some Raman lines appear in the librational region along the 1080 cm^{-1} line that is still the most intense line. Some explanations can however be drawn from the behavior of lithium azide in the presence of carbon nanotubes. The fact that the 1080 cm^{-1} line, that was also seen for sodium azide in the plasma procedure and the HTHP procedures, appears under specific circumstances especially when the 637 cm^{-1} is still weak and it is lost as the 637 cm^{-1} becomes prominent is a clear indication that a phase well characterized by the 1080 cm^{-1} is an intermediate phase in the polymerization process that nitrogen goes through before reaching the ultimate phase that bears the 637 cm^{-1} signature. The coexistence of both phases is the general case especially with sodium azide and the intensity ratios can be a measure of the abundance of each phase in the sample.

The origins of Raman frequencies that appear on lithium azide in the low-frequency region are not clearly understood, it might be due to a splitting of the IR active librational modes of lithium azide due to a symmetry reduction during the phase transition. In some plasma samples where the line about 600 cm^{-1} is still weak, more lines appear in the 100-500 region, a comparison can be made with Phase I in reference[32] obtained with sodium azide at pressures up to 19 GPa while the sample still didn't reach Phase II and also in Phase IV which is in the lowest pressure phase obtained upon decompression.

In the course of this investigation, it is clear that lithium azide presents a challenge during the plasma synthesis due to its lower temperature decomposition

and its sensitivity to the plasma bombardment. Also, encapsulating lithium azide by dipping didn't show a clear evidence of the nonmolecular phas synthesized from multiwall carbon nanotubes that are dipped with sodium azide. Only by exposing lithium azide to the plasma jet that it was possible to get the phase obtained from sodium azide. Lithium azide still has a relatively stronger nitrogen bond compared to other azides due to the smaller radius of lithium [71], its embodiment inside or on the sides of carbon nanotube sheets turns out to be more of a hindrance to the process unlike sodium azide where carbon nanotubes eventually helped in the polymerization process. Still, polymerization from LiN_3 tend to be faster and more efficient and runs where all lithium azide can be transformed is easier to obtain than from sodium azide (spectrum 3) in Figure. 4.13 and Figure. 4.12).

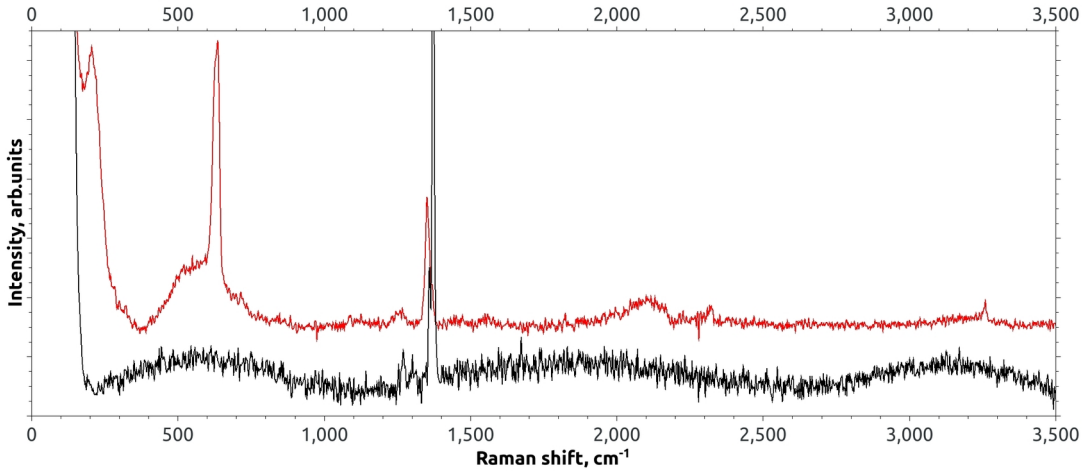

Figure 4.10 Raman spectra of LiN_3 powder before and after the plasma synthesis: The top spectrum from the plasma reaction is changed dramatically and exhibits a strong Raman line about 635 cm^{-1}, 210 cm^{-1} and 2325 cm^{-1} along with the broad line at the 2000 cm^{-1} region. Interestingly, these plasma Raman lines are the same as the ones observed with sodium azide. A mysterious line about 3260 cm^{-1} is also clear in this spectrum, its origins are not clear.

ATR-FTIR Spectroscopy of the Plasma Synthesized Phase As was the case with Raman spectra. ATR-FTIR of the plasma samples (Figure.s. 4.12 and 4.13)

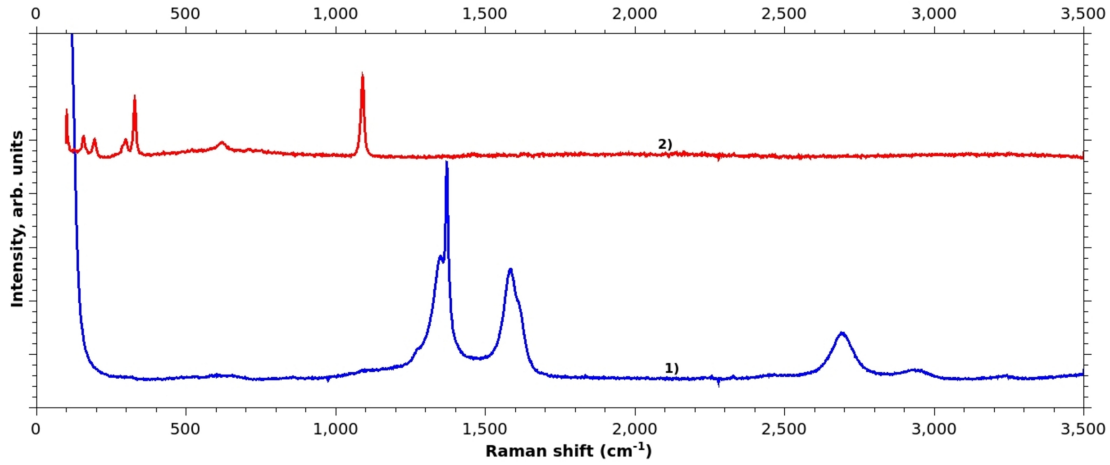

Figure 4.11 Raman spectra of 1) LiN_3-mwCNTs before and 2) after the plasma synthesis. Carbon nanotube Raman lines are not seen in spectrum 2) as the Raman laser beam was focused on areas of the sample that show signs of a nitrogen phase. The 1080 cm^{-1} line is prominent while the 600 cm^{-1} line is still weak, more lines appear in the librational region.

with LiN_3 that are in the same range as with NaN_3 can be clearly seen in the lines around 1400 and 900 cm^{-1} making the azide anion N_3^- the sole entity responsible for what happens as a consequence of this plasma treatment and valdiating the argument that polymerization could initiate from N_3^- regardless of the alkali metal in use.

4.6.4 X-Ray from Plasma Reacted Sodium and Lithium Azide

To gain more insight about the nature of the structure synthesized, X-Ray diffraction was carried out on the samples from sodium azide. In Figure. 4.14), spectra from sodium azide before and after the plasma synthesis are presented. While the plasma sample is still overwhelmed by the sodium azide X-ray diffraction patterns, some changes can be clearly seen. The only X-ray diffraction patterns that have ever been taken for polymeric nitrogen cubic gauche structure are the ones found in the work of Eremets and co-workers [4, 30] and only from molecular nitrogen as a starting material, the first reflection angles taken by the Synchrotron radiation at $\lambda \sim 0.41$ $\mathring{A}$

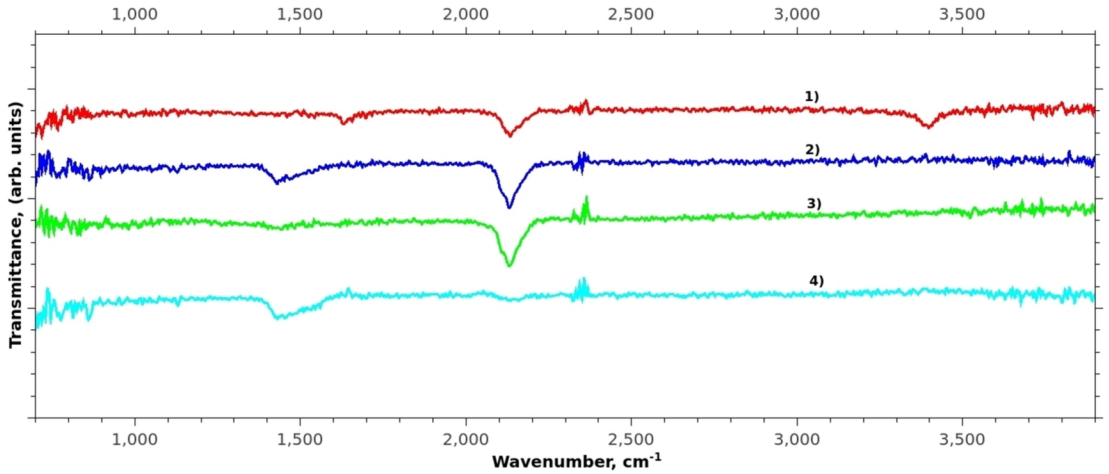

Figure 4.12 ATR-FTIR spectra of LiN_3 powder before and after the plasma synthesis : 1) Pristine LiN_3 powder sample before plasma synthesis, 2),3) and 4) same sample after plasma reaction . In Spectrum 2) lithium azide and the new phase coexist as the the 1428 cm^{-1} line is emerging, in spectrum 3) only left over lithium azide is detected while in spectrum 4) all lithium azide disappeared and only the 1400 cm^{-1} and 860 cm^{-1} lines can be noticed.

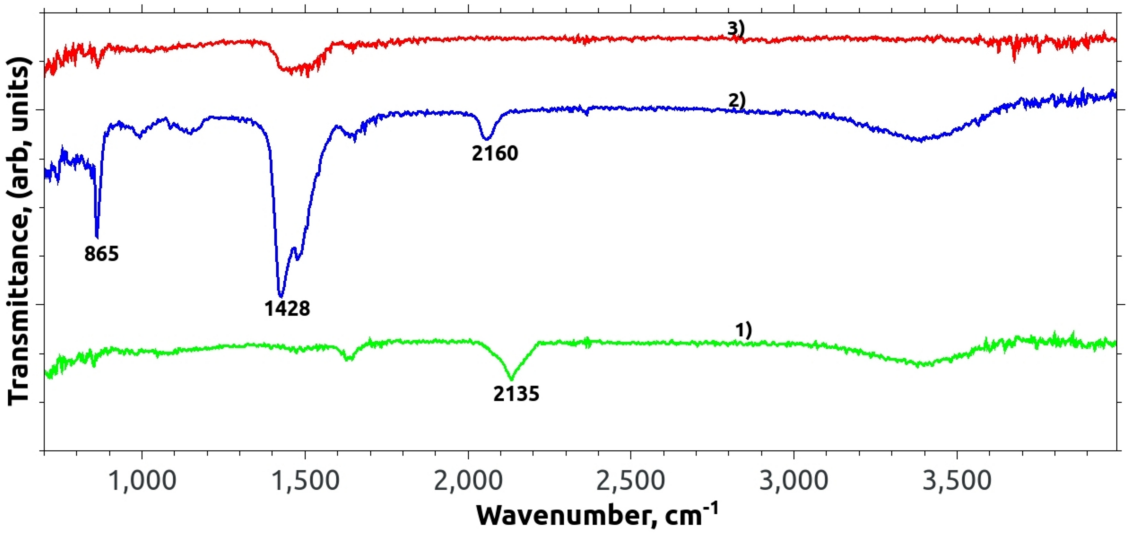

Figure 4.13 FTIR-ATR spectra of LiN_3 powder : 1) before plasma synthesis, 2) and 3) after synthesis in 30 mins and 3 hours plasma runs respectively. ν_3 of lithium azide is shifted from 2060cm^{-1} to 2135 cm^{-1} after annealing the pristine sample.The line at 1428 cm^{-1} has a shoulder at 1481 cm^{-1} on the 30 mins plasma sample, both lines become a broad band in the 3 hours plasma where ν_2 also disappears as all lithium azide was transformed.

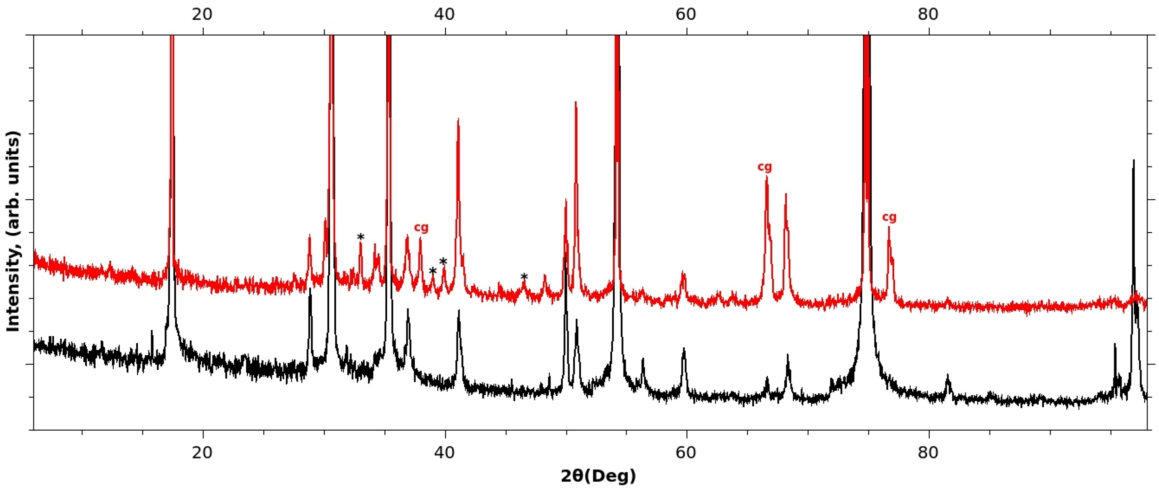

Figure 4.14 X-ray powder diffraction patterns taken using CuKα radiation for NaN_3 powder Before (Black) plasma reaction and after (Red) plasma reaction. The lines indicated by 'cg' at 37, 66 and 77 2θ degrees correspond closely to the (110), (211) and (220) reflections of the cubic gauche structure of polymeric nitrogen reported by Eremets and co-workers [4, 30]. The strong lines correspond to unreacted NaN_3 and the weak lines are probably either from sodium nitride or an unidentified phase.

are estimated to be at about 37, 54, 66 and 77 for 2θ values with a Cuα radiation. Interestingly, except for the third reflection which might be overshadowed by the strong sodium azide reflection around 54 degrees, the other three lines are very clear. Single crystals of polymeric nitrogen in the cubic gauche [30] added a great value to the understanding of this unique structure and new reflections at higher angles were obtained and confirmed to be relevant to the cubic gauche. The reflections relative intensities were also different from a different arrangement in the diamond anvil cell. X-ray data from lithium azide are shown in Figure. 4.15. The intense lines still correspond to the unreacted lithium azide and are depicted with red asterisks, there were speculations that lithium nitride might be forming in this plasma procedure as lithium nitride also has a strong Raman signature about 600 cm^{-1} along a weak line about 1000 cm^{-1} [72]. X-ray data doesn't support this claim because even some X-ray lines that might correspond to lithium nitride are seen in the plasma samples (marked

with delta symbol), some of the strong reflections in lithium nitride are totally absent (Table. 4.1). Some other lines including the strongest line in the green spectrum is still unindintified and might correspond to one of the synthesized phases. As discussed in the preceding sections, new nitrogen phases were obtained from sodium azide as a starting material and all the gathered Raman and Infrared data point to a single-bond structure. No X-ray data was taken to identify the structure of the these phases. Metastability of the polymeric nitrogen cubic gauche was suggested [5] and it is very likely that for this plasma synthesis this structure is the most likely candidate for the plasma synthesized phase at least from Raman and X-ray spectra. It is also possible that the cubic gauche structure is still contaminated with some intermediate phases.

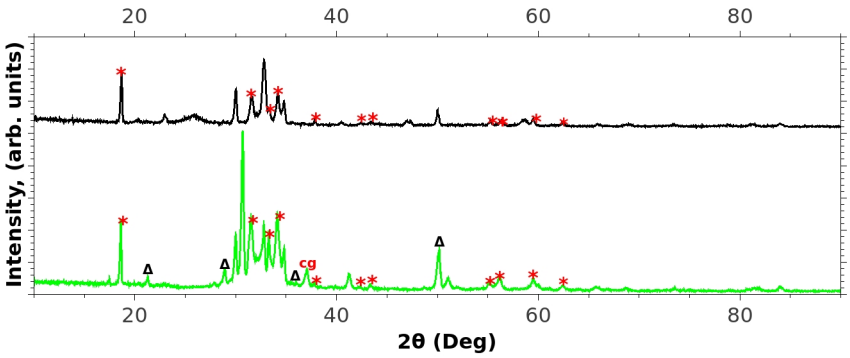

Figure 4.15 X-ray powder diffraction patterns taken using CuKα radiation for LiN_3 powder of two plasma reactions. Diffractions in red are for the sample with a strong Raman line about 637 cm^{-1} while the diffractions in black are for the sample with a moderate line at 637 cm^{-1}. Red asterisks correspond to the original diffraction angles of unreacted lithium azide as found in the litterature [73]. The lines with delta symbol were speculated to originate from lithium nitride Li_3N. However, many diffraction patterns with strong intensities are absent. It is likely that the line (marked cg) about 2θ=37 degrees corresponds to the cubic gauche structure of polymeric nitrogen.

Table 4.1 X-Ray Diffraction Patterns of Li_3N as Retrieved from JADE MDI Database

2θ	Intensity	(h k l)
22.783	100.0	(1 1 0)
28.036	100.0	(1 1 1)
32.533	70.0	(2 0 0)
36.040	70.0	
46.534	70.0	(2 2 0)
49.785	100.0	(2 2 1)
55.294	100.0	(3 1 1)
57.953	50.0	(2 2 2)
70.783	100.0	(4 1 0)
76.082	50.0	
78.304	20.0	
79.867	50.0	(4 2 1)
93.217	90.0	(5 1 1)
98.082	90.0	(5 2 0)

4.6.5 Temperature Programmed Desorption

The temperature programmed desorption (TPD) results from both sodium and lithium azide before and after the plasma reaction are shown in Figure.s 4.16 and 4.17. A dramatic change took place in the plasma sample from lithium azide powder as a new strong peak emerges about 400 °C indicating the formation of new entity completely different than lithium azide which only shows the natural peak about 225 °c due to lithium azide dissociation. The new nitrogen phase thus seems to have a dissociation temperature around 400 °C. This feature can be indistinguishable for the sodium azide sample after plasma reaction as pristine sodium azide also dissociates at this temperature range. However, The shape of the peaks before and after plasma reaction in the TPD analysis is very different. It is possible that the sharp strong signal of the plasma sample is mainly dominated by the new phase rather than the remnant unreacted sodium azide. No melting or dissociation temperature was reported for any polynitrogen except the $N_5^+AsF_6^-$ salt. In fact, speculations stil rise about the validity of X-Ray and Raman data obtained by Eremets [4, 30] as assumption were made about the stress that relaxes in the sample after heating.

Popov [33] argues that this assumption is unreasonable without any estimation of the melting point of the sample.

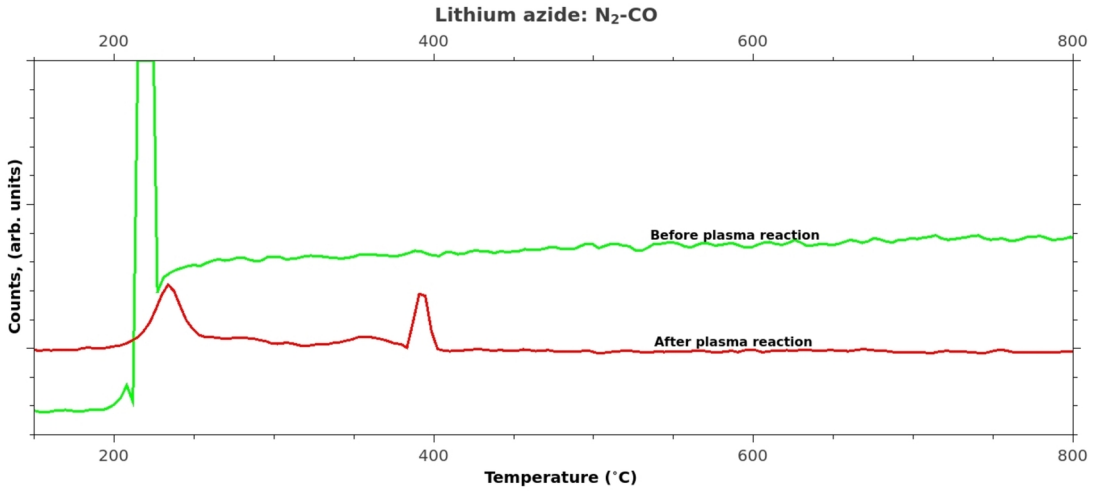

Figure 4.16 Temperature programmed desorption spectra of lithium azide before and after plasma reaction.

4.6.6 SEM Micrographs

SEM micrographs of the pristine nanopaper, and the sodium azide dipped carbon nanotubes before and after plasma synthesis are shown in Figure.s 4.18, 4.19 and 4.20, respectively. The fibrous features of multiwall carbon nanotubes are clearly seen from the pristine nanopaper. The plasma-reacted sample, on the other hand, looks cloudy and coated, and somehow more stretched. Although no damage appears to have taken place, this cloudy, coated appearance reinforces the belief that the PN structures form first on the outside surfaces and then inside the nanotubes. High-resolution TEM is planned to confirm this hypothesis. The dramatic increase in the defect D-mode Raman intensity provides strong support for this assumption as pointed out by the I_D/I_G ratio analysis.

SEM micrographs of lithium azide were taken without carbon nanotubes before and after plasma and are depicted in Figure.s 4.21 and 4.22 . Some needle-like

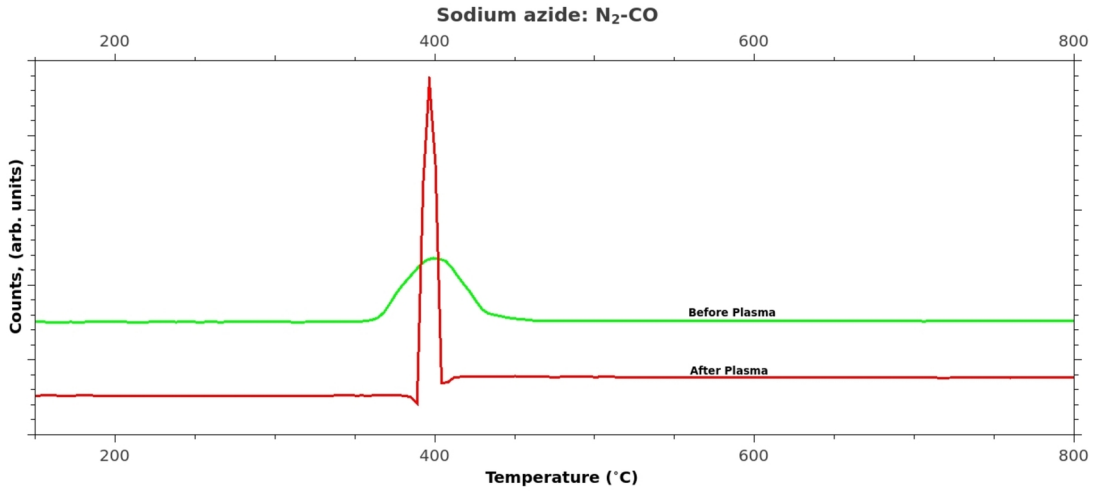

Figure 4.17 Temperature programmed desorption spectra of sodium azide before and after plasma reaction.

features appear on the pristine lithium azide powder before plasma reaction. In some runs where carbon nanotubes were used with lithium azide, some white needles appeared on carbon nanotubes after the plasma treatment. This was not observed before plasma. It appears that a good embodiement of lithium azide in carbon nanotubes takes place effectively, but the high sensitivity of lithium azide to the plasma bombardemet has the effect of getting this needle-features out of the nanopaper substrate. After plasma, the morphology of the sample is different and the synthesized phase seems to point in a uniforme specific direction.

EDX analysis (Figure. 4.23) was carried out to gain some quantitative insight about the elements present in the sample. Quantities of up to 17% of nitrogen were detected, part of which probably comes from remnants of sodium azide in the samples detected in the Raman spectra. Besides carbon and sodium, oxygen from the air present in the plasma reactor and nickel from the catalyst used in carbon nanotube synthesis, were detected.

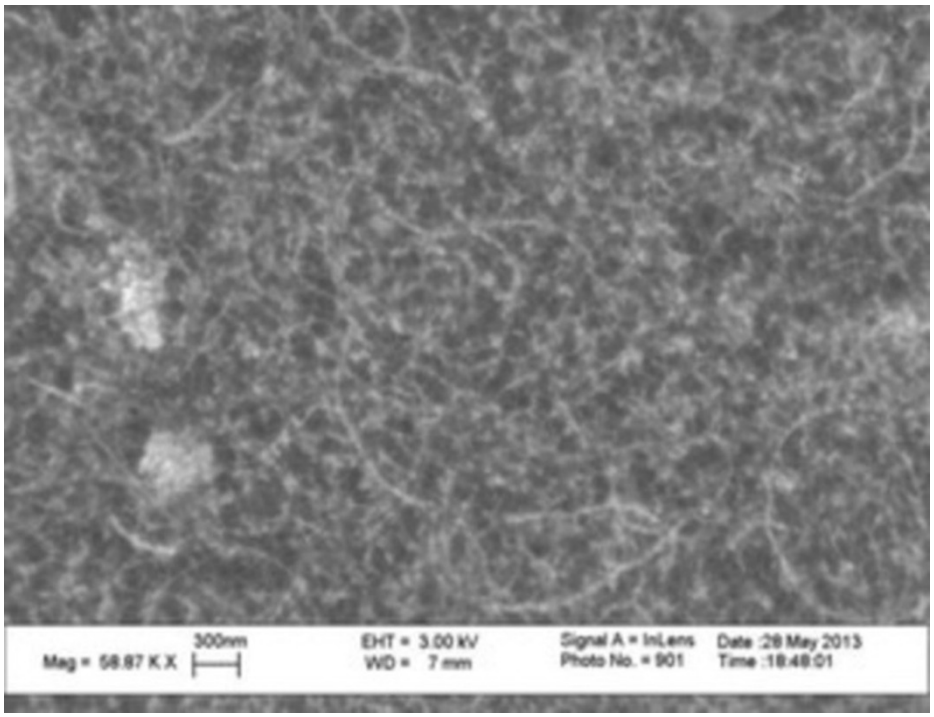

Figure 4.18 SEM image of the short multiwall carbon nanotubes used in this study.

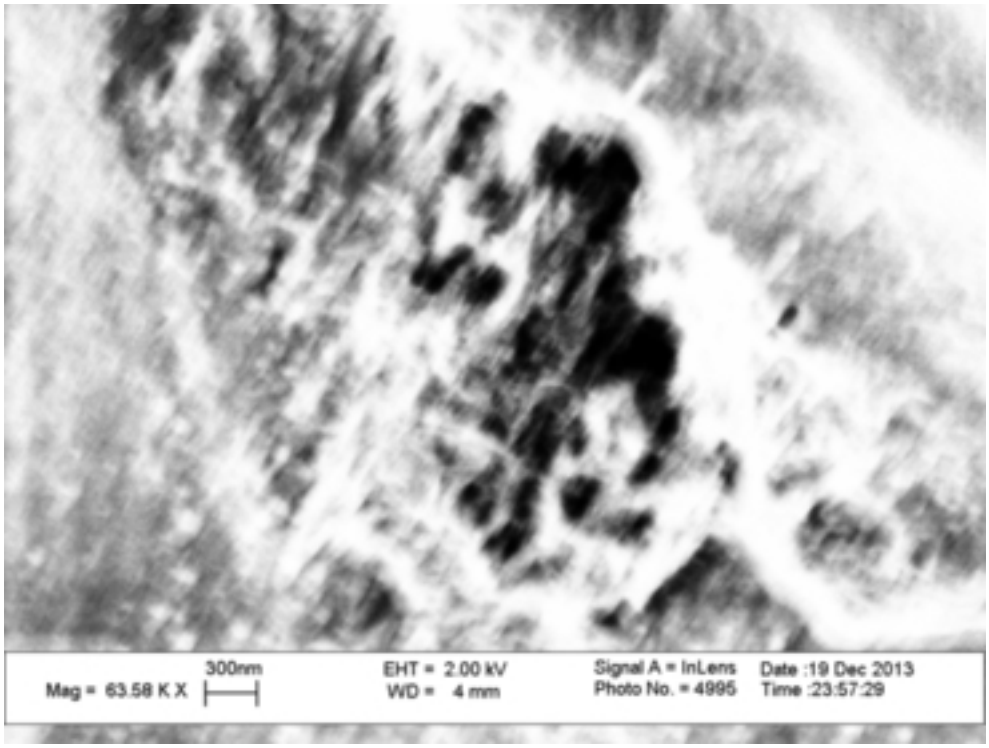

Figure 4.19 NaN_3 dipped Multiwall carbon nanotubes SEM.

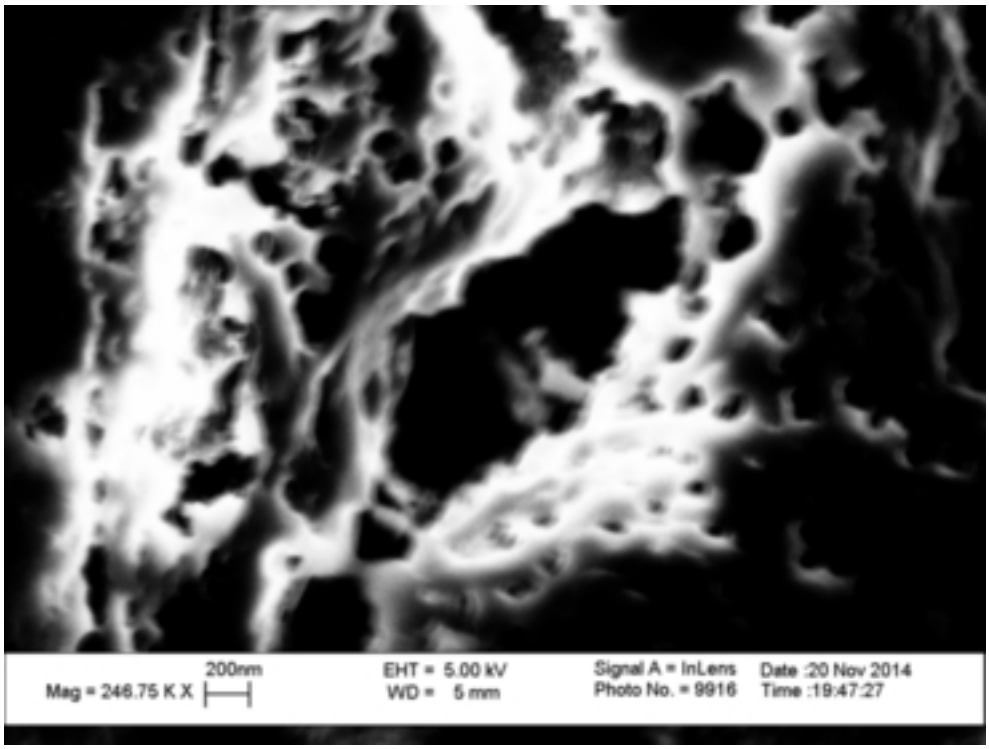

Figure 4.20 SEM image of NaN_3 dipped multiwall carbon nanotubes after plasma.

4.7 Plasma Synthesis of PN Without Azide Precursors

As mentioned earlier, tuning the plasma to the right conditions to synthesize the polymeric nitrogen clusters does not specifically require precursor nuclei like the azides. Gaseous ammonia or nitrogen in argon or hydrogen can be used to synthesize PN on nanopaper substrates, but the amounts produced have been typically small. The goal to synthesize PN without relying on azides is of great importance; therefore, optimizing a more environmentally friendly approach beyond the hazards of a chemical compound like sodium azide is of very important. Figure.ure 4.24 shows a high-resolution TEM of the sample prepared using nitrogen as the precursor was reported earlier in our group [63]. The TEM micrograph shows that the inside of the carbon nanotube is filled with a possibly nitrogen material based on electron energy loss spectroscopy. Although a reliable selected area electron diffraction could not be obtained, it was suggested that the solid structure formed is amorphous.

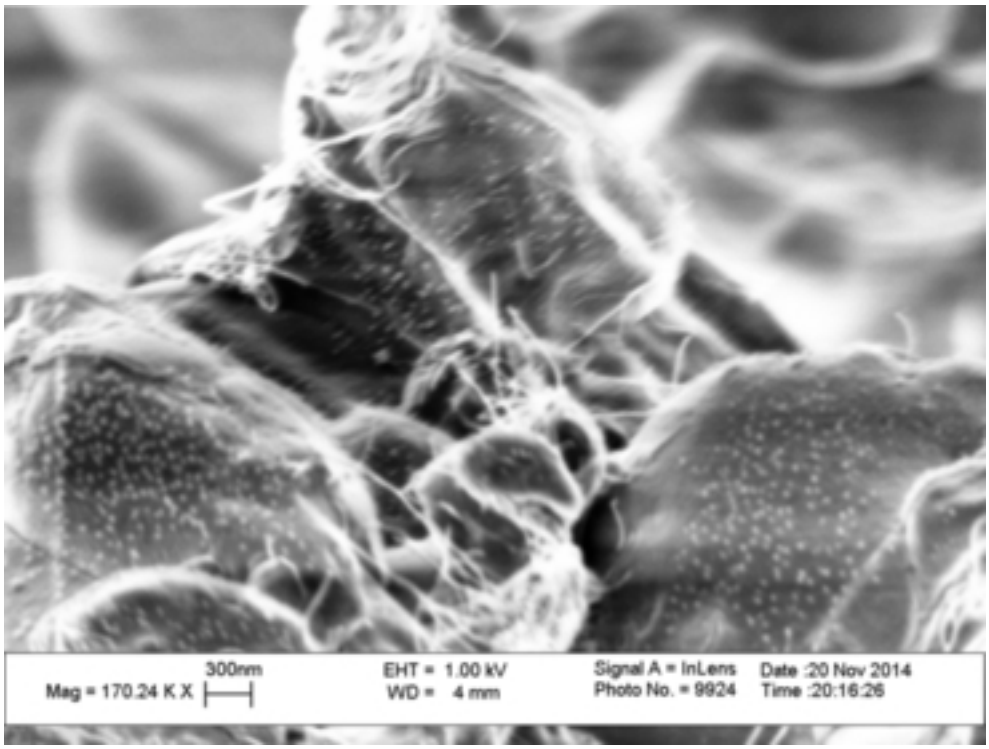

Figure 4.21 SEM image of LiN_3 powder.

This project was started with the idea of using plasma to synthesize polymeric nitrogen only from nitrogen gas precursors and without implementing azides. A SEM micrograph of carbon naotubes after plasma reaction using only molecular nitrogen and argon under plasma conditions of 65 watts is depicted in Figure. 4.25, spherical structures about 100 nm in diameter seem to form and are connected between carbon nanotubes, the carbon nanotubes connecting these particles look very stretched. No noticeable features were obtained from Raman and Infrared analysis of these samples. However, it is possible that the structure is truly amorphous with no Raman nor infrared activity. From the plasma experiments using azides as seeds to initiate polymerization, it was noticed that nitrogen plasma reacts more efficiently because of the alkali metals involved with azides. It will be interesting to explore a polymeric nitrogen synthesis route without azides but in the presence of an alkali metal that can play the role of a catalyst at the same time avoiding to form any nitrides.

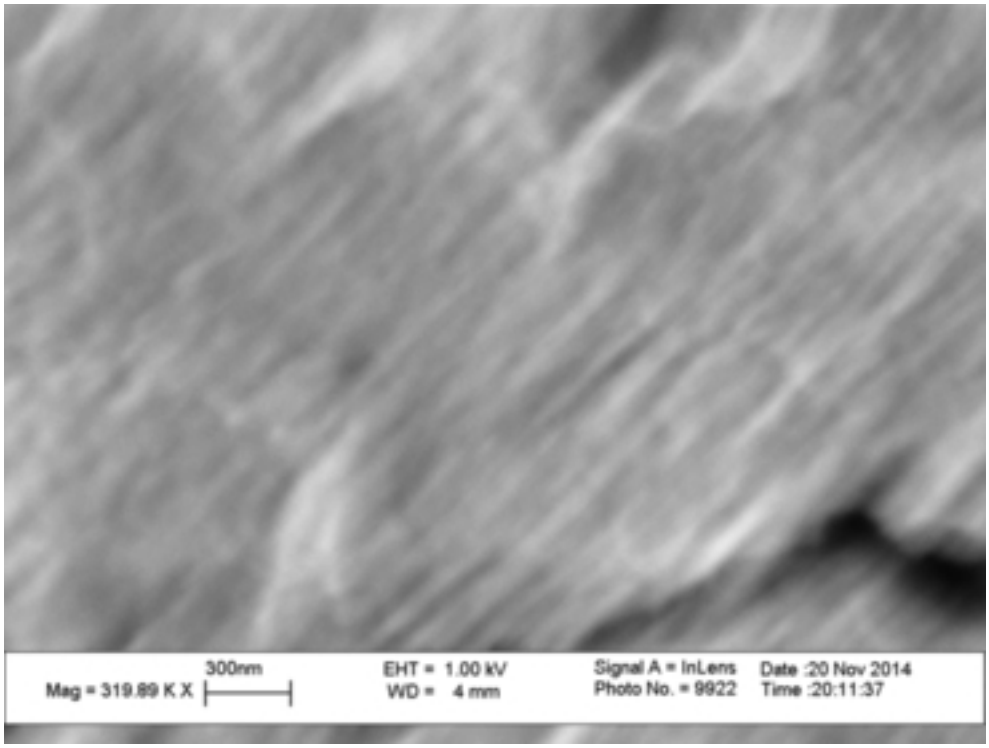

Figure 4.22 SEM image of LiN_3 after plasma.

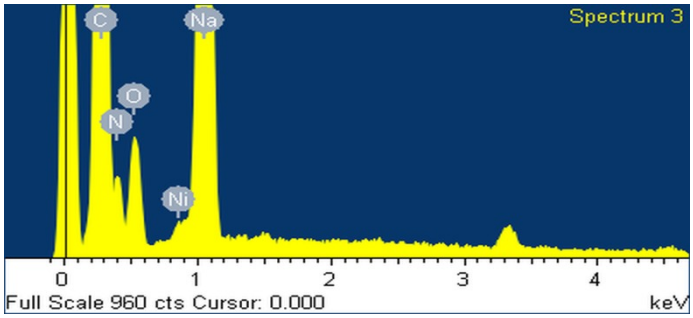

Figure 4.23 Elemental EDX analysis of a plasma-synthesized PN sample.

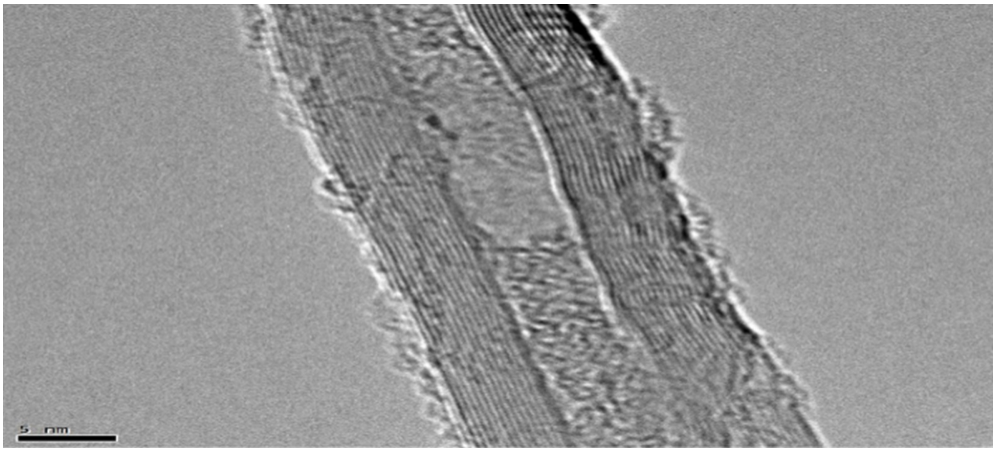

Figure 4.24 High-resolution TEM image of a PN/multiwall carbon nanotubes sample deposited under relatively low-RF plasma power of 65 W.
Source: *C. Wu. Plasma-Enhanced Chemical Vapor Deposition Synthesis of Stable Polymeric Nitrogen. Ph-d Thesis, New Jersey Institute of Technology, 2012.*

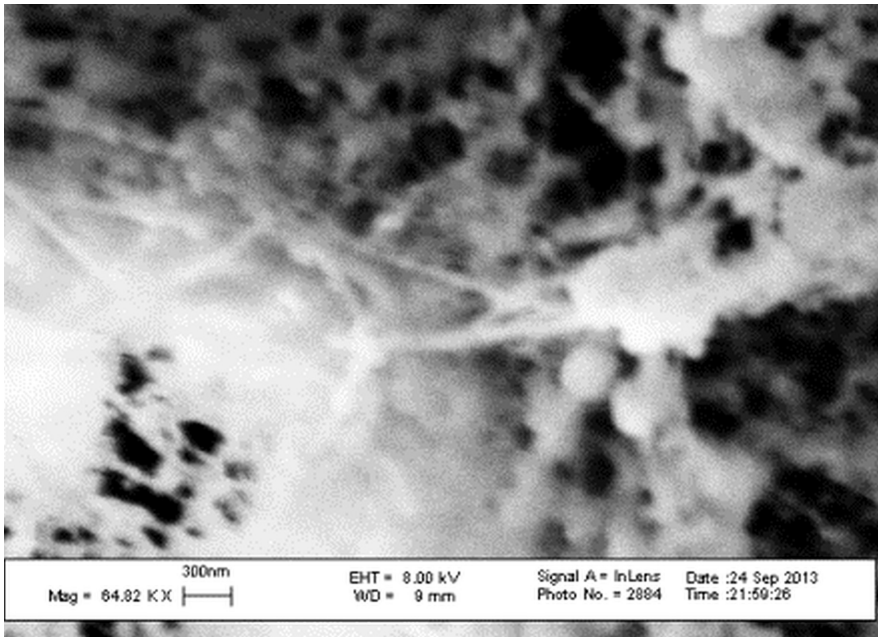

Figure 4.25 SEM image of a PN/multiwall carbon nanotubes sample prepared under the same conditions of the azide precursors.

CHAPTER 5

POLYMERIC NITROGEN: COMPUTATIONAL INVESTIGATION

5.1 Cg-PN by First Principle Calculations

5.1.1 Raman and Infrared Clues of the Phase Change to cg-PN

One year after the cg-PN was revealed as a potential structure that should exist as a metastable entity, Barbee [5] reported his calculations of the Raman and infrared active modes of the cubic gauche PN as a function of pressure using the linear response method LR [74, 75]. It was this pioneering work that helped the identification of the structure synthesized in 2004. The molecular nitrogen Raman frequency at relatively higher frequencies depending on pressure (2300- 2500 cm^{-1}) disappears in the HTHP procedure to give rise the the cg-PN Raman line about 840 cm^{-1} which was in good agreement with Barbee's predictions. Here, a general description of this phase is made: The cg-PN structure has four atoms per unit cell. Therefore, 3N-3=9 zone-center optical modes should either be Raman active, IR active or both. A summary of all the modes and their activity is depicted in Figure. 2.6. For pressures below 100GPa:

- A frequency somewhere between 600 and 800 cm^{-1}, depending on pressure,is Raman active.
- A frequency somewhere between 900 and 1200 cm^{-1} , depending on pressure, is Raman active.
- A frequency somewhere between 800 and 900 cm^{-1} , depending on pressure, is Raman and infrared active.
- A frequency somewhere between 1200 and 1400 cm^{-1} , depending on pressure, is Raman and infrared active.

The plasma synthesis revealed the most interesting line at 637 cm^{-1} from both sodium and lithium azide and the X-ray diffraction pattern reflections of cg-PN also emerged in the plasma synthesized sample. A theoretical investigation of the cg-PN at zero pressure is thus needed to better understand this interesting structure.

5.1.2 Computational Details

Most of the investigations, experimental and theoretical, about polymeric nitrogen in the cubic gauche structure were conducted under high pressure. But its metastability at ambient conditions has always been suggested. As discussed in the preceding chapter, cubic gauche nitrogen is one of the most likely structures of the plasma synthesized phase implemented in the course of this work. In this chapter, this structure will be discussed in more details and results of first-principle calculations regarding its structure and vibrational modes analysis will be discussed. Plane-wave pseudopotential density functional theory formalism as implemented in Quantum Espresso [76] was used. The lattice parameter and internal coordinates of the cg-PN were taken from the literature [5, 14, 16] to initiate a reasonable geometry optimization of the structure at zero pressure. Density functional theory [77, 78] as implemented in Quantum Espresso [76] was carried out in the general gradient density approximation (GGA)[79] with Perdew-Burke-Ernzerhof (PBE) functionals [80]. Even though ultrasoft potentials were used with the premise that they require less energy cutoffs, a high energy cutoff of at least 80 Ry was needed to achieve convergence which is typical for nitrogen as it has no p or d states in the core. For instance, Kotakoski and co-workers [81] reported the discrepancies found in the phonon dispersion and enthalpies of the black phosphorous (BP) nitrogen phase that's maybe due to the use of a small energy cutoff (39 Ry). A similar experience was faced in computing UV spectra of nitrogen clusters where reliable results were only obtained by implementing diffuse functions in the basis set as suggested by Tobita

and Bartlet[1]. K-point mesh of 10×10×10 in the Monkhorst-Pack formalism was maintained in all calculations. For Raman and Infrared calculations and due to restrictions in the software where no GGA functionals nor ultrasoft pseudopotentials can be used, the local density approximation LDA [78] was used with Pedrew-Zunger (PZ) [82] functionals and a norm conserving pseudopotential.

5.1.3 Geometry Optimization

Nitrogen cubic gauche is a body-centered with primitive cell atoms occupying the 8a(x,x,x) Wyckhoff positions. The Cartesian coordinates of the 4-atoms making the basis set are found at positions : (x,x,x), (0.5-x,-x ,0.5+x),(-x,0.5+x,0.5-x) and (0.5+x,0.5-x,-x) where x is an internal coordinate that entirely defines the structure along the lattice parameter. A typical energy minimization can be done by evaluating the total energy of the system with regards to the lattice constant while keeping the internal coordinate x constant. In Figure. 5.2 an optimal lattice parameter of 7.1148 Bohr (3.76 Angstrom) is found found from the E-V scheme at x=0.08945. A geometry optimization was conducted starting with these parameters using the variable cell dynamics as implemented in Quantum Espresso through the Newotonian Broyden-Fletcher-Goldfarb-Shanno (BFGS) algorithm for both ions and the cell itself. To ensure a reliable geometry optimization, a high threshold of 10^{-4}Ry/au was set for the forces on the atoms. That led us to a lattice parameter in the order of 7.1816 bohr (3.80 A). A new geometry optimization was again carried out with this lattice parameters by allowing only the ions to move in a dynamic relaxation without cell variation, the internal coordinates x was then found to be x=0.086 at zero pressure. The values for the cell parameters and internal coordinates agree well

[1]Structure and Stability of Polynitrogen Molecules and Their Spectroscopic Characteristics. `http://clas.ufl.edu/users/rodbartl/pdf_files/polynitrogen20Tobita.pdf`. accessed online (Dec 5 2014)

with the extrapolated values of Eremets and co-workers [4] (a=3.752) taken into account the tendency of GGA functionals in overestimating lattice parameters.

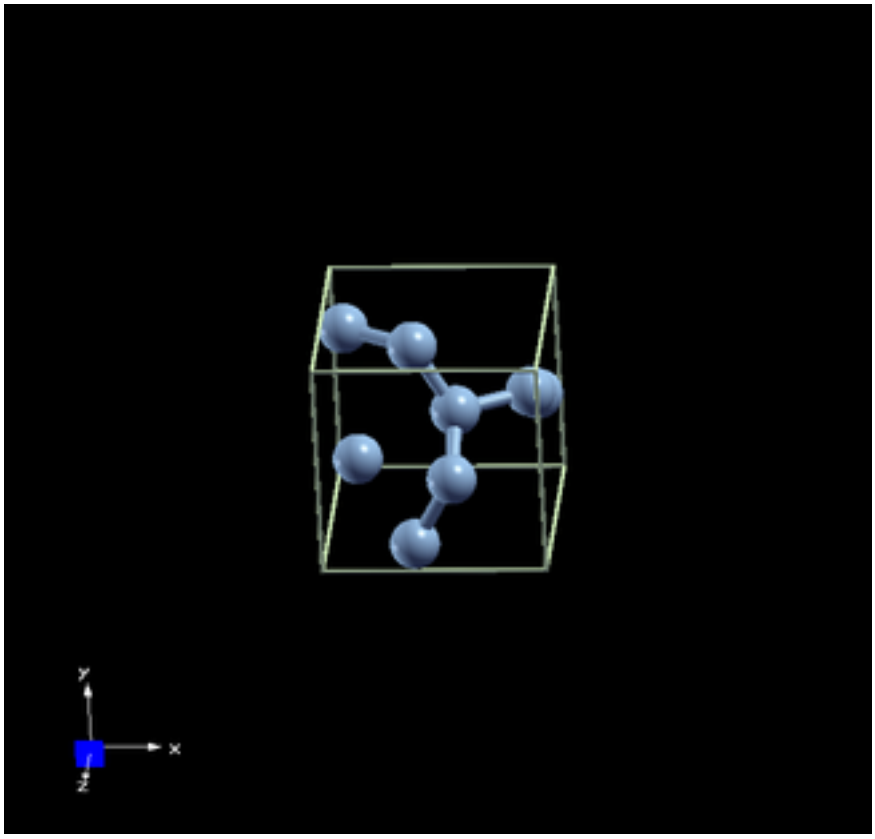

Figure 5.1 cg-PN unit cell

5.1.4 Phonons and Vibrational Modes

Phonon dispersion calculations were conducted with perturbation density functional theory. A richer grid of 20×20×20 was used to extract dynamical matrices for all phonon calculations. The phonon dispersion for the optimized nitrogen cubic gauche at zero pressure is shown in Figure. 5.3. The path from and to high symmetry points was in the following sequence: Γ $\frac{2\pi}{a}$(0 0 0), N $\frac{2\pi}{a}$(0.5 0.5 0), H $\frac{2\pi}{a}$(0.5 0 0), Γ $\frac{2\pi}{a}$(0 0 0), N $\frac{2\pi}{a}$(0.5 0.5 0), P $\frac{2\pi}{a}$(0.5 0.5 0.5). No negative phonon modes are detected at this level of theory which suggests the mechanical stability of the structure at zero pressure. The vibrational density of states was also computed and can be seen along

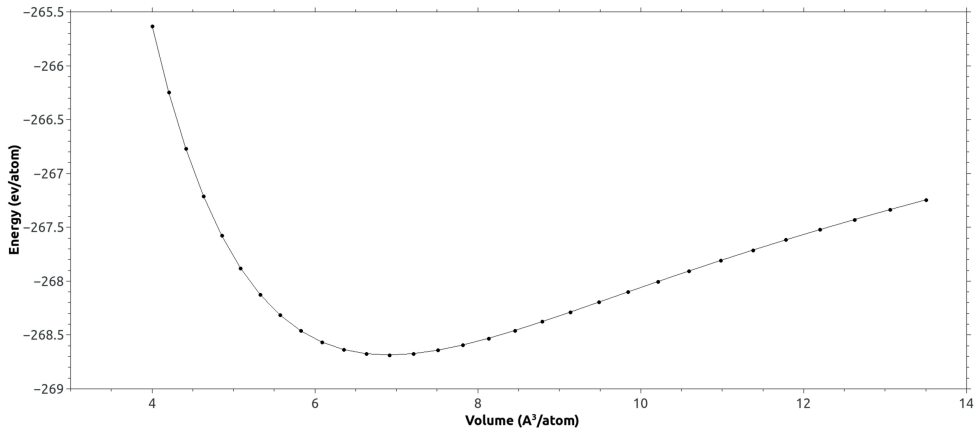

Figure 5.2 cg-N computed energy vs atomic volume at zero pressure

the phonon dispersion curve. All modes are highly dispersive when compared to the modes reported at high pressures [5, 31] where all modes harden by increasing their frequency in a nonlinear fashion. All modes are supposed to be degenerate at the Γ point. However, in the course of this investigation, the second optical mode slightly looses its degeneracy even at the Γ point due to the strong LO-TO splitting for this mode. Caracas [31] attributed the L0-TO splitting to the N-N bonds tilts relative to the direction of the polymeric chains. The splitting of this mode is stronger for cg-PN upon pressure decrease apparently because of the volume increase of the unit cell.

5.1.5 Raman and Infrared Spectra

For Raman and IR spectra, only phonons at the Γ point are involved. A linear response calculation is conducted at Γ by first computing the dielectric response then a second-order response to an external electric field and finally the linear response to lattice perturbation. As a result, effective charges, dielectric and Raman tensors were extracted along the dynamical matrix which allows for computing the cross sections by imposing the Acoustic Sum Rule. In Figure. 5.4, Raman (in red)and IR (in

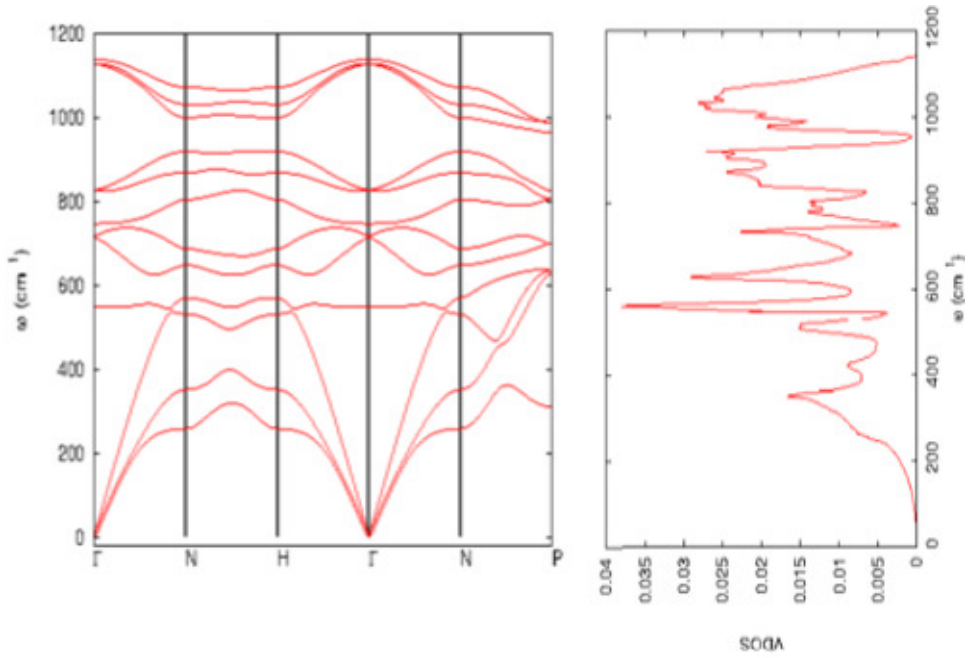

Figure 5.3 cg-PN phonon dispersion at zero Pressure and vibrational density of states.

green) intensities are plotted against wavenumbers, The spectrum is dominated by the Raman active mode which is located at 685 cm^{-1} after imposing the Acoustic Sum Rule which has the effect of forcing all translational and rotational modes to zero frequency. The second Raman-active mode at 960 cm^{-1} is about 14% in intensity and it is believed to be practically hard to detect in Raman spectra of the cg PN. In "The four lines controversy" discussed in Section 2.4, the emerging of a second line was pointed out after 10 times magnification of the Raman spectrum in Eremets work [13], but the line that emerged at 963 cm^{-1} is the second optical mode which is IR-Raman-active; in this investigation, it is the second Raman-active mode that should show up in the Raman spectrum. In fact, Eremets argument about this line is based on Caracas calculation [31] that does not specify which of the the other three lines can be detected in the Raman spectrum. The computed lines in the IR spectrum are all weak, the intensities shown are only due to numerical errors and

are practically at zero intensity. Caracas [31] evaluated the IR spectrum through the ideal reflectivity that only gives 0 or 100% but because of damping the real reflectivity can be anything in between. In summary, the cg PN structure will be only detected by Raman through a dominant band about 600 cm^{-1} with no IR activity.

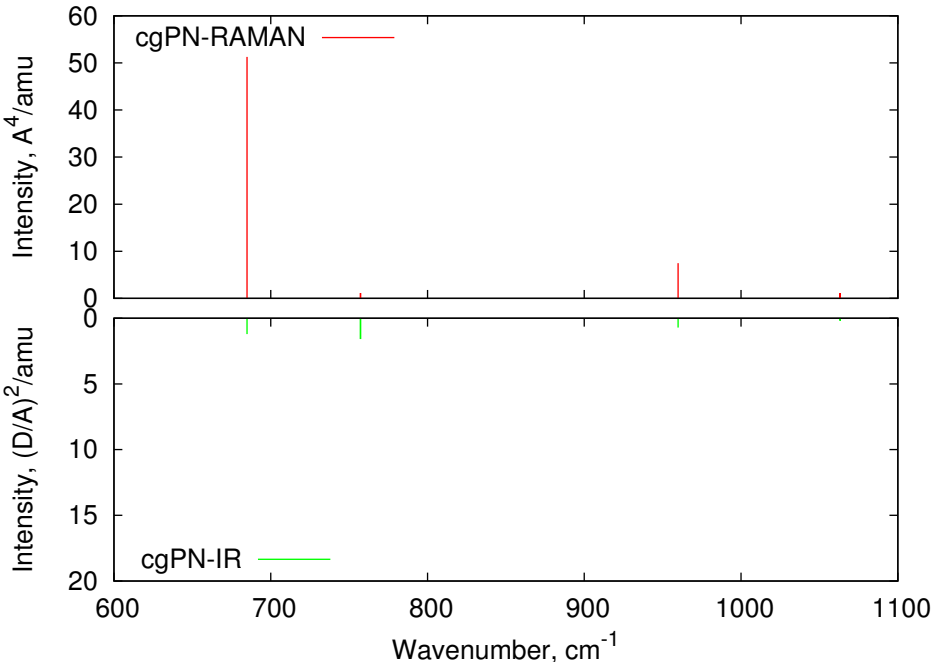

Figure 5.4 cg-PN Raman and infrared spectra at Zero Pressure.

5.2 Other Monoatomic Solid Nitrogen Compounds

Even though the cg-PN drew the most attention since its first prediction in 1990s because of the novelty of its structure and potential use as HDEM, plethora of phases were reported in the literature as energetically competitive to cg-PN first in terms of metastability and second for the complications that are still surrounding the cg-PN synthesis and thus its implementation for practical purposes. Probably one of the most interesting groundbreakings came recently in the work of Hirshberg et al. [83] where an all-nitrogen molecular structure consisting of two N_8 isomers (EEE and EZE) as shown in Figures. 5.5 and 5.5 is predicted to be more stable than cg-N at

pressures below 20GPa. About 0.524 eV.atom^{-1} stability gain relative to the cubic gauche. It is worth noting the striking resemblance between the two structures not in terms of their crystalline forms but the way nitrogen atoms arrange themselves preferring dihedral orientations as shown in Figure. 5.7 which should be taken into account in geometry optimization procedures for polymeric nitrogen structures in computational studies.

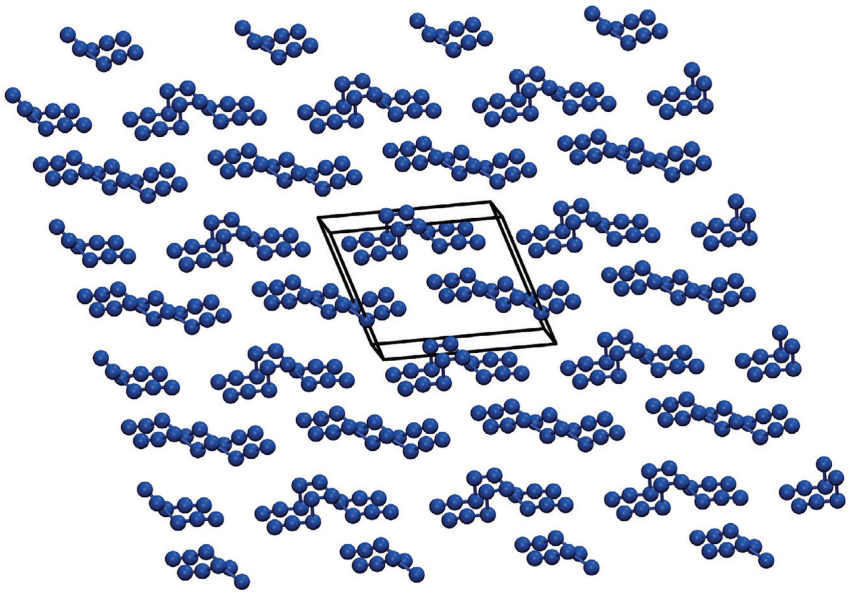

Figure 5.5 Unit cell of predicted N_8 solid. Top and bottom layer conformational isomer of N_8 in the unit cell is referred to as EZE and the middle layer as EEE. Source: *B. Hirshberg, R. B. Gerber, and A. I. Krylov. Calculations predict a stable molecular crystal of N_8 . Nat. Chem, 6:52, 2014.*

Before the recently discovered N_8 molecular structure, the so-called chaired web (CW) shown in Figure. 5.8 was another competitive to cg-PN at ambient conditions with more stability of 83 meV in free energy [84]. More forms of monoatomic solid nitrogen have been predicted to be metastable [85, 86, 87].

5.3 Polynitrogen Clusters

A great deal of theoretical studies was given to polynitrogen compounds that experimental success is, thanks to quantum first-principle methods, largely outnumbered

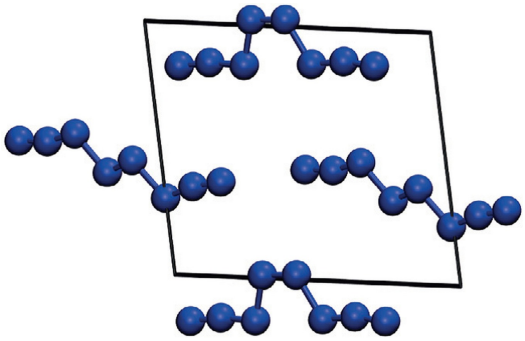

Figure 5.6 Crystal structure of N_8 solid showing unit cell detailed in Figure. 5.5.
Source: *B. Hirshberg, R. B. Gerber, and A. I. Krylov. Calculations predict a stable molecular crystal of N_8 . Nat. Chem, 6:52, 2014.*

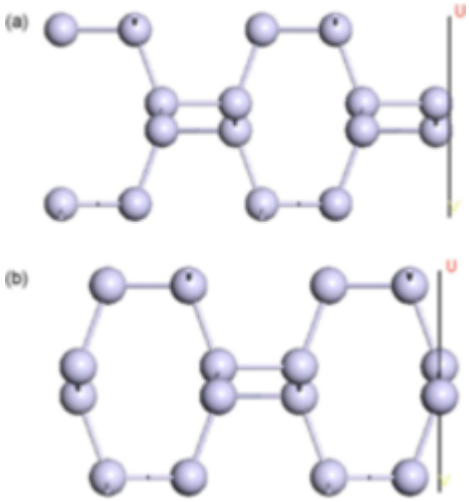

Figure 5.7 cg-PN (100) subsurfaces.
Source: *T. Zhang, S. Zhang, Q. Chen, and L.M. Peng. Phys. Rev. B 73, 094105, 2006.*

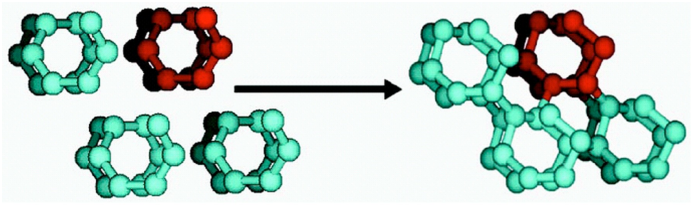

Figure 5.8 Six-fold helices forming the single-bonded CW phase.
Source: *F. Zahariev, J. Hooper, S. Alavi, F. Zhang, and T. K. Woo. Low-pressure metastable phase of single-bonded polymeric nitrogen from a helical structure motif and first-principles calculations. Phys. Rev. B, 75:140101, 2007.*

by what's available from computational studies. In almost all cases, thermodynamic stability is reached suggesting the possibility of a synthesis. Vibrational frequencies are often given to help experimentalists identify these structures. For example, a summary detailing a 30-year research in N_3 , N_4 and N_5 along with their ions were summarized by Nguyen [88]. Except for the azide anion N_3^-, these systems were only mere calculations but the experiental progress caught up with theory and one is now available in stable salt bulk quantities (N_5^+) while the others with only microseconds of lifetime in harsh experimental procedures. More structures ranging from N_6 to N_{10} are also abundant in the literature [89, 90, 91, 92]. A double chain semi-conducting nitrogen N_{24} structure was predicted by Owens [93] suggesting that encapsulation in a matrix is not necessary to gain stability. Higher oligomers went up to N_{60} and beyond. Another variant of these investigations is prioritizing the essential role of possible routes to form a compound. An example can be found in the work of Fau and Bartlett [94] on the possible route to N_8 synthesis from N_5^+ and N_3^- elements as both exist. It turns out, from this study, that a dissociation barrier that is at least 10 kcal/mol lower than needed is preventing the ion pair to lead such a route. On the other hand, it was suggested that such a hindrance doesn't exist for the N_5+/N_5^- pair to form N_{10} [95].

Another class of clusters with a great potential are the closed fullerene-like structures. Nitrogen by nature is sp^2 trivalent, in such structures, each nitrogen site can be single-bonded to three nearest neighbors. The N_{60}-buckyball-like of I_h symmetry is not stable but a concave cage C_{60} of symmetry S_6 is rather stable [96], More of these potential structures inlcude N_{18} and N_{20} [97, 98, 99].

5.4 The PECVD Synthesized Structure

In the search to identify the polynitrigen of the PECVD synthesis, a complete match was not found in the literature that should agree with the IR/Raman data that are

obtained from the plasma reacted samples. At first, closed structures were rulled because of the vibrational activity that is detected in the 2000 cm^{-1} frequency regions as structures from the literature and the calculations conducted along this experimental work are unlikely to give activity in that region. Assumptions were wade in the early phase of this project that the most likely structure had to be a linear chain. Couple structures were optimized and their computed Raman and IR spectra are depicted in Figure.s. 5.9 and 5.10. Neither of these structures are a good match and they are only presented to show the activity of such structures in the 2000 cm^{-1} region[2].

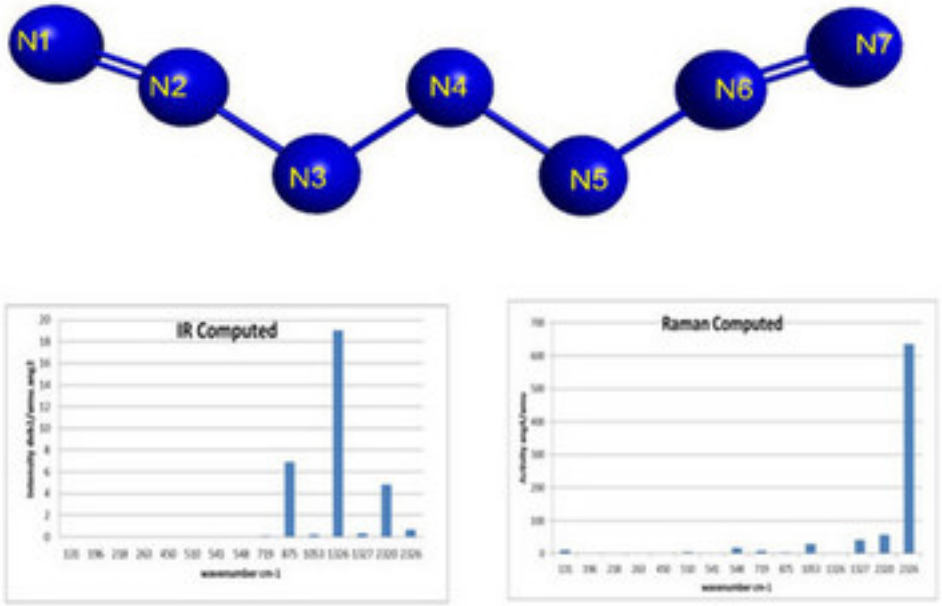

Figure 5.9 N_7^+ optimized structure and its IR/Raman spectra.

At some point, the N_{20} was thought of as a possibility because of it's strong Raman signatures in the vicinity of 600 cm^{-1}. Time of flight mass spectroscopy

[2]All linear chains of this type (up to N_{10}) containing single bonds and double bonds at both ends of the chain exhibit activity at the 2000 cm^{-1}. Another example is the N_8^- formed by our group in the electrochemistry procedure.

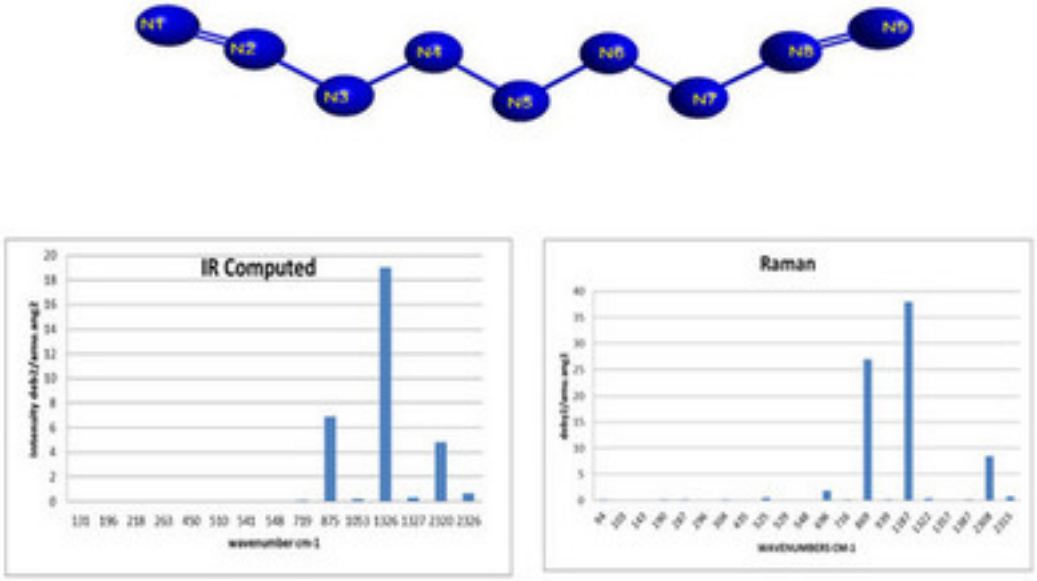

Figure 5.10 N_9^+ optimized structure and its IR/Raman spectra.

data obtained by Manning [62] using an electrochemical route to synthesize PN on single wall carbon nanotubes has a N_{20} signature. More theoretical and experimental investigations are needed to confirm that fullerenes of nitrogen can form and be synthesized. In Figure. 5.11 the optimized N_{20} of D_5 symmetry is presented and its vibrational frequencies are shown in Figure. 5.12. Similar to C_{60}, this structure can be detected only by one strong Raman signal but in the vicinity of 600 cm^{-1}. All calculations of nitrogen clusters were carried out by density functional theory at the 6-31+G (d, p) level using GamessUS [100, 101]. The structures were visualized with MacMolPlot [102], a graphical interface to GamessUS. The B3LYP [103] functional was adopted with the 6-31+G(d,p) as it yields the closest results for the well-known azide ion. Wave numbers are expressed in cm^{-1} , IR intensities in $debye^2/amu.ang^2$, whereas Raman intensities are expressed in ang^4/amu. The azide anion structure optimization was for the sole purpose of testing the validity of the method which gave a deviation of 2.9% for the IR antisymmetric stretching frequency at 2160 cm^{-1}, observed experimentally at 2100 cm^{-1}, while a deviation of only 0.29% was recorded for the symmetric stretching Raman frequency at 1,364 cm^{-1}, observed experimentally at 1360 cm^{-1}.

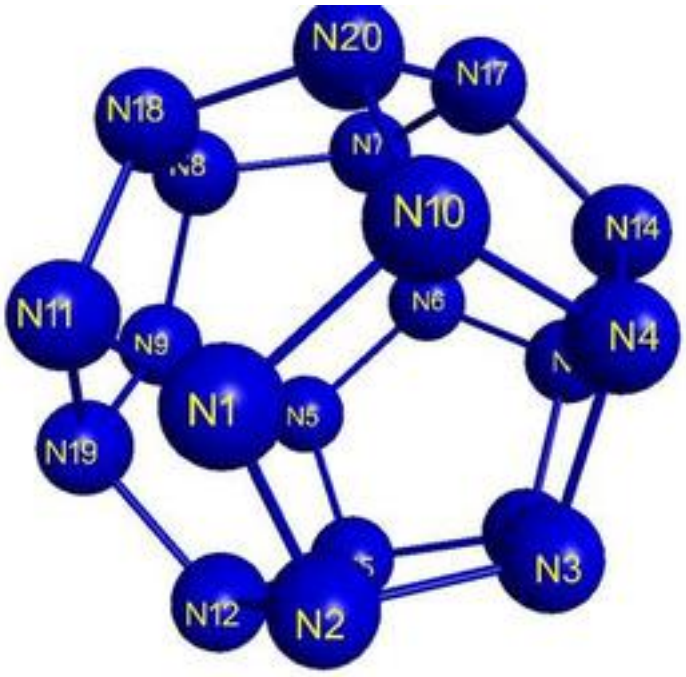

Figure 5.11 D_5 N_{20} closed structure.

Mode	Frequency (cm-1)	Symmetry	IR Intensity (Deby**2/Amu-Ang**2)	Raman Intensity (Ang**4/Amu)
7	322.608	E2U	0	0
8	322.608	E2U	0	0
9	324.442	E1U	0.000002	0
10	324.442	E1U	0.000001	0
11	324.976	A1U	0	0
12	450.842	E2G	0	63.4
13	450.842	E2G	0	10.76
14	451.929	E1G	0	24.668
15	451.929	E1G	0	10.783
16	453.746	A1G	0	323.783
17	575.454	E2U	0	
18	575.454	E2U	0	
19	577.945	E1U	0.00001	
20	577.945	E1U	0.000009	
21	591.053	A2U	0	0.001
22	594.873	E2U	0	
23	594.873	E2U	0	
24	598.078	A1G	0	102.547
25	609.828	A2G	0	
26	610.023	E2G	0	
27	610.023	E2G	0	12.199
28	640.622	E1G	0	6553.259
29	640.622	E1G	0	1.031
30	643.807	A1G	0	1.012
31	644.486	E2G	0	1648.377
32	644.486	E2G	0	1.003
33	662.995	A2U	0.00715	0
34	663.762	E1U	0.006753	0
35	663.762	E1U	0.006771	0
36	668.605	E1G	0	0.01
37	668.605	E1G	0	67.11
38	669.183	E2G	0	0.028
39	669.183	E2G	0	347.103
40	842.827	E2G	0	202.923
41	842.827	E2G	0	0
42	845.309	E1G	0	56.401
43	845.309	E1G	0	0
44	866.579	E2U	0	0
45	866.579	E2U	0	0
46	868.624	A2U	0.000002	0
47	890.756	E1U	0.000002	0
48	890.756	E1U	0.000001	0
49	890.889	E2U	0	0
50	890.889	E2U	0	0
51	916.981	E2U	0	0
52	916.981	E2U	0	0
53	917.37	E1U	0.000004	0
54	917.37	E1U	0.000003	0
55	920.366	A1U	0	0
56	979.652	E2G	0	1.386
57	979.652	E2G	0	188.786
58	981.848	A1G	0	856.414
59	982.138	E1G	0	1.344
60	982.138	E1G	0	1.345

Figure 5.12 D_5 N_{20} vibrational modes.

CHAPTER 6

SUMMARY AND FUTURE WORK

Although further optimization is necessary to enhance yields, plasma enhanced chemical vapor deposition has been shown to produce PN phases. In particular, fairly strong evidence has been obtained from X-ray diffraction data coupled with Raman spectroscopy for the ambient pressure metastable formation of cg-PN, particularly from sodium azide precursors, in general agreement with the results of Popov [33]. Moreover, a new crystalline PN phase (possibly the so- called Phase I) together with smaller amounts of cg-PN appears to form when lithium azide is used as the precursor. In the case of sodium azide, carbon nanotubes have been shown to enhance the formation of the PN phase possibly via stabilization of the structure on the nanotube sidewalls or inside the nanotubes. The ease with which PECVD is conducted gives it an edge over more expensive and harsh processes. More importantly, the synthesized phases of polymeric nitrogen obtained give indications of an unprecedented metastability at ambient conditions. In fact, from spectroscopic analysis, samples were preserved for extended periods without any noticeable change in their composition. Temperature programmed desorption studies indicated decomposition of the majority PN phase at 400°C. Energetic measurements using differential scanning calorimetric methods have not yet been conducted for safety reasons, although it is planned in future studies with US Army collaborators.

This work was shown to be reproducible as long as the plasma conditions were kept within the realm of the required parameters for a successful synthesis. Carbon nanotubes play an essential role as substrates as noted above, particularly when sodium azide is used as the precursor. Reasons for this are not clear and will be examined in planned future studies using transmission electron microscopy coupled with selected area electron diffraction and density functional simulations. More

detailed X-ray diffraction using a Synchrotron source will be conducted to determine the structure of the so-called Phase I and further details of cg-PN under ambient conditions.

BIBLIOGRAPHY

[1] S. Bräse, C. Gil, K. Knepper, and V. Zimmermann. Organic azides: An exploding diversity of a unique class of compounds. *Angew. Chem. Int. Ed*, 44:5188, 2005.

[2] C. Mailhiot, L. H. Yang, and A. K. McMahan. Polymeric nitrogen. *Phys. Rev. B*, 46:14419, 1992.

[3] K. O. Christe, W. W. Wilson, J. A. Sheehy, and J. A. Boatz. N_5^+: A novel homoleptic polynitrogen ion as a high energy density material. *Angew. Chem. Int. Ed*, 38:2004, 1999.

[4] M. I. Eremets, A. G. Gavriliuk, I. A. Trojan, D. A. Dzivenko, and R. Boehler. Single-bonded cubic form of nitrogen. *Nat. Mater*, 3:558, 2004.

[5] T. W. Barbee. Metastability of atomic phases of nitrogen. *Phys. Rev. B*, 48:9327, 1993.

[6] N. Hansen, A. M. Wodtke, S. J. Goncher, J. C. Robinson, N. E. Sveum, and D. M. Neumark. Photofragment translation spectroscopy of ClN_3 at 248 nm: Determination of the primary and secondary dissociation pathways. *Chem. Phys*, 123:305, 2005.

[7] F. Cacace, G. de Petris, and A. Troiani. Experimental detection of tetranitrogen. *Sci*, 295:480, 2002.

[8] A. Vij, J. G. Pavlovich, W. W. Wilson, V. Vij, and K. O. Christe. Experimental detection of the pentaazacyclopentadienide (pentazolate) anion, cyclo N_5. *Angew. Chem*, 114:3177, 2002.

[9] G. Junk and H. J. Svec. The presence of N_3^+ and N_4^+ in the mass spectra of molecular mitrogen. *Am. Chem. Soc*, 80:2908, 1958.

[10] M. Yamashita and J. B. Fenn. Electrospray ion source. another variation on the free-jet theme. *Phys. Chem*, 88:4451, 1984.

[11] R. Kalescky, E. Kraka, and D Cremer. Identification of the strongest bonds in chemistry. *Phys. Chem. A*, 117:8981, 2013.

[12] George B. Kaufman. Inorganic chemistry: principles of structure and reactivity, 4th ed. *Chem. Ed*, 70:A279, 1993.

[13] M. Eremets, I. A. Trojan, A. G. Gavriliuk, and S. A. Medvedev. *Synthesis of High-Nitrogen Energetic Material*. Shock Wave and High Pressure Phenomena. Springer Berlin Heidelberg, 2008.

[14] X. Q. Chen, C. L. Fu, and R. Podloucky. Bonding and strength of solid nitrogen in the cubic gauche (cg-n) structure. *Phys. Rev. B*, 77:064103, 2008.

[15] H. J. McSkimin, P. Andreatch, and P. Glynn. The elastic stiffness moduli of diamond. *App. Phys*, 43:985, 1972.

[16] H. L. Yu, G. W. Yang, X. H. Yan, Y. Xiao, Y. L. Mao, Y. R. Yang, and M. X. Cheng. First-principles calculations of the single-bonded cubic phase of nitrogen. *Phys. Rev. B*, 73:012101, 2006.

[17] Z. Wu, E. M. Benchafia, Z. Iqbal, and X. Wang. N_8^- polynitrogen stabilized on multi-wall carbon nanotubes for oxygen-reduction reactions at ambient conditions. *Angew. Chem. Int. Ed*, 53:12555, 2014.

[18] K. Gong, F. Du, Z. Xia, M. Durstock, and L Dai. Nitrogen-doped carbon nanotube arrays with high electrocatalytic activity for oxygen reduction. *Sci*, 323:760, 2009.

[19] D. Geng, Y. Chen, Y. Chen, Y. Li, R. Li, X. Sun, S. Ye, and S. Knights. High oxygen-reduction activity and durability of nitrogen-doped graphene. *Energy. Environ. Sci*, 4:760, 2011.

[20] M. Liu, Y. Song, S. He, W. W. Tjiu, J. Pan, Y. Y. Xia, and T. Liu. Nitrogen-doped graphene nanoribbons as efficient metal-free electrocatalysts for oxygen reduction. *Acs. Appl Mater. Inter*, 6:4214, 2014.

[21] F. J. DiSalvo. Solid-state chemistry: A rediscovered chemical frontier. *Sci*, 247:649, 1990.

[22] C. Mailhiot, J. B. Grant, and A. K. McMahan. High-pressure metallic phases of boron. *Phys. Rev. B*, 42:9033, 1990.

[23] C. Mailhiot and A. K. McMahan. Atmospheric-pressure stability of energetic phases of carbon. *Phys. Rev. B*, 44:11578, 1991.

[24] D. B. Boercker. Constant-pressure simulation of carbon in the bc8 structure. *Phys. Rev. B*, 44:11592, 1991.

[25] H. E. Lorenzana, C. S. Yoo, M. Lipp, T. III Barbee, A. K. McMahan, and C. Mailhiot. *Novel high energy density materials: Synthesis by megabar hot pressing. LDRD final report.* 1996.

[26] A. F. Goncharov, E. Gregoryanz, H. K. Mao, Z. Liu, and R. J. Hemley. Optical Evidence for a Nonmolecular Phase of Nitrogen above 150 GPa. *Phys. Rev. Lett*, 85:1262, 2000.

[27] A. K. McMahan and R. LeSar. Pressure dissociation of solid nitrogen under 1 mbar. *Phys. Rev. Lett.*, 54:1929, 1985.

[28] M. I. Eremets, R. J. Hemley, H. k. Mao, and E Gregoryanz. Semiconducting non-molecular nitrogen up to 240 gpa and its low-pressure stability. *Nat*, 411:170, 2001.

[29] K. Nordlund, A. Krasheninnikov, N Juslin, J. Nord, and K. Albe. Structure and stability of non-molecular nitrogen at ambient pressure. *Europ. Lett*, 65:400, 2004.

[30] M. I. Eremets, A. G. Gavriliuk, and I. A. Trojan. Single-crystalline polymeric nitrogen. *App. Phys. Lett*, 90, 2007.

[31] R. Caracas. Raman spectra and lattice dynamics of cubic gauche nitrogen. *Chem. Phys*, 127(14), 2007.

[32] M. I. Eremets, M. Yu. Popov, I. A. Trojan, V. N. Denisov, R. Boehler, and R. J. Hemley. Polymerization of nitrogen in sodium azide. *Chem. Phys*, 120(22), 2004.

[33] M. Popov. Raman and ir study of high-pressure atomic phase of nitrogen. *Phys. Lett. A*, 334:317, 2005.

[34] P. Pyykkö and N. Runeberg. Ab initio studies of bonding trends: Part 9. the dicyanamide-carbon suboxide-dicyanoether-cyanogen azide isoelectronic series abcde. *Molec. Str*, 234:279, 1991.

[35] L. Tonks and I. Langmuir. Oscillations in ionized gases. *Phys. Rev.*, 33:195, 1929.

[36] M. Meyyappan, D. Lance, C. Alan, and H. David. Carbon nanotube growth by pecvd: a review. *Plsm. Src. Sci. and Techn*, 12:205, 2003.

[37] P. Chabert and N. Braithwaite. *Physics of Radio-Frequency Plasmas*. Cambridge University Press, 2011.

[38] B. Eliasson and U. Kogelschatz. Nonequilibrium volume plasma chemical processing. *Plsm Sci, IEEE Trans*, 19:1063, Dec 1991.

[39] I. Fabio, C. Giulio, and L. Francesco. Structural properties of SiO_2 films prepared by plasma-enhanced chemical vapor deposition. *Mater. Sci. in Semicon. Proc*, 4:43, 2001. Advanced Characterisation of Semiconductor Materials.

[40] A. A. Howling, J. L. Dorier, C. Hollenstein, U. Kroll, and F. Finger. Frequency effects in silane plasmas for plasma enhanced chemical vapor deposition. *Vac. Sci. Tech. A.*, 10:1080, 1992.

[41] R. B. Jackman, J. Beckman, and J. S. Foord. Diamond chemical vapor deposition from a capacitively coupled radio frequency plasma. *App. Phys. Lett*, 66, 1995.

[42] J. J. Lander and j. Morrison. Low energy electron diffraction study of the (111) diamond surface. *Sur. Sci*, 4:241, 1966.

[43] Y. Muranaka, H. Yamashita, K. Sato, and H. Miyadera. The role of hydrogen in diamond synthesis using a microwave plasma in a CO/H_2 system. *App. Phys*, 67, 1990.

[44] D. L. Smith. Controlling the plasma chemistry of silicon nitride and oxide deposition from silane. *Vac. Sci. & Techn*, 11, 1993.

[45] P. K. Bachmann, D. Leers, and H. Lydtin. Towards a general concept of diamond chemical vapour deposition. *Diam. & Reltd Mater*, 1:1, 1991.

[46] S. H. Chan, S. H. Chen, W. T. Lin, M. C. Li, Y. C. Lin, and C. C Kuo. Low-temperature synthesis of graphene on cu using plasma-assisted thermal chemical vapor deposition. *Nanosca. Res. Lett*, 8:285, 2013.

[47] F. Piallat, C. Valle, R. Gassilloud, P. Michallon, B. Pelissier, and P. Caubet. Pecvd rf versus dual frequency: an investigation of plasma influence on metal?organic precursors' decomposition and material characteristics. *Phys D. App Phys*, 47:185201, 2014.

[48] R. Hayakawa, T. Yoshimura, A. Ashida, N. Fujimura, H. Kitahata, and M. Yuasa. Analysis of nitrogen plasma generated by a pulsed plasma system near atmospheric pressure. *App. Phys*, 96, 2004.

[49] A. Lofthus and P .H . Krupenie. *The Spectrum of Molecular Nitrogen.* Journal of physical and chemical reference data: Reprint. American Chemical Society and the American Institute of Physics for the National Bureau of Standards, 1977.

[50] J. J Camacho, J. M. L. Poyato, L. Daz, and M Santos. Optical emission studies of nitrogen plasma generated by ir CO_2 laser pulses. *Phys B: Atom, Molec and Opti Phys*, 40:4573, 2007.

[51] G. Baravian, J. Godart, and G. Sultan. Multiphoton ionization of molecular nitrogen by a neodymium-glass laser. *Phys. Rev. A*, 25:1483, 1982.

[52] A. A Sorokin, S. V. Bobashev, K Tiedtke, and M Richter. Multi-photon ionization of molecular nitrogen by femtosecond soft x-ray fel pulses. *Phys B: Atom, Molec and Opti Phys*, 39:L299, 2006.

[53] W. H. Soon and J. A. Kunc. Nitrogen-plasma continuum emission associated with $N^-(^3p)$ and $N^-(^1d)$ ions. *Phys. Rev. A*, 41:4531–4533, 1990.

[54] F. P Bundy, H. T. Hall, H. M. Strong, and R. H. Wentorf. Man-made diamonds. *Nat*, 176:51, 1955.

[55] Kazuaki Kurihara, Kenichi Sasaki, Motonobu Kawarada, and Nagaaki Koshino. High rate synthesis of diamond by dc plasma jet chemical vapor deposition. *App. Phys. Lett*, 52, 1988.

[56] Atsuhito Sawabe, Hiroaki Yasuda, Tadao Inuzuka, and Kazuhiro Suzuki. Growth of diamond thin films in a dc discharge plasma. *App. Sur. Sci*, 33:539, 1988.

[57] D. E. Meyer, N. J. Ianno, J. A. Woollam, A. B. Swartzlander, and A. J. Nelson. Growth of diamond by rf plasma-assisted chemical vapor deposition. *Materials. Res*, 3:1397, 1988.

[58] H. W. Kroto, J. R. Heath, R. F. Curl, and R. E. Smalley. C_{60}: Buckminsterfullerene. *Nat*, 318(10):162, 1985.

[59] H. Abou-Rachid, A. Hu, V. Timoshevskii, Y. Song, and L. Simon. Lussier. Nanoscale high energetic materials: A polymeric nitrogen chain N_8 confined inside a carbon nanotube. *Phys. Rev. Lett.*, 100:196401, 2008.

[60] V. Timoshevskii, W. Ji, H. Abou-Rachid, L. S. Lussier, and H. Guo. Polymeric nitrogen in a graphene matrix: An ab initio study. *Phys. Rev. B*, 80:115409, 2009.

[61] W. Ji, V. Timoshevskii, H. Guo, H. Abou-Rachid, and L. S Lussier. Thermal stability and formation barrier of a high-energetic material N_8 polymer nitrogen encapsulated in (5,5) carbon nanotube. *App. Phys. Lett*, 95:021904, 2009.

[62] T. Manning. *Novel micron and nano-scale energetic materials for advanced gun propulsion, their material properties and their effects on balistic performance.* diploma thesis, New Jersey Institute of Technology, 2010.

[63] C. Wu. *Plasma-Enhanced Chemical Vapor Deposition Synthesis of Stable Polymeric Nitrogen.* diploma thesis, New Jersey Institute of Technology, 2012.

[64] M. Popov. Raman and ir study of high-pressure atomic phase of nitrogen. *Phys. Lett. A*, 334:317, 2005.

[65] M. Zhang, H. Yan, Q. Wei, H. Wang, and Z. Wu. Novel high-pressure phase with pseudo-benzene N_6 molecule of LiN_3. *EPL*, 101:26004, 2013.

[66] J. Li, X. Wang, N. Xu, D. Li, D. Wang, and L. Chen. Pressure-induced polymerization of nitrogen in potassium azides. *EPL*, 104:16005, 2013.

[67] S. M. Peiris and T. P. Russell. Photolysis of compressed sodium azide (NaN_3) as a synthetic pathway to nitrogen materials. *The Journal of Physical Chemistry A*, 107:944, 2003.

[68] N. E. Massa, S. S. Mitra, H. Prask, R. S. Singh, and S. F. Trevino. Infraredactive lattice vibrations in alkali azides. *Chem. Phys*, 67, 1977.

[69] A. F. Goncharov, E. Gregoryanz, H. K. Mao, Z. Liu, and R. J. Hemley. Optical evidence for a nonmolecular phase of nitrogen above 150 gpa. *Phys. Rev. Lett.*, 85:1262, 2000.

[70] S. Vepřek, Z. Iqbal, J. Brunner, and M. Schärli. Preparation and properties of amorphous phosphorus nitride prepared in a low-pressure plasma. *Phil. Mag. B*, 43:527, 1981.

[71] X. Wang, J. Li, J. Botana, M. Zhang, H. Zhu, L. Chen, H. Liu, T. Cui, and M. Miao. Polymerization of nitrogen in lithium azide. *Chem. Phys*, 139, 2013.

[72] H. R. Chandrasekhar, G. Bhattacharya, R. Migoni, and H. Bilz. Phonon spectra and lattice dynamics of lithium nitride. *Sol. St. Comm*, 22:681, 1977.

[73] G. E. Pringle and D. E. Noakes. The crystal structures of lithium, sodium and strontium azides. *Acta. Cryst*, B24:262, 1968.

[74] S. Baroni, P. Giannozzi, and A. Testa. Greens-function approach to linear response in solids. *Phys. Rev. Lett.*, 58:1861, 1987.

[75] X. Gonze and J. P. Vigneron. Density-functional approach to nonlinear-response coefficients of solids. *Phys. Rev. B*, 39:13120, 1989.

[76] P. Giannozzi, S. Baroni, N. Bonini, M. Calandra, R. Car, C. Cavazzoni, D. Ceresoli, G. L. Chiarotti, M. Cococcioni, I. Dabo, A. Dal Corso, S. de Gironcoli, S. Fabris, G. Fratesi, R. Gebauer, U. Gerstmann, C. Gougoussis, A. Kokalj, M. Lazzeri, L. Martin-Samos, N. Marzari, F. Mauri, R. Mazzarello, S. Paolini, A. Pasquarello, L. Paulatto, C. Sbraccia, S. Scandolo, G. Sclauzero, A. P. Seitsonen, A. Smogunov, P. Umari, and R. M. Wentzcovitch. Quantum espresso: a modular and open-source software project for quantum simulations of materials. *Phys. Cond. Mat*, 21:395502, 2009.

[77] P. Hohenberg and W. Kohn. Inhomogeneous electron gas. *Phys. Rev.*, 136:B864, 1964.

[78] W. Kohn and L. J. Sham. Self-consistent equations including exchange and correlation effects. *Phys. Rev.*, 140:A1133, 1965.

[79] J. P. Perdew, K. Burke, and Y. Wang. Generalized gradient approximation for the exchange-correlation hole of a many-electron system. *Phys. Rev. B*, 54:16533, 1996.

[80] J. P. Perdew, K. Burke, and M. Ernzerhof. Generalized gradient approximation made simple. *Phys. Rev. Lett.*, 77:3865, 1996.

[81] J. Kotakoski and K. Albe. First-principles calculations on solid nitrogen: A comparative study of high-pressure phases. *Phys. Rev. B*, 77:144109, 2008.

[82] J. P. Perdew and Alex Zunger. Self-interaction correction to density-functional approximations for many-electron systems. *Phys. Rev. B*, 23:5048, 1981.

[83] B. Hirshberg, R. B. Gerber, and A. I. Krylov. Calculations predict a stable molecular crystal of N_8. *Nat. Chem*, 6:52, 2014. Article.

[84] F. Zahariev, J. Hooper, S. Alavi, F. Zhang, and T. K. Woo. Low-pressure metastable phase of single-bonded polymeric nitrogen from a helical structure motif and first-principles calculations. *Phys. Rev. B*, 75:140101, 2007.

[85] Y. Ma, A. R. Oganov, Z. Li, Y. Xie, and J Kotakoski. Novel high pressure structures of polymeric nitrogen. *Phys. Rev. Lett.*, 102:065501, 2009.

[86] X. Wang, F. Tian, L. Wang, T. Cui, B. Liu, and G. Zou. Structural stability of polymeric nitrogen: A first-principles investigation. *Chem. Phys*, 132:024502, 2010.

[87] W. Xiaoli, T. Fubo, W. Lin, J. Xilian, D. Defang, H. Xiaoli, L. Bingbing, and C. Tian. Predicted novel metallic metastable phases of polymeric nitrogen at high pressures. *New. Jrn. of Phys*, 15:013010, 2013.

[88] M. T Nguyen. Polynitrogen compounds: 1. structure and stability of N_4 and N_5 systems. *Coord. Chem. Rev*, 244:93, 2003.

[89] Walter J. Lauderdale, John F. Stanton, and Rodney J. Bartlett. Stability and energetics of metastable molecules: tetraazatetrahedrane (N_4), hexaazabenzene (N_6), and octaazacubane (N_8). *Phys. Chem*, 96:1173, 1992.

[90] T. K. Ha and M. T Nguyen. The identity of the six nitrogen atoms (N_6 species. *Chem. Phys. Lett*, 195:179, 1992.

[91] L. Gagliard, S. Evangelisti, B. O. Roos, and P.O Widmark. A theoretical study of ten N_8 isomers. *Mol. Str. Theochem*, 428:1, 1998.

[92] Li Jie Wang, Paul G. Mezey, and Marek Z. Zgierski. Stability and the structures of nitrogen clusters N_{10}. *Chem. Phys. Lett*, 391:338, 2004.

[93] F. J. Owens. Prediction of a stable free standing nitrogen oligomer. *Comput and Theor. Chem*, 966:137, 2011.

[94] S. Fau and R. J. Bartlett. Possible products of the end-on addition of N_3^- to N_5^+ and their stability. *Phys. Chem. A*, 105:4096, 2001.

[95] L. Gagliardi, G. Orlandi, S. Evangelisti, and B. O. Roos. A theoretical study of the nitrogen clusters formed from the ions N_3^- , N_5^+ , and N_5^-. *Chem. Phys*, 114:10733, 2001.

[96] J. W. Li and Z. Z Marek. Super-high energy-rich nitrogen cluster N_{60}. *Chem. Phys. Lett*, 36:698, 2003.

[97] J. D. Gu, K. X. Chen, H. L. Jiang, J. Z. Chen, R. Y. Ji, Y. Ren, and A. M. Tian. N_{18}: a computational investigation. *Mol. Str. Theochem*, 428:183 – 188, 1998.

[98] J. S. Wright, D. J. McKay, and G. A. DiLabio. Dodecahedral molecular nitrogen (N_{20}) and related structures. 424:47, 1998.

[99] F. J. Owens. Density functional calculation of structure and stability of nitrogen clusters N_{10}, N_{12}, and N_{20}. *Mol. Str. Theochem*, 623:197, 2003.

[100] M. W. Schmidt, K. K. Baldridge, J. A. Boatz, S. T. Elbert, M. S. Gordon, J. H. Jensen, S. Koseki, N. Matsunaga, K. A. Nguyen, S. Su, T. L. Windus, M. Dupuis, and J. A. Montgomery. General atomic and molecular electronic structure system. *Comput. Chem*, 14:1347, 1993.

[101] M. S. Gordon and M. W. Schmidt. Chapter 41 - advances in electronic structure theory: Gamess a decade later. In C. E. Dykstra, G. Frenking, K. S. Kim, and G. E. Scuseria, editors, *Theory and Applications of Computational Chemistry*, page 1167. Elsevier, Amsterdam, 2005.

[102] B. M. Bode and M. S. Gordon. Macmolplt: a graphical user interface for gamess. *Mol. Graph. and Model.*, 16:133, 1998.

[103] C. Lee, W. Yang, and R. G. Parr. Development of the colle-salvetti correlation-energy formula into a functional of the electron density. *Phys. Rev. B*, 37:785, 1988.